Forschungszentrum Karlsruhe
in der Helmholtz-Gemeinschaft

Wissenschaftliche Berichte

FZKA 7447

Behavior of BWR-type Fuel Elements with B_4C/Steel Absorber Tested under Severe Fuel Damage Conditions in the CORA Facility

L. Sepold, S. Hagen, P. Hofmann, G. Schanz

Institut für Materialforschung
Programm Nukleare Sicherheitsforschung

Januar 2009

Forschungszentrum Karlsruhe

in der Helmholtz-Gemeinschaft

Wissenschaftliche Berichte

FZKA 7447

Behavior of BWR-type Fuel Elements with B_4C/Steel Absorber Tested under Severe Fuel Damage Conditions in the CORA Facility

L. Sepold, S. Hagen, P. Hofmann, G. Schanz

Institut für Materialforschung
Programm Nukleare Sicherheitsforschung

Forschungszentrum Karlsruhe GmbH, Karlsruhe

2008

Note: This document was prepared in 1994 for publication as KfK report 4560 but was not released then. Due to timeliness of the topics and in context with the follow-up research program “QUENCH” it is published in 2008 as report FZKA 7447.

Forschungszentrum Karlsruhe GmbH
Postfach 3640, 76021 Karlsruhe

Mitglied der Hermann von Helmholtz-Gemeinschaft
Deutscher Forschungszentren (HGF)

ISSN 0947-8620

urn:nbn:de:0005-074476

Inhaltsverzeichnis

Abstract

The CORA experiments carried out in an out-of-pile facility at the Kernforschungszentrum Karlsruhe (KfK), Federal Republic of Germany, are part of the "Severe Fuel Damage" (SFD) program.

The experimental program was to provide information on the failure mechanisms of Light Water Reactor (LWR) fuel elements in a temperature range from 1200°C to 2000°C and in a few cases up to 2400°C.

In the CORA experiments two different bundle configurations were tested: PWR (Pressurized Water Reactor) and BWR (Boiling Water Reactor) bundles. The BWR-type bundles consisted of 18 fuel rod simulators (heated and unheated rods), an absorber blade of steel containing eleven absorber rods filled with boron carbide powder. The larger bundle CORA-18 contained the same number of absorber rods but was made up of 48 fuel rod simulators. All BWR bundles were surrounded by a zircaloy shroud and the absorber blades by a channel box wall on each side, also made of zircaloy. The test bundles were subjected to temperature transients of a slow heatup rate in a steam environment. Thus, an accident sequence was simulated, which may develop from a small-break loss-of-coolant accident of a LWR.

The transient phases of the tests were initiated with a temperature ramp rate of 1 K/s. The temperature escalation due to the exothermal zircaloy(Zry)-steam reaction started at about 1100 °C, leading the bundles to maximum temperatures of approximately 2000 °C.

In all experiments bundle destruction started in the upper region (axially) with melting of the absorber blade and the absorber rod cladding at about 1250 °C by interaction of boron carbide and steel. After destruction of the channel box walls this melt attacked the zircaloy fuel rod cladding and and started to interact with the UO_2 pellets.

The test bundles also resulted in severe oxidation of the following components made of zircaloy: shroud, cladding, and grid spacers at the central and upper positions. Relocated absorber melt formed extended blockages at lower elevations of the bundles. This distribution of absorber material could in the type of reactor accident described with subsequent flooding of the partially destroyed reactor core with unborated water lead to local recriticalities.

There was no difference in the behavior of the large bundle CORA-18 compared to the BWR test bundles of regular size, i.e. CORA-16 and CORA-17.

Quenching (flooding) of a degraded BWR-type bundle (CORA-17) exhibits identical behavior as observed in the PWR-type quenching experiments: The bundle results in locally enhanced zircaloy/steam reaction causing a renewed temperature rise, an additional meltdown of materials, and an additional strong hydrogen generation.

Verhalten von Siedewasserreaktor-typischen Brennelementen mit Borkarbid/Stahl-Absorbermaterial, die unter sog. Severe-Fuel-Damage-Bedingungen in der CORA-Versuchsanlage getestet wurden

(Nachuntersuchungsergebnisse der Experimente CORA-16, CORA-17, und CORA-18)

Kurzfassung

Die CORA-Experimente, die in einer Out-of-pile Versuchsanlage des Kernforschungszentrums Karlsruhe (KfK) durchgeführt wurden, gehören zum Severe-Fuel-Damage-Programm, d. h. zum Programm zur Untersuchung schwerer Kernschäden in Leichtwasserreaktoren (LWR).

Mit Hilfe der CORA-Versuche sollen die Versagensmechanismen von LWR-Brennelementen im Temperaturbereich bis 2000 °C und in einigen Fällen bis 2400 °C ermittelt werden.

In diesen Versuchen wurden zwei unterschiedliche Typen von Brennstabbündeln getestet: DWR (Druckwasserreaktor)- und SWR (Siedewasserreaktor)-Bündel. Die SWR-Bündel bestanden aus 18 Brennstabsimulatoren (elektrisch beheizte und unbeheizte Stäbe), einem Absorberkasten aus Stahl mit elf Absorberstäben (B_4C) mit Stahlhülle. Das größere SWR-Bündel CORA-18 enthielt die gleiche Anzahl von Absorberstäben, war jedoch mit 48 Brennstabsimulatoren bestückt. Alle Testbündel waren von einem sog. Shroud (aus Zirkaloy) und ihre Absorberkästen zusätzlich von einer Zirkaloy-Kühlkanalwand auf jeder Seite umgeben. Die Bündel wurden Temperaturtransienten mit langsamer Aufheizrate und in Dampfatmosphäre ausgesetzt. Damit wurde ein Unfallablauf für einen LWR simuliert, der sich aus einem Kühlmittelverluststörfall durch Auftreten eines sogenannten kleinen Lecks entwickeln kann.

Die Aufheizraten für alle Versuche betrugen zu Transientenbeginn 1 K/s, bis die Temperatureskalation aufgrund der exothermen Zirkaloy (Zry)-Wasserdampfreaktion ab ca. 1100 °C einsetzte. Die Höchsttemperaturen betrugen 2000 °C.

In den Versuchen begann die Bündelzerstörung in der oberen Bündelhälfte mit dem Schmelzen des Absorberkastens bei etwa 1250 °C durch die Wechselwirkung zwischen Stahl (Absorberkasten und Absorberstabhülle) und Borkarbid. Nach der Zer-

störung der Kühlkanalwände begann die Absorberschmelze die Hüllrohre anzugreifen und mit den UO_2-Tabletten zu reagieren.

Die Versuchsbündel zeigten auch starke Oxidation der folgenden Zry-Komponenten: des Shrouds, der Hüllrohre und der mittleren und oberen Abstandshalter. Die Umverlagerung von Absorberschmelze in den unteren Teil des Bündels führte zur Bildung ausgedehnter Blockaden. Diese Umverteilung von Absorbermaterialien dürfte ferner bei einem derartigen Unfallablauf mit nachfolgendem Fluten des teilzerstörten Reaktorkerns mit unboriertem Wasser zu lokalen Rekritikalitäten führen.

Ein wesentlicher Unterschied im Verhalten des größeren Bündels CORA-18 im Vergleich zu den Bündeln regulärer Größe (CORA-16, CORA-17) konnte nicht festgestellt werden.

Das Abschrecken eines teilzerstörten SWR-typischen Bündels (CORA-17) ergab ein gleiches Verhalten, wie es in den DWR-typischen Experimenten beobachtet worden ist: Im Bündel kam es während des Flutvorgangs zu einer verstärkten Zirkaloy/Wasserdampf-Reaktion und damit zu einem erneuten Temperaturanstieg, einem zusätzlichen Abschmelzen von Bündelkomponenten und einer zusätzlichen, starken Wasserstofferzeugung.

1. Introduction

Safety studies have demonstrated that so-called small break loss-of-coolant accidents in Light-Water Reactors (LWR), in combination with failure of the required safety systems, can lead to overheating of the core and thus result in severe fuel damage (SFD) and fission product release.

In such an accident the nuclear fuel rods may be subjected to temperatures beyond the present design basis accident limit of 1200 °C. The temperature transient, however, will not necessarily escalate to an uncontrolled core meltdown accident, as was learned from the TMI accident in 1979.

The transient of a SFD-type accident is initiated by a slow temperature rise in the order of 0.5 - 1.0 K/s, followed by a rapid temperature escalation (several tens of degrees Kelvin per second) due to the exothermal heat produced by the Zry cladding oxidation in steam environment. Besides oxidation and embrittlement of the fuel rod cladding, local melting of the cladding and an interaction between molten zircaloy and uranium oxide pellets will occur, leading to destruction of fuel rod elements and other core structure far below the melting point of the fuel. The concern with melting of fuel rod materials in a SFD accident is relocation, solidification, and therefore the formation of coolant channel blockages.

To investigate the relevant damage mechanisms acting with increasing temperature on an uncovered core, and to develop models for estimating core damage initiation and propagation, research programs have been defined in various countries. In these programs in-pile and out-of-pile experiments are being performed under severe fuel damage conditions, i.e. temperature escalation to about 2000°C with termination of the transient before complete core meltdown.

At the Kernforschungszentrum Karlsruhe (KfK) a series of out-of-pile experiments on SFD research has been performed in the CORA facility. The entire experimental program is provided with Table 1 (CORA test matrix). As can be seen from this list, a total of 19 experiments was conducted. All of the CORA experiments were performed with UO_2 as pellet material and with absorber material (except for CORA-2 and -3). Two different absorber materials were used within different bundle configurations, i.e. (Ag,In,Cd) rods representing PWR (Pressurized Water Reactor) conditions /2, 3, 4/, whereas boron carbide refers to the experiments simulating BWR (Boiling Water Reactor) fuel elements. Pellets,

claddings, and grid spacers were typical for those of commercial LWRs with respect to their chemical compositions and dimensions.

This report describes the results of the first BWR-type experiments designated CORA-16, CORA-17, and CORA-18.

2. Test Description

2.1 Description of the Test Facility

A simplified flow diagram of the test facility is given in Figure 1 and a detailed description of the CORA facility in reference /1/. In the axial cross section of Figure 2 the main components of the CORA facility are shown schematically. The test bundle is surrounded by a high-temperature shield which is insulated by ZrO_2 and Al_2O_3/SiO_2 fiber ceramics (Figs. 3 and 4). The fiber ceramics are proven to be excellent insulators with a low heat capacity due to the low density of the material.

The high-temperature shield is located within the pressure tube. Through a number of holes in the shield, the test bundle is being inspected during the test by several video and still cameras. The holes are also used for temperature measurements by two-color pyrometers complementing the thermocouple readings at elevated temperatures.

Steam generator and steam superheater are placed inside the CORA containment. Using the total electric power of the steam generator, a maximum steam temperature of more than 800°C can be reached. The maximum steam flow rate amounts to 33 g/s.

Two different condensers are installed in the CORA facility: A vent condenser and a surge condenser. Under normal operating conditions the steam which is not consumed by oxidation of the bundle, is condensed in two vent condenser units. The surge condenser is physically separated from the high pressure system by four rupture disks. In case of emergency, e.g. due to an extremely high evaporation rate caused by quenching of the bundle, the void volume of the surge condenser serves as a pressure suppression system.

The condensate from the vent condensers and - in the case of emergency - the excess spray water of the surge condenser are collected in the condensate tank.

After each test the amount of water in the condensate tank is determined to perform a water mass balance.

To avoid any hazard of hydrogen formed during the zircaloy oxidation, the non-condensable gases are expanded and diluted in a mixing chamber (see Fig. 1). In particular the hydrogen is diluted to a concentration below explosion limits by adding compressed air to the gas.

The test facility has a quench capability which is activated by raising a water-filled quench cylinder into the test section at a controlled speed. After the test the high-temperature shield can be lowered into the quench unit without moving the bundle. So, the tested bundle can be inspected and photographed posttest in its original condition that existed at the termination of the transient.

2.2 Test Bundle Design

The philosophy of simulating the BWR-type configuration in the CORA test section is rendered in Fig. 5. In this figure the observation windows in the insulation of the CORA bundle can be seen. Test bundles CORA-16 and CORA-17 consisted of 18 fuel rod simulators, test bundle CORA-18 was built of 48 rods. The test rods were arranged within the large bundle as shown in the schematic cross section of Fig. 7. The rod designation of test bundles CORA-16 and CORA-17 can be taken from Fig. 6. Twelve of the 18 fuel rods and 28 of the 48 rods, respectively, were electrically heated by using tungsten pins as heater elements. The heated rods (fuel rod simulators) were filled with annular UO_2 pellets whereas the unheated rods contained full UO_2 pellets of the same outer diameter.

The design of the heated and unheated types of rods corresponds to that used in the PWR-type test bundles /2/, /3/, /4/ and is given with Fig. 8.

So, the cladding of the test rods is of Zircaloy-4 as is the case in the PWR-type test bundles. The rods are surrounded by a shroud made of Zircaloy-4. The shroud itself is insulated with a 20 mm-thick layer of ZrO_2 fiber material to guarantee a uniform radial temperature distribution.

Three grid spacers of approximately 40 mm length were mounted below the heated region, in its center, and in the upper zone. The three grid spacers were made of Zircaloy-4. Details on the location of the spacers and the fuel rod simulator design characteristics are given in Tables 2 and 3.

The test train instrumentation comprised thermocouples and two-color pyrometers for the various temperature measurements. The test section was instrumented with thermocouples (W/Re and NiCr/Ni type thermoelements) to measure steam temperature, rod cladding temperature, shroud temperature, absorber blade and channel box wall temperatures. The high-temperature thermocouples were made of W5Re/W26Re wires, insulated with HfO_2 and sheathed in tantalum or in Ta/Zry duplex tubing. The positions of the different types of thermocouples for the three test bundles are given in Tables 4 through 6 and in Figs. 9a and 9b.

Ten videoscopes (CORA-16) and six videoscopes (CORA-17 and CORA-18), respectively, were used in the tests to observe the materials behavior and the relocation of material during transient testing. The positions of the videoscopes can be taken from Figs. 10a and 10b. A schematic of the videoscope system with video camera and 35-mm still camera is given with Fig. 11.

The operational data, e.g. voltage, current, electric power, pressure, and temperatures were recorded by a data acquisition system as were the temperatures of the test section.

The hydrogen produced during the test by the steam/Zr reaction is usually measured at two different positions, i.e. above the test section and in the mixing chamber (see Fig. 1).

A schematic of the probes, gas lines, and gas analysis system is provided with Fig. 12. To dilute the gas taken at the location above the test section a dilution chamber with flow meters is installed. The off-gas mixture which contains hydrogen among other gases is being transported to the spectrometer via capillary tubes. It is analyzed by two quadrupole mass spectrometers of the type Leybold PQ 100. The ion currents representing the concentrations of the respective gases are determined. From these data the mass production rate of hydrogen as well as of the other gases is calculated with the ratio of the partial pressure of the particular gas and that one of argon (carrier gas) and multiplied by the argon flow rate through the test bundle.

3. Test Conduct and Results

In the CORA experiments the test sequence can be distinguished in the following phases:

- Pre-heating 0000 - 3000 s (argon only)
- Heat-up 3000 - 3900 s (argon + steam)
- Escalation 3900 - 4900 s (argon + steam)
- Cool-down > 4900 s (argon only).

During the preheating phase argon of about 500 °C entered the test bundle with a flow rate of 5 - 8 g/s that was kept constant during the transient phase. System pressure, steam flow, and electric power input are given in Fig. 13 for test CORA-16, in Fig. 14 for test CORA-17, and in Fig. 15 for test CORA-18. Except for test CORA-17, termination the test conduct was the same for the three tests:

- Argon flow 8 g/s (CORA-16 und -17), 16 g/s (CORA-18)
- Steam flow 2 g/s between 3300 and 4800 s (CORA-16 und -17), 4 g/s between 3300 and 4080 s (CORA-18)
- Electric power input between 3000 and 4800 s (CORA-16 und -17) and between 3000 and 4145 s (CORA-18)
- Initiation of quenching (CORA-17) at 5000 s.

Between 3000 s and 4500 s within the transients of CORA-16 and CORA-17 the electric power was increased from 6 kW to about 22 kW. In test CORA-18 the power was run from 12 kW to about 38 kW between 3000 and 4145 s. In both cases the power ramp rate (linear function of time) was chosen to achieve the initial heatup rate of 1 K/s. At 3300 s within the test a constant flow of superheated steam was established in addition to the argon flow. In the escalation phase, i.e. starting from about 1100 °C, the slow temperature rise was followed by a rapid increase caused by the energy from the exothermal zirconium - steam reaction which becomes significant at the temperature mentioned and - in addition - the electric power input. The contribution of the exothermal heat to the total energy, i.e. electrical and chemical power, is generally between 30 and 50 %. For CORA-16, CORA-17, and CORA-18 the chemical reaction contributes to 48, 44, and 33 %, respectively.

The tests CORA-16 and CORA-18 were terminated by power reduction (slow cooldown) whereas CORA-17 was terminated by power reduction and quenching with water (fast cooldown). In both cases the steam supply is turned off with the shutoff of the electric power.

The response of the bundle temperatures during the CORA transients at different elevations is provided with Figs. 16 through 20. The maximum temperature reached in the CORA tests amounts to about 2000 °C, except for test CORA-18 where the turnaround occurred at about 1900 °C (see Table 7) due to the shutoff of the steam supply at 4080 s.

The temperatures of absorber blade and channel box walls show basically the same behavior as the unheated or heated rods as is demonstrated with Figs. 17 and 19.

The conduct of tests CORA-16, CORA-17, and CORA-18 resulted in a behavior typical for BWR-type CORA experiments: The flame front, i.e. the temperature escalation developed first above the axial centerline and then moved to the upper and lower part of the bundle. The damage process started in the upper bundle region with melting of the absorber blade by interaction of boron carbide and steel at about 1200 °C. The resulting melt attacked the zircaloy channel box walls by the steel - zirconium interaction. After destruction of the walls the melt was able to penetrate the coolant channels starting the interaction with the rod claddings. The so liquefied zircaloy interacted with the UO_2 fuel pellets.

The early melt or the absorber - steel reaction seemed to have a similar viscosity as water so that it could easily exit at the observation windows as was observed during the tests and can be imagined by the postest view in Fig. 21.

The quenching of the test bundle CORA-17 had an impact on temperature behavior and hydrogen release. Before the quench process temperatures of CORA-17 were similar to those of test CORA-16. During the quench phase, however, a strong temperature increase was registered prior to the final cooldown (Fig. 19). In Fig. 22 the hydrogen production versus time is plotted for comparison for tests CORA-16 and CORA-17. At the upper part of the bundle the temperatures of bundle CORA-17 showed a temporary increase which coincided with the additional peak in the hydrogen production. This peak is due to an extremely strong reaction between saturated steam of the quench water and the zirconium that was not yet completely consumed during the first part of the transient /5, 6/. It is a remarkable amount of hydrogen (79 %) that was generated

during the flooding phase. The amount of hydrogen produced during test CORA-18 is given in Fig. 23.

Based on the accumulated H_2 productions of 167 g, 150 g, and 106 g the oxidation energies were determined to be 25.4 MJ, 22.8 MJ, and 16.1 MJ, respectively for the three experiments. Also on the basis of the total H_2 production the percentages of zirconium oxidized was calculated to be 47 %, 43 %, and 15 % (referred to a bundle length that had experienced the temperature escalation and a total mass of zircaloy that includes cladding, channel box walls, and shroud). These percentages represent integral values and do not reflect local differences in oxidation.

The fractions of steam consumed during the transient (heatup) phases, i. e. prior to quenching in test CORA-17, were calculated to be 76 %, 14 %, and 60 %, for CORA-16, CORA-17, and CORA-18, respectively. These, too, are integral (average) values that are based on flow rate and a time at temperature above 1400 °C.

4. Posttest Appearance of the Bundles

Overall views of the test bundles CORA-16, CORA-17, and CORA-18 at different orientations are given in Figs. 24, 25, 31,and 35.

Fig. 24 shows the entire bundle CORA-16 before and after the test and with and without shroud insulation. Fig. 25 gives the posttest appearance of bundle CORA-16 after removal of the high-temperature insulation but before taking off the shroud itself. The interaction between shroud and its insulation is to be seen as well as the deformation and cracking of the shroud. In the upper bundle region (Fig. 26) the absorber blade had molten away with the consequence of a clear change in the distribution of absorber material. The more detailed views of this bundle (Figs. 26 through 29) show the typical patterns as oxidized shroud, grid spacer and rod claddings, cladding - fuel reaction, and absorber - steel melt. This melt which had flown out of the observation windows at 100 mm and 300 mm elevation can be seen in Fig. 30.

Appearances of the bundles CORA-17 (Figs. 31 - 34) and CORA-18 (Figs. 35 - 40) are similar. The quench phase of CORA-17, however, had led to a significant amount of rubble, distributed over the bundle but at the bottom, i.e. in the water of the quench tube (Fig. 34).

The following description of the posttest appearances of the individual test bundles was made possible with help of cross sections. The sections were obtained as follows.

After visual inspection, photographic documentation, and collecting of fragments (see Tables 8 through 11) the test bundles were encapsulated in epoxy resin and sectioned according to the lists in Tables 12 through 14. The locations of the sections are illustrated in figures of the Appendix together with schematics of additional cuts.

For encapsulation of the bundle the epoxy system Rütapox 0273 with the hardener designated LC (Epoxy resin and hardener manufactured by Bakelite GmbH, D-5860 Iserlohn 7) was chosen. For this a mold of plastic ("plexiglas") was set up around the bundle. Then the bundle was filled from the bottom, through the steam inlet line, to avoid air entrainment in the encapsulant (see Fig. 41). The mould was filled to an elevation above the top of the shroud. The epoxy showed some heating during the curing stage but the shrinkage effect was negligible. After epoxying the bundle the resin was allowed to harden for one week.

A saw with a 2.3 mm-thick diamond blade (mean diamond size 138 µm) of 500 mm OD was used to do the cutting of the slab at 3200 rpm. The thickness of a slice from the epoxied bundle resulted in 13 mm corresponding to the distance of the marks of 15 mm (see lists of cross sections).

As the horizontal and vertical cross sections of bundle CORA-16 (Figs. 42 through 47) demonstrate, absorber blade and channel box walls had failed between the 100-mm and 1100-mm elevation. Cross sections below and above this region exhibit intact steel blades with the boron carbide absorber gone. The zircaloy grid spacers remained in their positions but were oxidized. Molten material had mainly solidified at around 100 mm. On the basis of these pictures, temperature measurements, and video camera observations the damage process went as follows. Melting of material started at about 1200 °C in the upper bundle region by interaction between boron carbide and steel of the absorber blade. By contacting the zircaloy channel box walls this melt dissolved the zirconium and spread in the bundle. The so generated zirconium-rich melt then started to dissolve the UO_2 pellets.

The damage process described is the same for CORA-17 (see also Fig. 48) and CORA-18 (Figs. 49 - 56). Absorber blade and channel box walls were destroyed in the same region as in CORA-16, with the major blockages between 100 mm and 200 mm in bundle CORA-17 and between 120 and 200 mm in bundle CORA-18. No

essential difference between the smaller and larger bundle was found, even that the absorber blade was eccentrically positioned (at the 300 ° side) in bundle CORA-18. No preference for melt relocation at the voided side or at the region of the absorber blade was detected.

5. Material Distribution

Axial profiles of the cross-sectional areas (end state) of the bundles CORA-16 and CORA-17 were evaluated. The result of bundle CORA-16 is presented with Fig. 57 and that of test CORA-17 is presented with Fig. 58, both figures taken from reference /9/. The data of the volume profile in Fig. 57 were obtained by using the epoxying process. As can be seen in Fig. 41 the epoxy resin is filled into the mould from the bottom end. By wheighing the resin left in the supply container after each step, i.e. when the resin level has raised in the bundle by 1 cm, the difference of mass allows the calculation of the void volume of the bundle as a function of axial height.

The blocked areas of CORA-16 and CORA-17 at 100 mm and 150 mm (maximum), respectively, can be seen in Figs. 57 and 58.

6. Destructive Post-test Examinations of Melt Generated During the Early Phase of the Transient (CORA-16)

When the BWR-bundle CORA-16 was heated to a maximum temperature of 2000°C, liquid reaction products have formed as early as from 1200°C on, due to the chemical interactions of the bundle components, some of them occurring even well below the melting point of the components. Liquefaction of the bundle components, beginning at 1200°C, could be visualised by means of the ten video-cameras installed, simultaneously to the temperature measurements, and characterised with a view to temperature. The melts formed are radially and axially relocated in the bundle and give rise to local blockages as they cool down. Some of these melts escaped from the view ports in the lower zone of the bundle and solidify. This process is visible from Fig. 30 which shows the melts from the initial phase of the test which had been solidified outside the bundle. The metallographic and chemical-analytical investigations of these materials provide first information on the chemical interactions taking place in the bundle which are characteristic of incipient damage and early damage propagation.

Figure 59 shows a solidified nose of melt extracted from the view port in the bundle at 200 mm elevation. Transverse micro-sections from two points were subjected to detailed chemical analysis. The macroscopic representations of the transverse micro-sections 1-1 and 2-2 make evident two facts. Most of the relocated material are metals with different microstructures. The interfaces within the solidified melt are an indication of melts of different chemical compositions which were relocated at different times and had solidified at that point. The microstructures of the zones investigated make visible greatly differing phase formations (Figure 60). Position 1 shows the formation of an approximately 20 µm thick oxide layer on the surface of the melt; this is already an indication of the high Zr-content of the melt. Detailed chemical analyses of the phases formed during solidification at one position are represented in Fig. 61. The table in the figure shows the chemical composition of the seven phases observed in total; two of them are oxide phases, the rest are metal phases. Despite the occurrence of the two oxide phases, the metal phase portion dominates in quantitative terms. The fact that in one phase (no. 7) also uranium was detected is an indication of precocious failure of the Zircaloy flow channel walls and of the neighbouring fuel element cladding tubes, followed by the dissolution through the B_4C/steel melt of UO_2 at temperatures below the melting point of Zircaloy (approx. 1760°C). The flow channel walls and the cladding material of the fuel element fail as a result of eutectic interactions with the B-

and C-containing steel melt. The B_4C absorber material enters into a reaction with its steel cladding, beginning at approximately 1000°C, and liquefies the cladding very quickly above 1200°C. It appears from the integral analysis (Fig. 61) that the dominating portion of the melt consists of zirconium metal.

Diagrams of the distribution of elements of some of the phases formed are shown in Fig. 62 and 63. Depending on the chemical composition of the solidified melt, (Fe, Cr)-borides or Zr-borides are formed which do not contain carbon. Also Zr-carbides were detected at some points. Generally, carbon has been dissolved relatively homogeneously in the multi-phase metal matrix, which consists primarily of Zr and Fe. Similar phase formations were observed also in the other relocated melts, which likewise escaped from the bundle.

7. Metallographic Examinations of Selected Cross Sections

For the analysis of cross sections and longitudinal sections the selected samples were infiltrated by "Araldit" resin to close up residual pores then ground and polished.

The procedure of the preparation for the metallographic examination is given with Table 15. The steps described in the list were performed using a semi-automatic machine with a closed water circuit for grinding and an automatic lubricant feeder for the polishing steps. The cross sections that were selected for polishing can be taken from Table 16.

7.1 Posttest Examination of Bundle CORA-16

The BWR fuel element before and after the test has been represented in Fig. 24. The external steam pipe and the ZrO_2-insulation with the view ports provided at different axial levels can be recognised (figures on the left-hand side). The insulation has survived the high-temperature transient in a relatively good condition, whereas the steam pipe degraded heavily (figures on the right-hand side). A detail of the bundle recorded at the elevation 800-1050 mm makes visible in addition several relocated melts (Fig. 26). Moreover, it can be recognised that the absorber material has been completely removed from that zone by melting; one can look through the absorber channel. This finding is evident even more clearly from the transverse micro-sections of the destroyed bundle CORA-16 (Fig. 64). They also make evident the extent of chemical interactions as a function

of the bundle elevation. The transverse micro-section of CORA 16-08 shows the nearly undisturbed fuel element cross-section. The transverse micro-section CORA 16-07 is free from absorber material and the flow channel walls have almost completely disappeared. Some of the Zircaloy cladding material has molten and chemically dissolved some of the UO_2 fuel. The melts formed in the upper part of the bundle are relocated towards the bottom part of the bundle where they develop blockages of different radial and axial extensions. On account of their heat content, the melts consisting mainly of metals are capable of destroying also in the colder zones of the bundle the cladding tubes and the B_4C-containing absorber rods (Fig. 64; transverse micro-section CORA 16-01).

The various axial transverse micro-sections of the CORA-16 bundle to which different temperatures can be attributed reflect the material behaviour as a function of the temperature. The CORA 16-08 transverse micro-section (Fig. 65), prepared from a section outside the heated bundle zone, clearly shows the onset of the chemical interactions of B_4C and stainless steel (type AISI 316) at temperatures ranging from 1100 to 1200°C. B_4C reacts with stainless steel eutectically while forming liquid phases. The boride phase is clearly visible as a border around the B_4C-particles. The B_4C-particles are dissolved chemically by it.

The lowest bundle cross-section investigated, CORA 16-01 (Figs. 66 and 67), exhibits the advanced destruction of the absorber rods due to relocated metal (Zr, U, O) melts. A large portion of the B_4C particles were already dissolved chemically while releasing free carbon (position 2). Boron is present dissolved in the steel matrix. Various phases are formed in addition whose chemical compositions have been entered in Fig 68. Scanning electron microscopic examinations performed at other points of the solidified melts show in addition that discrete phases have been formed (Fig. 69).

At the higher temperatures occurring in the top part of the bundle, some of the B_4C is completely dissolved chemically (Fig. 70). During solidification of the B_4C/steel melt various phases are formed (positions 1 and 3). The B_4C/steel melt reacts with the Zircaloy cladding material and dissolves it chemically. The resulting Zr-containing melt is capable of liquefying UO_2 fuel about 1000 K below its melting point (position 2). Above all the UO_2 solid pellets exhibit signs of considerable dissolution. The still existing Zircaloy steam pipe has completely oxidised - like the Zircaloy spacer - which appears from the transverse micro-section CORA 16-09.

It should be added that the chemical composition of the various phases, together with the phase diagrams available, provide important indications of the degree of chemical interactions and of the reaction temperatures. The determination of critical temperatures beyond which the reaction products are liquid and thus easily amenable to relocation, is of particular importance. B_4C, melting point approximately 2350°C, can be liquefied from approximately 1250°C on due to chemical interactions with the Fe, Cr and Ni steel components /7/. This process was observed with video-cameras during the heating phase of the BWR bundle CORA 16. The subsequent relocation of the B_4C-containing melt produces relatively large axial sections of bundles containing no more B_4C absorber material. Under realistic accident conditions flooding of the overheated, partly destroyed reactor core with boron-free water might give rise to criticality problems.

Results of the element analyses with the scanning electron microscope are provided in reference /8/.

7.2 Posttest Examination of Bundle CORA-17

The post-test examination of the bundle was intended to confirm the relation to oxidation of the remaining metal structures.

In all parts of the bundle upper half destruction of the fuel rods has progressed to a considerable extent and only negligible residues of material can still be detected. In case of advanced cladding tube oxidation and embrittlement, fuel rod damage is caused by mechanical failure and even intensified by thermal shock ahead of the quenching front. Likewise in this experiment, a conspicuously large number of fuel rod fragments were formed which consisted of the pellet and the partly oxidised cladding attached to it (Fig. 71). Also the melts rich in zirconium which accumulated on the external side of the shroud (Fig. 72) and in the interior of the bundle were surprising. It often appears that these melts have been dislocated repeatedly (empty oxide hulls) and are highly porous and, as a consequence of both phenomena, exhibit large specific surfaces only partly oxidised (Fig. 73). Such structures might not only have been produced by melting (and possibly foaming) preceding the quenching process, but also have contributed through violent oxidation to raise the temperature and to release hydrogen.

The post-test examination of the lower half of the bundle concentrated on the formation and relocation of melts starting from the absorber assembly. In agreement with results obtained earlier for the CORA-16 bundle, B_4C in contact with CrNi-steel reacts first while forming a melt rich in absorber material (Fig. 74). In the external zone of the original absorber blade the boron and carbon contents of the melt might be much lower (Fig. 75). This melt, in contact with the Zircaloy of the channel box wall, is capable of dissolving this wall and of reacting similarly with the cladding tube material. Finally, the melt formed in this way which is rich in zirconium might already initiate the dissolution of UO_2-fuel (Fig. 76). However, it has been observed that only a minor portion of the absorber melt penetrates into the bundle via the adjacent row of fuel rods, whereas the major portion is relocated downwards and remains in the mid-plane of the channel box, respectively, as porous, partly oxidised residual structures.

Figure 77 shows - in a longitudinal section running transverse to the absorber - an example of distribution of the various melts and of the fragment relocations in the zone of the bundle blockage. It will be a task of further detailed post-test examinations and analyses to determine the range of variations in the compositions of the melts and to reconstruct the sequence of damage events on the bundle.

7.3 Posttest Examination of Bundle CORA-18

As had been expected from the test conditions chosen, a state of moderate damage of the fuel rods has been detected in the post-test examinations. A transverse micro-section of the upper part of the bundle (Fig. 78) shows the residues of the channel box walls as well as solidified material of the fully destroyed and largely molten absorber. Further down in the bundle a zone follows within which not only the absorber structure, but also the channel box walls have been completely destroyed and vanished, with the exception of small residues of solidified reaction products. At the fuel rods oxidation-induced damage (deformation and rupture of the cladding tubes) as well as incipient cladding tube/fuel reaction and cladding tube melting are visible.

In the neighbourhood of the medium spacer (Fig. 79) which has been completely converted into ZrO_2 and disintegrated into many fragments, the heaviest destructions occurred at the fuel rods. Whereas only fragments and deformed residues are left of the cladding tubes, solidified reaction products of the

dissolved fuel as well as pellet fragments are present at some locations. A small portion of all the absorber melt formed has solidified, most of it attached to the channel box and the neighbouring fuel rods. A longitudinal section through the channel made evident the widespread propagation, the high porosity, and the heterogeneity of this material and allowed the melt, rich in absorber material, to be distinguished, with B_4C-residues of diluted melt and high fractions of steel constituents.

Figure 80 is an illustration of the bottom part of the bundle where most of the fuel rods are still intact, some of them, however, embedded in the melts consisting of cladding tube ((Zr, O) and fuel rod and (Zr, U, O) melts), respectively. The channel box accommodates the absorber blade, broken down into single rods, fallen down fragments, and (Zr,O) and (Zr,U,O) melts, respectively. The longitudinal micro-section (Fig. 81) of the channel box in the next downward bundle section exhibits complete blockage consisting of metal melt. In the lowest, first relocated zone, where more porosity can be observed, this blockage is probably attributable to melt-down of the absorber whereas melt in the the central and top zones accumulated during melt-down of the fuel rods.

8. Summary of the Major Results

Results from tests with BWR absorber material can be summarized in the following way:

The destructive post-test examinations of the bundle showed strong chemical interactions over the whole bundle length.

The presence of B_4C absorber material causes the formation of a "low-temperature" melt at around 1250 °C that attacks the zircaloy channel box and the zircaloy fuel rod cladding. The liquefaction is due to an interaction between B_4C and steel (of the absorber rod cladding and the absorber blade). The distribution of the absorber-rich melts also leads to dissolution of the UO_2 fuel at the temperature indicated. The liquefied B_4C/ss absorber blade relocates completely from the upper half of the CORA test bundle, i.e. the absorber material is missing in the upper regions of fuel elements whereas it is concentrated at the bottom. This fact may cause recriticality problems with the injection of unborated emergency cooling water into a dried-out reactor core.

Oxidative embrittlement of the cladding tubes as well as the formation of (Zr,O) and (Zr,UO)-melts, respectively, take place while the temperature transient continues. While the oxidation was intensified once more during the process of quenching of the hot bundle CORA-17, fuel fragments and, locally, the formation and propagation of metal melts are observed to an increasing extent.

The large BWR-type bundle shows the same damage behavior as the bundles of regular size. Consequently, regarding the size of the bundle, the results of the CORA programme can be transferred to a fuel element. The asymmetric configuration of the absorber blade did not lead to a preferential relocation of melt.

9. References

/1/ S. Hagen, K. Hain, "Out-of-pile Bundle Experiments on Severe Fuel Damage (CORA-Program): Objectives, Test Matrix, and Facility Description", KfK 3677, 1986

/2/ S. Hagen, P. Hofmann, G. Schanz, L. Sepold, "Interactions in Zry/UO_2 Fuel Rod Bundles with Inconel Spacers at Temperatures above 1200°C; (Posttest Results of Severe Fuel Damage Experiments CORA-2 and CORA-3)", KfK 4378, 1990

/3/ S. Hagen, V. Noack, L. Sepold, P. Hofmann, G. Schanz, G. Schumacher, "Results of SFD Experiment CORA-13 (OECD International Standard Problem 31)", KfK 5054, 1993.

/4/ S. Hagen et al., "Behavior of Ag/In/Cd Absorber Material in Zry/UO_2 Fuel Rod Simulator Bundles at High Temperatures; (Posttest Results of Severe Fuel Damage Experiments CORA-5, CORA-12, CORA-15, CORA-9, CORA-7)", KfK 4419, to be published

/5/ S. Hagen, F. Seibert, L. Sepold, P. Hofmann, G. Schanz, G. Schumacher, "Influence of Reflood in the CORA Severe Fuel Damage Experiments", Heat Transfer and Fuel Behavior in Nuclear Reactor Accidents, 27th ASME/AIChE/ANS National Heat Transfer Conference, Minneapolis, 28-31 July 1991, AIChE Symposium Series 283, Vol. 87, ISBN-0-8169-0548-7, pp. 120-129.

/6/ S. Hagen, P. Hofmann, G. Schanz, G. Schumacher, F. Seibert, L. Sepold, "Effects of Quenching on LWR Fuel Rod Behavior Observed in the CORA Severe Fuel Damage Experiments", Proceedings ANS International Topical Meeting "Safety of Thermal Reactors", Portland, July 21-25, 1991, ISBN 0-89448-159-2, pp 85-91

/7/ W. Hering, P. Hofmann, "Material Interactions During Severe LWR Accidents; Summary of Separate-Effects Test Results", KfK 5125, 1994

/8/ J. Burbach, "Ergebnisse von REM/EDX-Mikrobereichsanalysen des Siedewasser-Bündelabschmelzexperiments CORA-16", (in German), KfK 5282, 1994

/9/ W. Hering, unpublished report, 1989

10. Acknowledgements

Various kinds of support for preparation, conduct, and evaluation of the experiment are gratefully acknowledged.

The fuel elements were designed by Mr. H. Junker. The test rods were assembled by Mr. E. Mackert, the test bundles by Messrs. H. Giesmann and R. Röder. The authors would like to thank Messrs. H. Benz, C. Grehl, W. Rötzel, and H.J. Röhling for test preparations and conduct.

Mr. K.P. Wallenfels is acknowledged for arrangement of camera and video systems and for the preparation of temperature measurements. Messrs. R. Huber, H. Malauschek, and Ms. I. Schub prepared and conducted the on-line measurements of the off-gas samples.

The authors would like to thank Mr. L. Anselment for sectioning of the epoxied bundle and for preparation of the metallographic samples, Mr. H. Metzger for investigation of the metallographic samples by optical microscope, and Mr. J. Burbach for the SEM investigations.

11. List of Tables

12. List of Figures

Appendix

Table 1: CORA Test Matrix

Test No.	Max. Cladding Tempera-tures	Absorber Material	Other Test Conditions	Date of Test
2	≈ 2000°C	-	UO_2 refer., inconel spacer	Aug. 6, 1987
3	≈ 2400°C	-	UO_2 refer., high temperature	Dec. 3, 1987
5	≈ 2000°C	Ag, In, Cd	PWR-absorber	Febr. 26, 1988
12	≈ 2000°C	Ag, In, Cd	quenching	June 9, 1988
16	≈ 2000°C	B_4C	BWR-absorber	Nov. 24, 1988
15	≈ 2000°C	Ag, In, Cd	rods with internal pressure	March 2, 1989
17	≈ 2000°C	B_4C	quenching	June 29, 1989
9	≈ 2000°C	Ag, In, Cd	10 bar system pressure	Nov. 9, 1989
7	< 2000°C	Ag, In ,Cd	57-rod bundle, slow cooling	Febr. 22, 1990
18	< 2000°C	B_4C	59-rod bundle, slow cooling	June 21, 1990
13	≈ 2200°C	Ag, In, Cd	OECD/ISP; quench initiation at higher temperature	Nov. 15, 1990
29*	≈ 2000°C	Ag, In, Cd	pre-oxidized,	April 11, 1991
31*	≈ 2000°C	B_4C	slow initial heat-up (≈ 0.3 K/s)	July 25, 1991
30*	≈ 2000°C	Ag, In, Cd	slow initial heat-up (≈ 0.2 K/s)	Oct. 30, 1991
28*	≈ 2000°C	B_4C	pre-oxidized	Febr. 25, 1992
10	≈ 2000°C	Ag, In, Cd	cold lower end 2 g/s steam flow rate	July 16, 1992
33	≈ 2000°C	B_4C	dry core conditions, no extra steam input	Oct. 1, 1992
W1	≈ 2000°C	-	VVER-test	Febr. 18, 1993
W2	≈ 2000°C	B_4C	VVER-test with absorber	April 21, 1993

Table 2 Design characteristics of test bundles CORA-16 and CORA-17

Bundle type:			BWR
Bundle size:			29 rods
Number of heated rods:			12
Number of unheated rods:			6
Pitch:			14.3 mm
Rod outside diameter:			10.75 mm
Cladding material:			Zircaloy-4
Cladding thickness:			0.725 mm
Rod length			2175 mm
Heated length:			1000 mm
Heater material:			Tungsten (W)
Heater diameter:			6 mm
Fuel pellets (UO_2)			
	- heated rods:		annular pellets
	- unheated rods:		full pellets
Pellet stack length	- heated rods:		0 to 1000 mm
	- unheated rods:		-200 to 1300 mm
U-235 enrichment			0.2 %
Pellet outer diameter (nominal)			9.1 mm
Grid spacer	- material:		Zircaloy-4
	- length:		42 mm
	- location	lower:	- 33 mm
		center:	+ 578 mm
		top:	+ 1167 mm
Shroud	- material:		Zircaloy-4
	- wall thickness:		1.2 mm
	- outside dimensions:		86 x 112 mm
	- elevation:		40 mm - 1235 mm
	- insulation material:		ZrO_2 fiber
	- insulation thickness:		20 mm
Absorber rod	- number of rods:		11
	- material:		B_4C powder
	- cladding:		Steel 1.4919
	- cladding OD:		5.77 mm
	- cladding ID:		4.57 mm
	- length inside:		1578 mm
	outside:		1600 mm
Absorber blade			
	- material:		Steel 1.4919
	- dimensions inside:		66 x 6 mm
	- wall thickness:		1 mm

Note: Elevations are referred to the bottom of the heated zone (0 mm = EL 5121). The values for the grid spacers refer to the top end.

Table 3 Design characteristics of test bundles CORA-18

Bundle type:			BWR
Bundle size:			59 rods
Number of heated rods:			28
Number of unheated rods:			20
Pitch:			14.3 mm
Rod outside diameter:			10.75 mm
Cladding material:			Zircaloy-4
Cladding thickness:			0.725 mm
Rod length	- heated rods:		1840 mm
	(elevation		-369 to 1471 mm)
	- unheated rods:		1672 mm
	(elevation		-201 to 1471 mm)
Heated length:			1000 mm
Heater material:			Tungsten (W)
Heater diameter:			6 mm
Fuel pellets	- heated rods:		UO_2 annular pellets
	- unheated rods:		UO_2 full pellets
Pellet stack	- heated rods:		0 to 1000 mm
	- unheated rods:		-200 to 1300 mm
U-235 enrichment			0.2 %
Pellet outer diameter (nominal)			9.1 mm
Grid spacer	- material:		Zircaloy-4
	- length:		42 mm
	- location	lower	- 33 mm
		center	+ 578 mm
		top	+ 1167 mm
Shroud	- material		Zircaloy-4
	- wall thickness		1.2 mm
	- outside dimensions		138 x 135 mm
	- elevation		40 mm - 1235 mm
	- insulation material		ZrO_2 fiber
	- insulation thickness		20 mm
Absorber rod	- number of rods		11
	- material		B_4C powder
	- cladding		Stainless steel
	- cladding OD		5.77 mm
	- cladding ID		4.57 mm
	- length inside		1578 mm
	outside		1600 mm
Absorber blade			
	- material		Stainless steel
	- dimensions inside		66 x 6 mm
	- wall thickness		1 mm

Note: Elevations are referred to the bottom of the heated zone (0 mm = EL 5121). The values for the grid spacers refer to the top end.

Table 4 Positions of thermocouples (CORA-16)

Positions of thermocouples in unheated rods (CORA-16)			
Slot number	Elevation [mm]	Rod number	Type of TC
2	950	2.4	WRe *
1	750	4.2	WRe *
5	550	2.4	WRe *
6	550	2.6	WRe *
9	550	6.2	WRe*
8	350	4.6	WRe *
7	150	4.2	WRe *
10	50	6.4	WRe *

Positions of thermocouples at heated rods (CORA-16)			
Slot number	Elevation [mm]	Rod number	Type of TC
3	950	5.3	WRe *
4	750	3.5	WRe *
11	550	5.3	WRe *
14	550	1.7	WRe *
12	350	3.5	WRe *
13	150	5.3	WRe *

Positions of thermocouples located inside the absorber blade (CORA-16)			
Slot number	Elevation [mm]	Orientation of TE	Type of TC
52	1330	30°	WRe **
53	1150	30°	WRe**
46	950	30°	WRe **
47	800	30°	WRe **
48	550	30°	WRe **
49	450	30°	WRe**
50	350	30°	WRe **
51	250	30°	WRe **
44	150	30°	WRe **
45	50	30°	WRe **
60	50	30°	NiCrNi
61	-50	30°	NiCrNi
57	-150	210°	NiCrNi

Positions of thermocouples at the channel box wall (CORA-16)			
Slot number	Elevation [mm]	Orientation of TE	Type of TC
15	1150	210°	WRe *
16	950	210°	WRe *
17	750	210°	WRe *
18	550	210°	WRe *

Positions of thermocouples at the channel box wall (CORA-16)			
Slot number	Elevation [mm]	Orientation of TE	Type of TC
43	550	210°	WRe*
40	350	210	WRe *
41	150	210	WRe *
42	50	210	WRe *
75	50	210	NiCrNi

Positions of thermocouples at the shroud insulation (CORA-16).			
Slot number	Elevation [mm]	Orientation of TE	Type of TC
54	950	255°	NiCrNi
55	750	255°	NiCrNi
74	550	255°	NiCrNi
59	350	255°	NiCrNi
56	150	255°	NiCrNi

Positions of thermocouples at the grid spacer (CORA-16)			
Slot number	Elevation [mm]	Orientation of TE	Type of TC
24	568	210°	NiCrNi
27	568	210°	NiCrNi
26	-43	210°	NiCrNi
62	-43	210°	NiCrNi

Positions of thermocouples for gas temp. and at steam distribution tube (CORA-16)			
Slot number	Elevation [mm]	Orientation of TE	Type of TC
76	1450	90°	NiCrNi
72	1245	120°	NiCrNi
58	30	120°	NiCrNi
19	0	180°	NiCrNi
20	0	180°	NiCrNi

*) WRe wires,duplex sheath (Ta/Zr)

**) WRe wires,Ta sheath

Table 5 Positions of thermocouples (CORA-17)

Positions of thermocouples in unheated rods (CORA-17)			
Slot number	Elevation [mm]	Rod number	Type of TC
2	950	2.4	WRe *
1	750	4.2	WRe *
5	550	2.4	WRe *
6	550	2.6	WRe *
8	350	4.6	WRe*
7	150	4.2	WRe *
10	50	6.4	WRe *

Positions of thermocouples at heated rods (CORA-17)			
Slot number	Elevation [mm]	Rod number	Type of TC
3	950	5.3	WRe *
4	750	3.5	WRe *
11	550	5.3	WRe *
12	350	3.5	WRe *
13	150	5.3	WRe *

Positions of thermocouples located inside the absorber blade (CORA-17)			
Slot number	Elevation [mm]	Orientation of TE	Type of TC
52	1350	300°	WRe **
46	950	120°	WRe**
47	800	300°	WRe **
48	550	300°	WRe **
50	350	300°	WRe **
51	250	120°	WRe**
44	150	120°	WRe **
45	50	120°	WRe **
54	50	300°	NiCrNi
55	-50	120°	NiCrNi
24	-150	300°	NiCrNi

Positions of thermocouples at the channel box wall (CORA-17)			
Slot number	Elevation [mm]	Orientation of TE	Type of TC
15	1150	300°	WRe *
16	950	300°	WRe *
17	750	120°	WRe *
18	550	300°	WRe *

Positions of thermocouples at the channel box wall (CORA-17)			
Slot number	Elevation [mm]	Orientation of TE	Type of TC
40	350	300°	WRe*
41	150	120°	WRe *
42	50	120°	WRe *
26	50	300°	NiCrNi

Positions of thermocouples at the shroud insulation (CORA-17).			
Slot number	Elevation [mm]	Orientation of TE	Type of TC
57	950	255°	NiCrNi
58	750	255°	NiCrNi
60	550	255°	NiCrNi
61	350	255°	NiCrNi
62	150	255°	NiCrNi

Positions of thermocouples for gas temp. and at steam distribution tube (CORA-17)			
Slot number	Elevation [mm]	Orientation of TE	Type of TC
76	1450	90°	NiCrNi
27	1245	120°	NiCrNi
56	1245	300°	NiCrNi
19	0	180°	NiCrNi
20	0	180°	NiCrNi
59	0	120°	NiCrNi

*) WRe wires,duplex sheath (Ta/Zr)

**) WRe wires,Ta sheath

Table 6a Positions of thermocouples (CORA-18)

Positions of thermocouples in unheated rods (CORA-18)			
Slot number	Elevation [mm]	Rod number	Type of TC
153	1450	4	NiCrNi
154	1450	0.4	NiCrNi
155	1250	0.2	NiCrNi
156	1250	6.8	NiCrNi
157	1250	8.4	NiCrNi
158	1250	0.8	NiCrNi
159	1250	0.6	NiCrNi
160	1250	4.8	NiCrNi
101	1150	2.4	WRe *
102	950	4.6	WRe *
103	750	8.6	WRe *
104	750	6.4	WRe *
105	750	4.2	WRe*
106	750	2	WRe *
107	750	6.2	WRe *
108	750	8	WRe *
109	750	2.6	WRe *
201	550	4.6	WRe *
202	350	2.4	WRe *
203	150	0.2	WRe *
231	50	8.6	NiCrNi
232	50	6.4	NiCrNi
233	50	4.2	NiCrNi
234	50	2	NiCrNi
204	50	6.8	NiCrNi
235	50	8.4	NiCrNi
236	50	4	NiCrNi
237	50	0.8	NiCrNi
238	50	0.4	NiCrNi

Positions of thermocouples at heated rods (CORA-18)			
Slot number	Elevation [mm]	Rod number	Type of TC
197	1468	T3	NiCrNi
110	950	1.3	WRe *
111	950	5.7	WRe *
112	750	3.1	WRe *
113	691	7.5	WRe *
205	550	1.3	WRe*
206	550	5.7	WRe *
207	350	3.1	WRe *
208	350	7.5	WRe *
209	150	3.5	WRe *
210	150	R7	WRe *

Positions of thermocouples located inside the absorber blade (CORA-18)			
Slot number	Elevation [mm]	Orientation of TE	Type of TC
114	1350	300°	WRe **
115	1150	300°	WRe**
116	950	300°	WRe **
117	750	300°	WRe **
211	550	300°	WRe **
212	450	300°	WRe**
213	350	300°	WRe **
214	250	300°	WRe **
215	150	300°	WRe **
216	50	300°	WRe **

Positions of thermocouples located outside the absorber blade (CORA-18)			
Slot number	Elevation [mm]	Orientation of TE	Type of TC
131	1150	300°	NiCrNi
134	1150	120°	NiCrNi
135	1050	120°	NiCrNi
132	950	300°	NiCrNi
136	950	120°	NiCrNi
137	850	120°	NiCrNi
133	750	300°	NiCrNi
138	750	120°	NiCrNi
139	650	120°	NiCrNi
239	550	300°	NiCrNi
244	550	120°	NiCrNi
245	450	120°	NiCrNi
241	350	300°	NiCrNi
246	350	120°	NiCrNi
247	250	120°	NiCrNi
242	150	300°	NiCrNi
248	150	120°	NiCrNi
243	50	300°	NiCrNi
249	50	120°	NiCrNi
250	-50	120°	NiCrNi

*) WRe wires,duplex sheath (Ta/Zr)

**) WRe wires,Ta sheath

Table 6b Positions of thermocouples (CORA-18), continued

Positions of thermocouples near by the bundle head (CORA-18)			
Slot number	Elevation [mm]	Orientation of TE	Type of TC
152	1937	180°	NiCrNi
148	1740	180°	NiCrNi
151	1734	180°	NiCrNi
150	1531	180°	NiCrNi
149	1511	180°	NiCrNi
198	1491	345°	NiCrNi
196	1450	90°	NiCrNi
195	1120	180°	NiCrNi

Positions of thermocouples at the channel box wall (CORA-18)			
Slot number	Elevation [mm]	Orientation of TE	Type of TC
124	1150	300°	WRe*
125	1150	120°	WRe *
126	950	300°	WRe *
127	950	120°	WRe *
128	750	300°	WRe*
129	750	120°	WRe*
217	550	300°	WRe *
218	550	120°	WRe *
219	350	300°	WRe *
220	350	120°	WRe*
221	150	300°	WRe *
222	150	120°	WRe *
223	50	300°	WRe *
224	50	120°	WRe*

Positions of thermocouples at the shroud (CORA-18).			
Slot number	Elevation [mm]	Orientation of TE	Type of TC
130	950	75°	WRe*
141	950	255°	WRe*
142	765	75°	WRe*
143	780	255°	WRe*
225	550	75°	WRe*
226	350	75°	WRe*
227	350	255°	WRe*
228	150	255°	WRe*
199	50	75°	NiCrNi

Positions of thermocouples at the shroud insulation (CORA-18)			
Slot number	Elevation [mm]	Orientation of TE	Type of TC
251	950	75°	NiCrNi
252	750	75°	NiCrNi
253	550	75°	NiCrNi
254	350	75°	NiCrNi
255	150	75°	NiCrNi
256	50	75°	NiCrNi

Positions of thermocouples between bundle and shroud (CORA-18)			
Slot number	Elevation [mm]	Orientation of TE	Type of TC
146	1350	165°	NiCrNi
147	1350	345°	NiCrNi
144	1250	165°	NiCrNi
145	1250	345°	NiCrNi

Positions of thermocouples btw. bundle and shroud in ceramic tube (CORA-18)			
Slot number	Elevation [mm]	Orientation of TE	Type of TC
118	965	345°	WRe*
122	920	120°	WRe*
119	840	165°	WRe*
121	820	75°	WRe*
120	710	255°	WRe*
123	710	120°	WRe*

Positions of thermocouples for gas temp. and at steam distribution tube (CORA-18)			
Slot number	Elevation [mm]	Orientation of TE	Type of TC
257	0	315°	NiCrNi
258	0	135°	NiCrNi
259	0	180°	NiCrNi
260	0	180°	NiCrNi
193	0	15°	NiCrNi
194	0	195°	NiCrNi

*) WRe wires,duplex sheath (Ta/Zr)

**) WRe wires,Ta sheath

Table 7 Maximum temperatures reached during test CORA-18

Elevation (mm)	Temperature (°C)
0	500
100	880
200	1315
300	1705
400	1825
500	1885
600	1905
700	1905
800	1880
900	1780
1000	1575
1100	1280
1200	965
1300	660
1400	405

Table 8 Fragments taken from bundle CORA-16 for chemical analysis

Sample No.	Elevation (mm)	Orientation (degrees)	Remarks
16-101	-	300	Melt lump of absorber material (gray) solidified below the heated zone
16-102	100	300	Lowest part of melt (black, silver rupture surface) that had run out of window H 23
16-103	200	120	Thick black, glossy, melt taken at window H 25
16-104	70	120	Black (very hard and heavy) and gray melt lumps solidified at the elevation of the steam inlet pipe
16-105	-100	90	Gray thin melt solidified at the steam inlet pipe
16-106	280	75	Piece of shroud black at both sides taken from the outer shell

Note: First fragments (16-101 through 16-105) were taken prior to the removal of the shroud insulation; sample 16-106 was taken after the removal of the insulation.

Table 9 Fragments taken from bundle CORA-17 for chemical analysis

Sample No.	Elevation (mm)	Orientation (degrees)	Remarks
17-101	-	-	Melt lump of edged shape (black, hard) solidified below the heated zone
17-102	-	-	Melt lump of spheric shape (gray) solidified below the heated zone

Table 10 Chemical analysis of the fragments taken from bundle CORA-16

Sample No.	Elements in [wt.-%]							
	Fe	Mn	Cr	Ni	Mo	B	U	Zr
16-101	50.0	0.77	11.4	6.7	0.08	2.6	1.6	24.70
16-105	65.5	1.10	15.2	9.1	0.11	4.5	-	0.04

Note: The given data are mean values

Table 11 Chemical analysis of the fragments taken from bundle CORA-17

Sample No.	Elements in [wt.-%]						
	Fe	Cr	Ni	B	Sn	Mo	Zr
17-101	11.0	2.0	1.0	0.5	1.5	<0.01	84.0
17-102	67.3	17.0	8.0	1.5	<0.1	0.1	6.0

Note: The given data are mean values

Table 12 List of cross sections for test bundle CORA-16

Sample	Sample length	Axial position bottom	top	Remarks
16-a1			- 39 mm	Lower remnant
Cut	2 mm			
16-a2	100 mm	- 37 mm	+ 63 mm	
Cut	2 mm			
16-b	30 mm	65 mm	95 mm	Additional longitudinal cut
Cut	2 mm			Transition round - square
16-01	13 mm	97 mm	110 mm	Cross section
Cut	2 mm			
16-c	83 mm	112 mm	195 mm	Two additional longitudinal cuts
Cut	2 mm			
16-02	13 mm	197 mm	210 mm	Cross section
Cut	2 mm			
16-d	83 mm	212 mm	295 mm	
Cut	2 mm			
16-03	13 mm	297 mm	310 mm	Cross section
Cut	2 mm			
16-e	83 mm	312 mm	395 mm	
Cut	2 mm			
16-04	13 mm	397 mm	410 mm	Cross section
Cut	2 mm			
16-f	83 mm	412 mm	495 mm	
Cut	2 mm			
16-05	13 mm	497 mm	510 mm	Cross section
Cut	2 mm			
16-09	13 mm	512 mm	525 mm	Cross section
Cut	2 mm			

16-g	68 mm	527 mm	595 mm	
Cut	2 mm			
16-06	13 mm	597 mm	610 mm	Cross section
Cut	2 mm			
16-h	110 mm	612 mm	722 mm	
Cut	2 mm			
16-i	110 mm	724 mm	834 mm	
Cut	2 mm			
16-j	112 mm	836 mm	948 mm	
Cut	2 mm			
16-07	13 mm	950 mm	963 mm	Cross section
Cut	2 mm			
16-k	85 mm	965 mm	1050 mm	
Cut	2 mm			
16-l	91 mm	1052 mm	1143 mm	
Cut	2 mm			
16-08	13 mm	1145 mm	1158 mm	Upper grid spacer
Cut	2 mm			
16-m	xxx mm	1160 mm	xxxx mm	Upper remnant

Table 13 List of cross sections for test bundle CORA-17

Sample	Sample length	Axial position bottom	top	Remarks
17- a1	xx mm		-85 mm	Lower remnant
Cut	2 mm			
17- a2	140 mm	-83 mm	57 mm	Additional longitudunal cut
Cut	2 mm			Transition round - square
17- b	143 mm	59 mm	202 mm	Two additional longitudinal cuts
Cut	2 mm			
17-01	13 mm	204 mm	217 mm	Cross section
Cut	2 mm			
17- c	140 mm	219 mm	359 mm	Additional longitudinal cut
Cut	2 mm			
17-02	13 mm	361 mm	374 mm	Cross section
Cut	2 mm			
17- d	140 mm	376 mm	516 mm	Additional longitudinal cut
Cut	2 mm			
17-03	13 mm	518 mm	531 mm	Cross section
Cut	2 mm			
17- e	140 mm	533 mm	673 mm	Additional longitudinal cut
Cut	2 mm			
17-04	13 mm	675 mm	688 mm	Cross section
Cut	2 mm			
17- f	140 mm	690 mm	830 mm	
Cut	2 mm			
17-05	13 mm	832 mm	845 mm	Cross section
Cut	2 mm			
17- g	140 mm	847 mm	987 mm	
Cut	2 mm			

17- h	140 mm	989 mm	1129 mm	
Cut	2 mm			
17- i	94 mm	1131 mm	1225 mm	Upper remnant

Table 14 List of cross sections for test bundle CORA-18

Sample	Sample length	Axial position bottom	top	Remarks
18-a	ca. 40 mm	ca.-100 mm	-45 mm	
Cut	2 mm			Lower grid spacer
18-b	140 mm	-43 mm	97 mm	
Cut	2 mm			
18-02	13 mm	99 mm	112 mm	Cross section
Cut	2 mm			
18-c	140 mm	114 mm	254 mm	Two add. longit. cuts (18-c-L)
Cut	2 mm			
18-03	13 mm	256 mm	269 mm	Cross section
Cut	2 mm			
18-d1	63 mm	271 mm	334 mm	Additional longitudinal cut
Cut	2 mm			
18-d2-L	47 mm	336 mm	383 mm	18-d2-R top 398 mm
Cut	2 mm			
18-01	13 mm	385 mm	398 mm	18-d2-L shortened by 18-01
Cut	2 mm			
18-04	13 mm	400 mm	413 mm	Cross section, lower window
Cut	2 mm			
18-e1	64 mm	415 mm	479 mm	18-e with 2 longit. cuts (18-e-L)
Cut	2 mm			
18-e2	64 mm	481 mm	545 mm	18-e-L not horizontally divided
Cut	2 mm			
18-05	13 mm	547 mm	560 mm	Cross section, central spacer
Cut	2 mm			
18-f	140 mm	562 mm	702 mm	
Cut	2 mm			

18-06	13 mm	704 mm	717 mm	Cross section
Cut	2 mm			
18-g	140 mm	719 mm	859 mm	
Cut	2 mm			
18-07	13 mm	861 mm	874 mm	Cross section
Cut	2 mm			
18-h	140 mm	876 mm	1016 mm	
Cut	2 mm			Above heated zone
18-i	140 mm	1018 mm	1158 mm	
Cut	2 mm			Upper grid spacer
18-j	xx mm	1160 mm	xxxx mm	Upper remnant

Table 15: Procedure of the preparation of the samples for the metallographic examination

	Horizontal grinding	Grinding	Lapping	Polishing		
Abrasive	Corrundum disc 120 µm Diamond disc 64 µm	Diamond disc 20 µm	Petrodisc-M or DP Net*)	PAW cloth	PAN-W	NAP cloth
Particle size			Diamond spray 6 µm	6 µm	3 µm	1 µm
Lubricant	Water	Water	W. lubric. **)	W. lub.	W. lub.	W. lub.
Revolutions of disc	300 rpm	300 rpm	150 rpm (Net) or 300 rpm (Petrod.)	150 U/min	150 U/min	150 U/min
Pressure	200-400 N	200-300 N	200 N	100 N	100 N	100 N
Time	to level	25 min	30 min	30 min	60 min	60 min

*) Petrodisc-M and DP Net are registered trade marks of Struers company

**) "White lubricant" of Struers; liquid on an oil/alcohol/glycerin basis

Table 16 Polished cross sections of bundles CORA-16, CORA-17, and CORA-18

- Sample CORA-16-01 top and bottom 97 mm and 110 mm (absorber melt)
- Sample CORA-16-03 top 310 mm
- Sample CORA-16-09 top 525 mm
- Sample CORA-16-07 top 963 mm
- Sample CORA-16-08 bottom 1145 mm
- Sample CORA-16-c-L 112 - 195 mm (longitudinal section with absorber melt)

- CORA-17-02 bottom 361 mm
- CORA-17-03 bottom 518 mm
- CORA-17-04 bottom 675 mm
- CORA-17-05 bottom 832 mm
- CORA-17-b-R 59 mm - 202 mm (longitudinal section of the blockage zone)

- CORA-18-03 top 269 mm
- CORA-18-04 top 413 mm
- CORA-18-05 top 560 mm (central grid spacer)
- CORA-18-06 top 717 mm
- CORA-18-07 top 874 mm
- CORA-18-c-L 114 mm - 254 mm (longitudinal section of the blockage zone)
- CORA-18-e-L 415 mm - 545 mm (longitudinal section with the grid spacer)

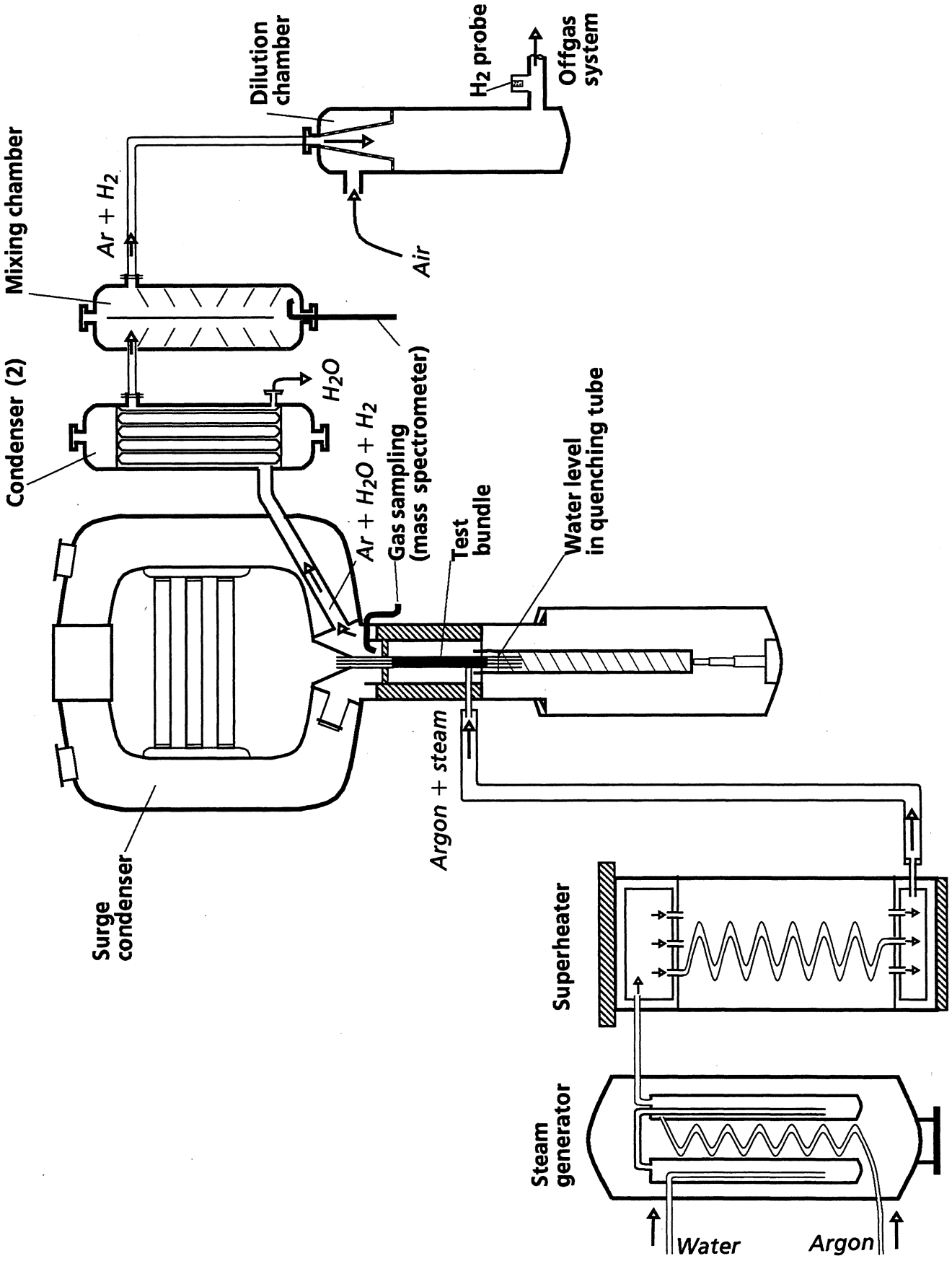

Fig. 1 SFD Test Facility CORA (Simplified flow diagram)

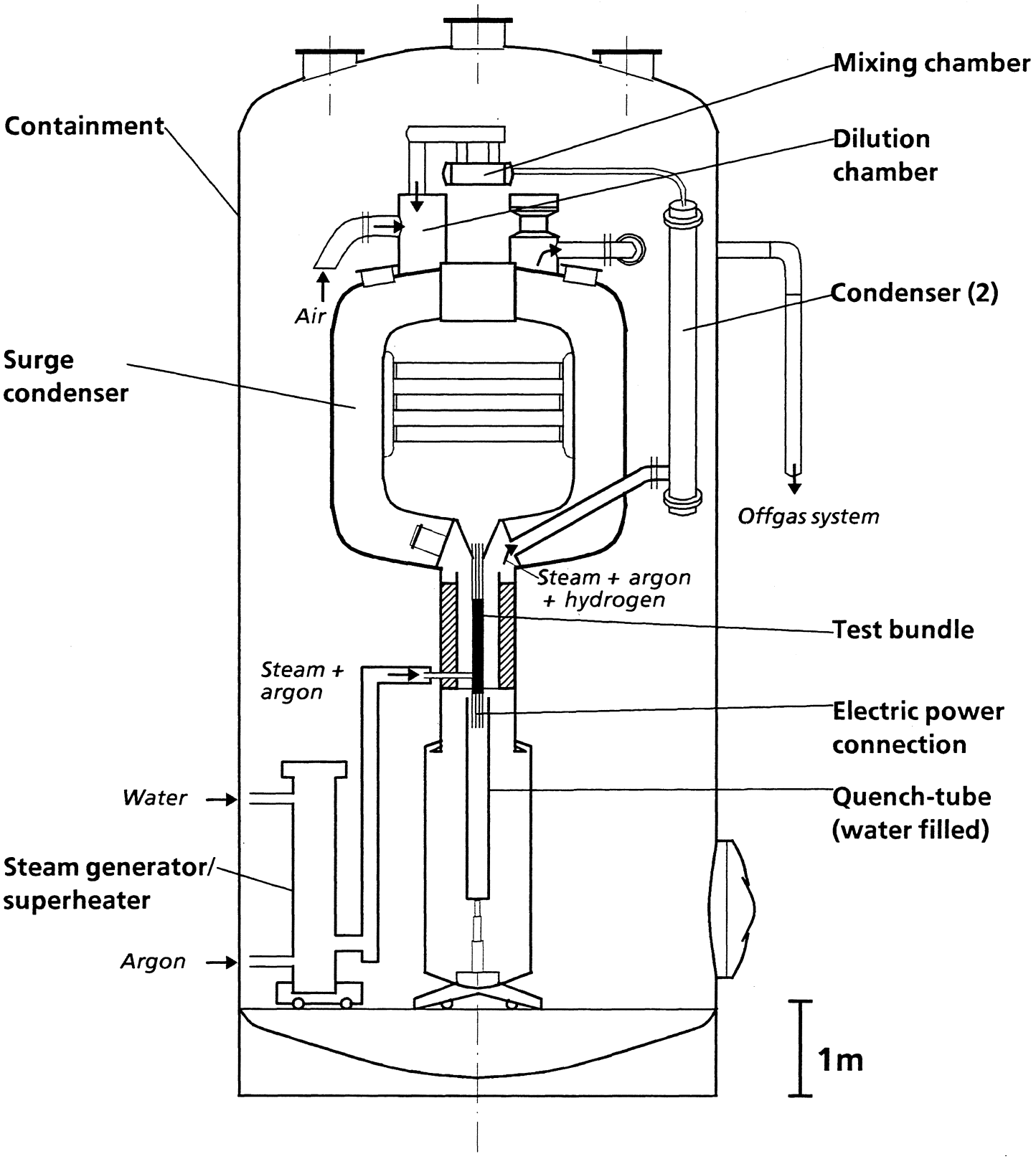

Fig. 2 SFD Test Facility CORA (Main components)

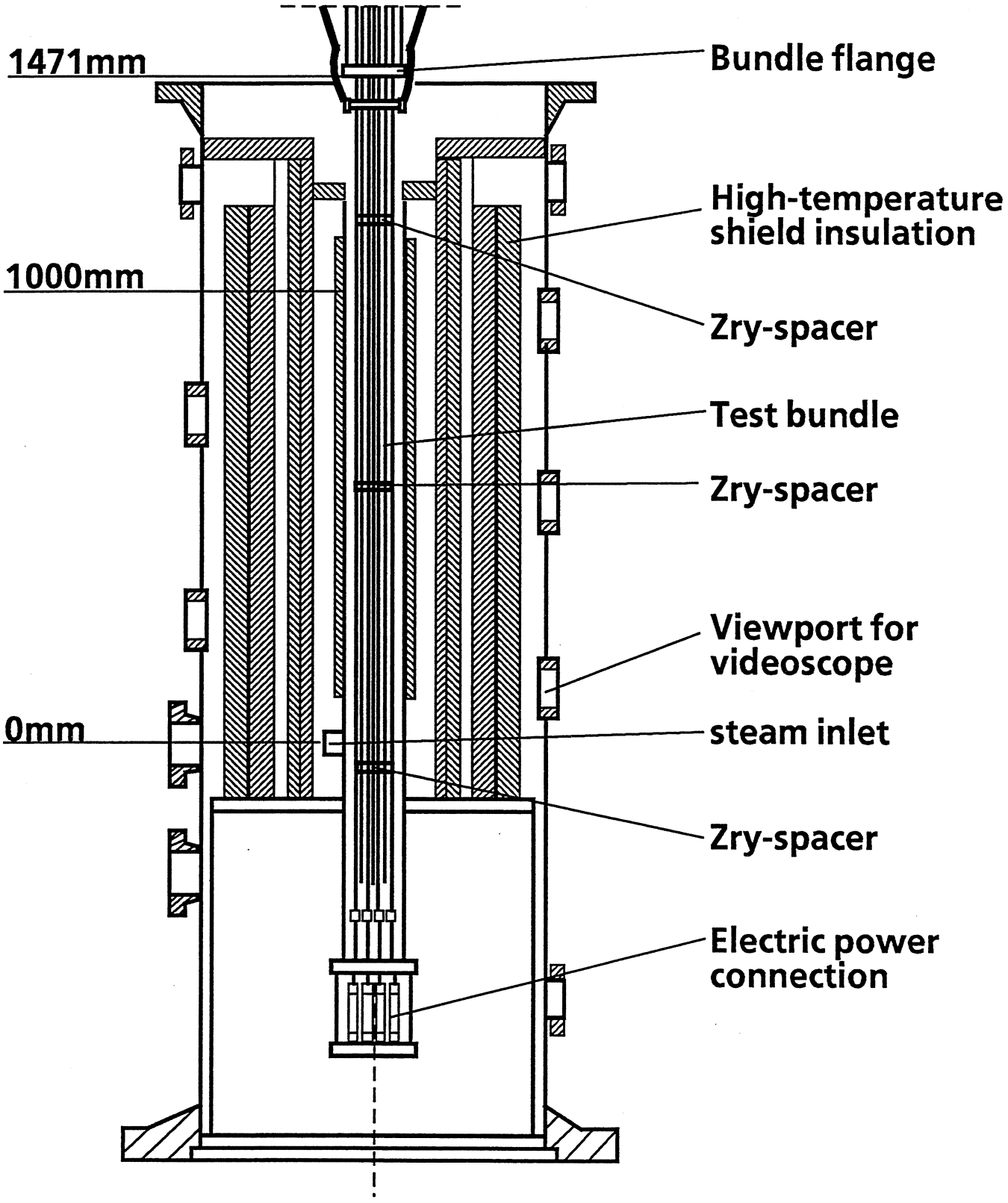

Fig. 3 CORA BWR-type bundle arrangement

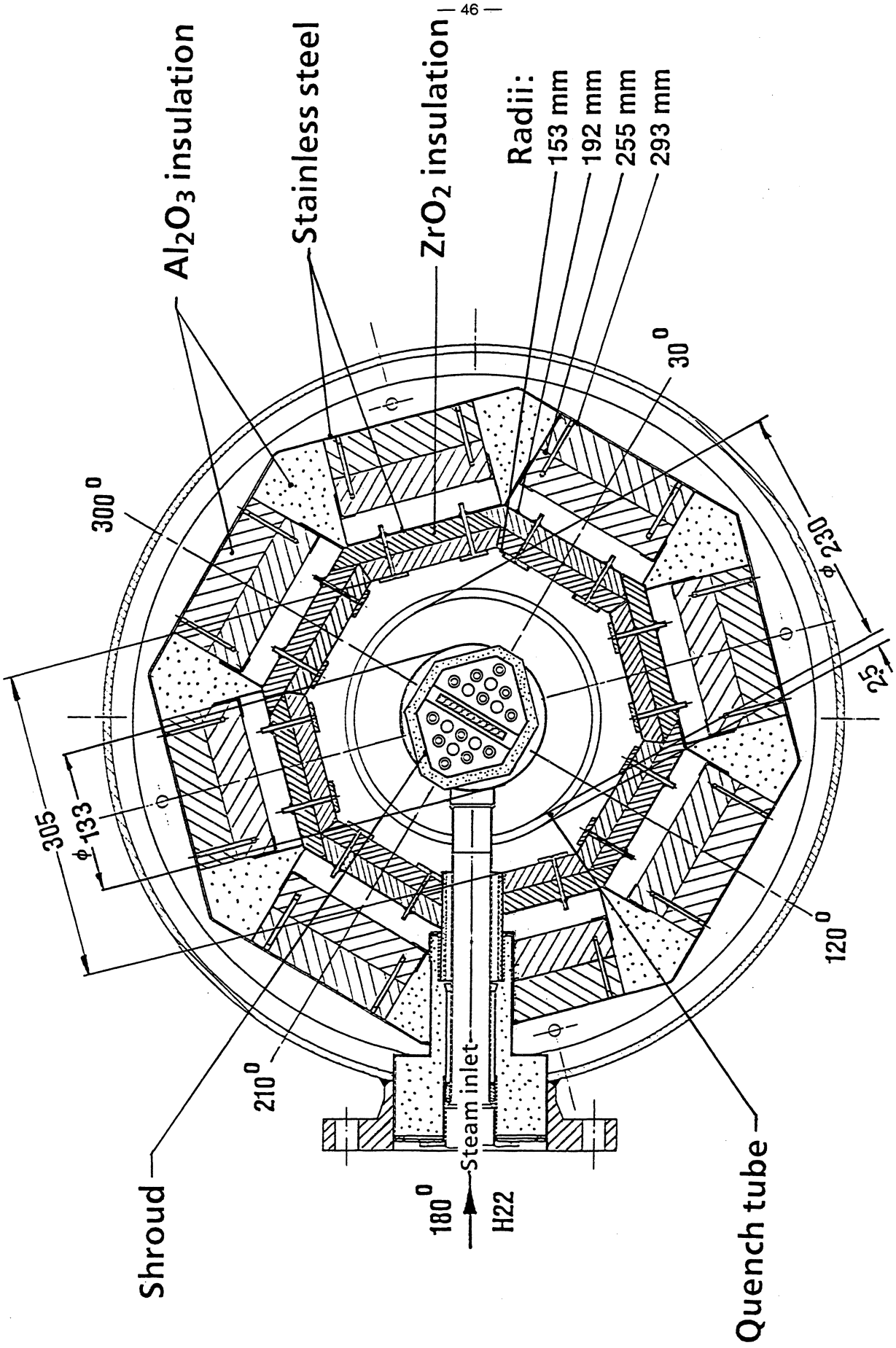

Fig. 4 **Horizontal cross section of the high-temperature shield**

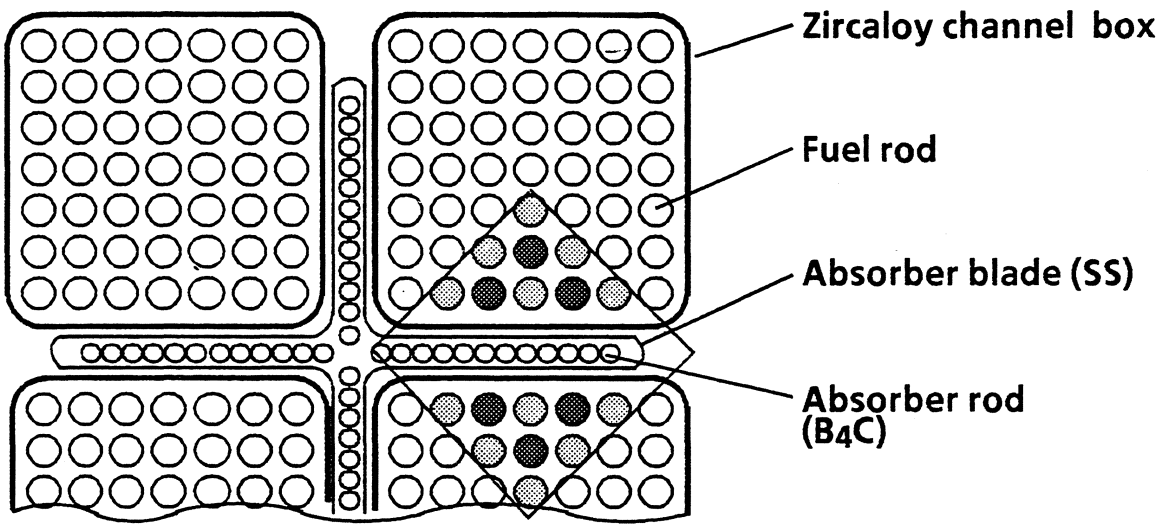

BWR

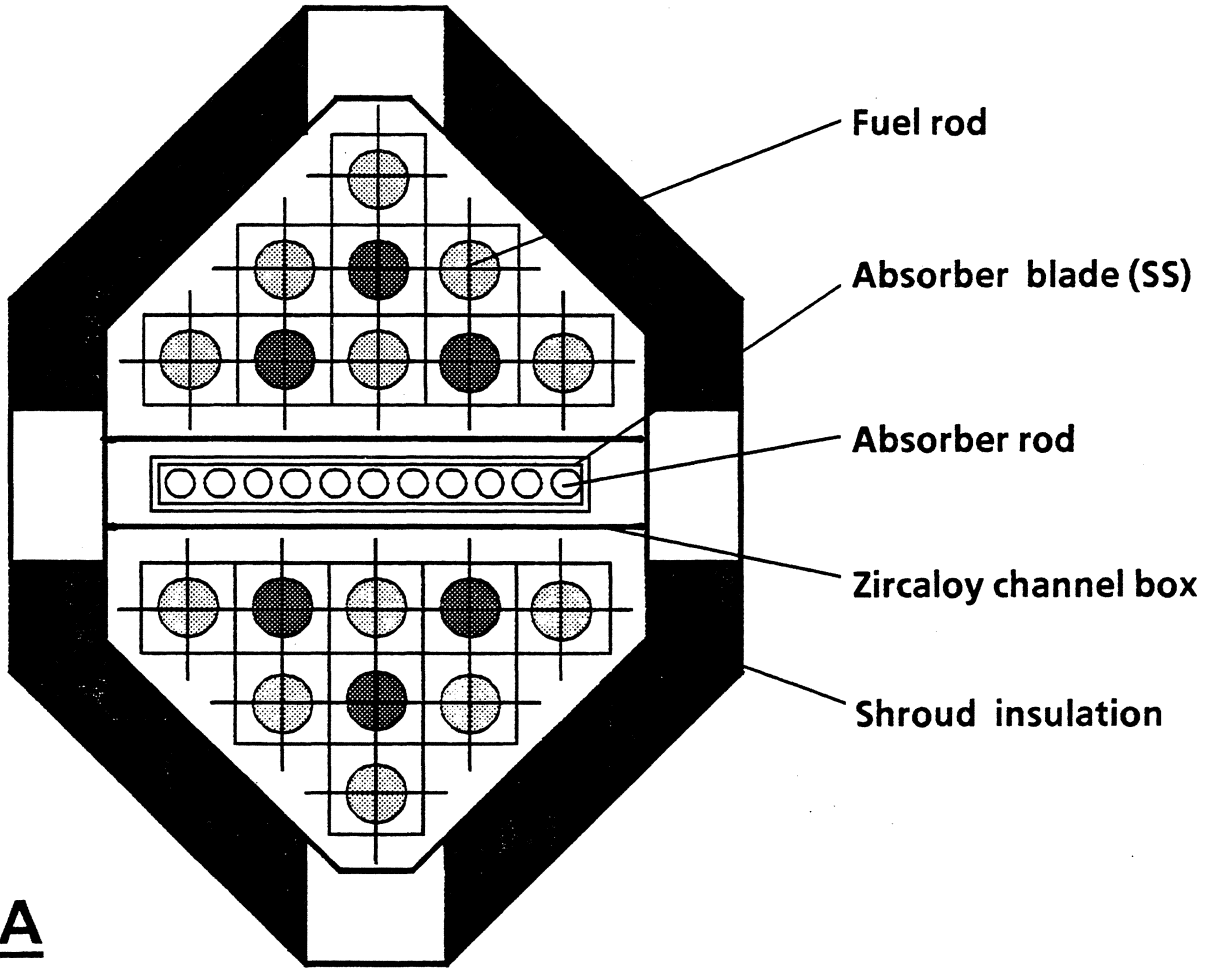

CORA

Fig. 5: BWR-type configuration and simulation in the CORA test bundle

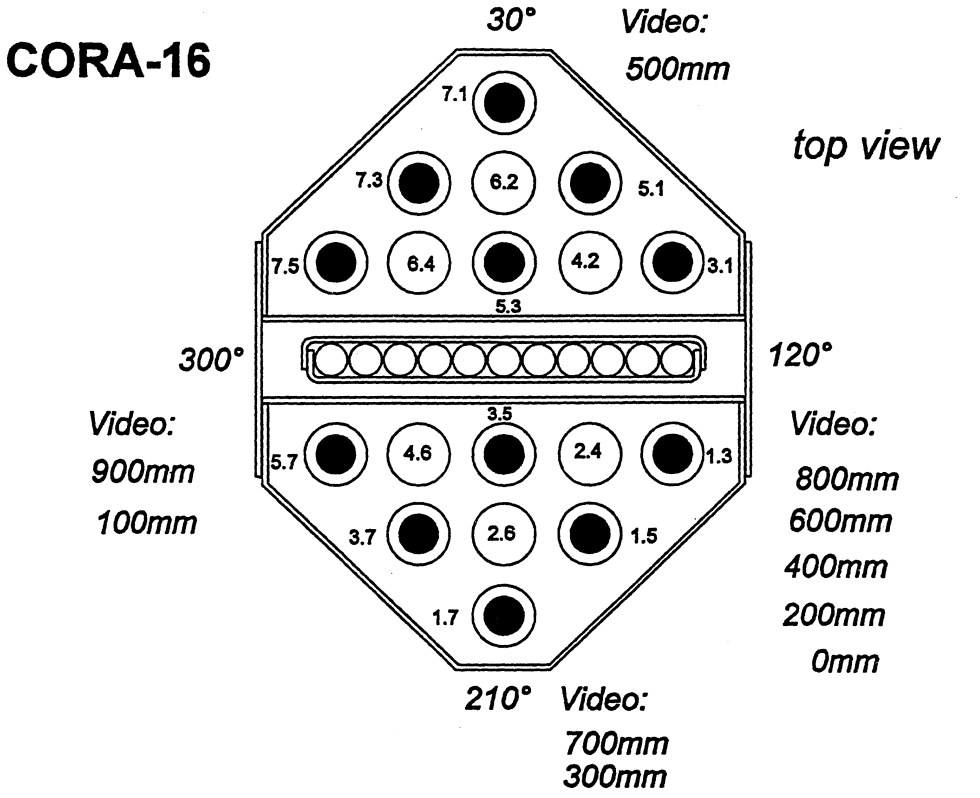

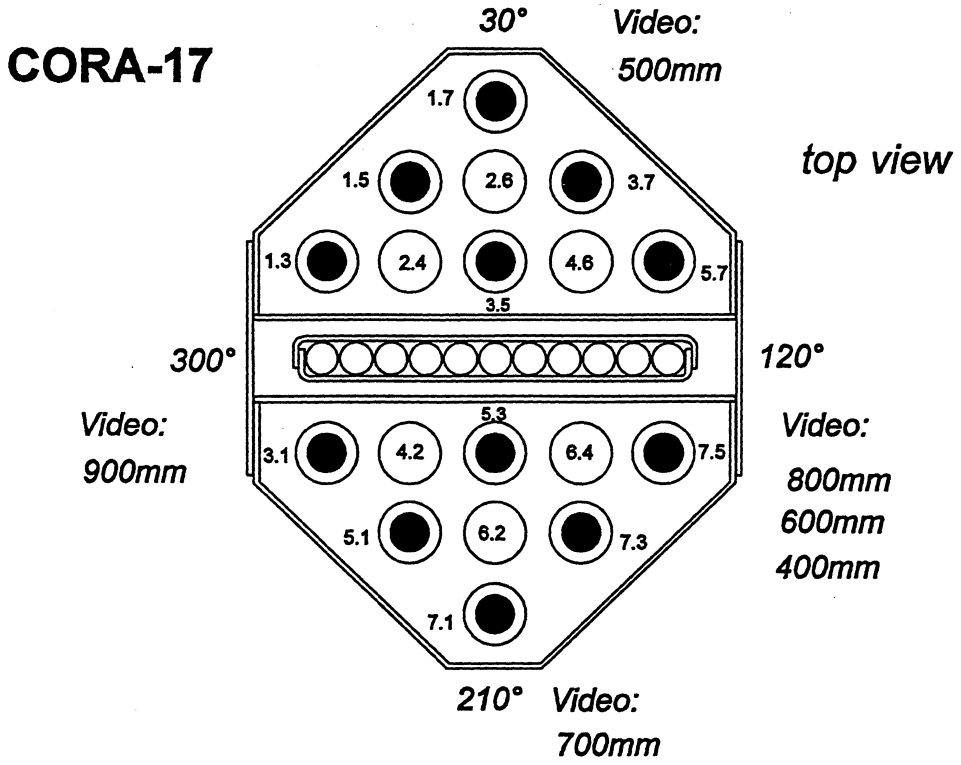

Fig. 6 **Test rod designation in bundles CORA-16 and CORA-17**

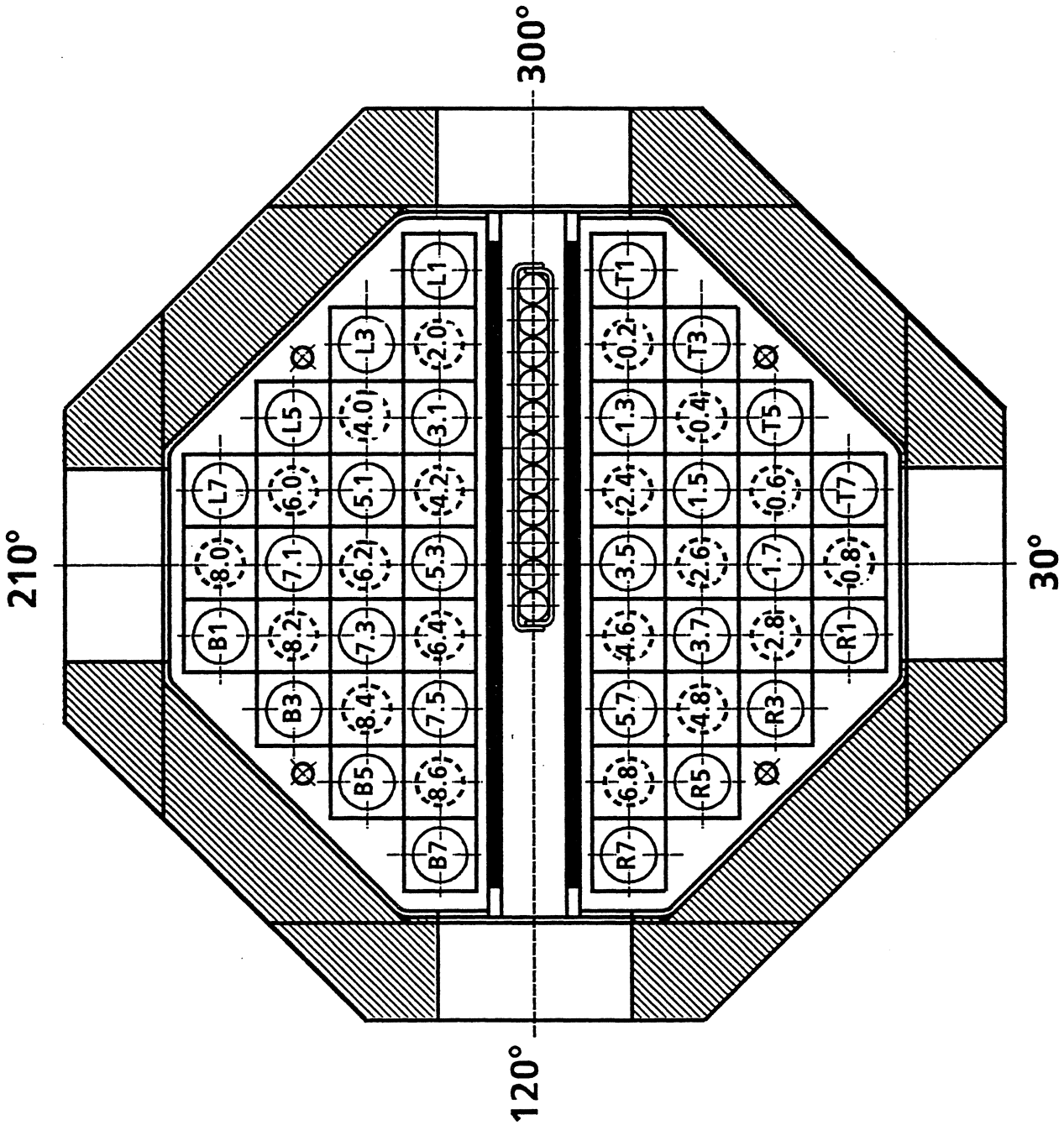

Fig. 7 Test bundle arrangement for CORA-18

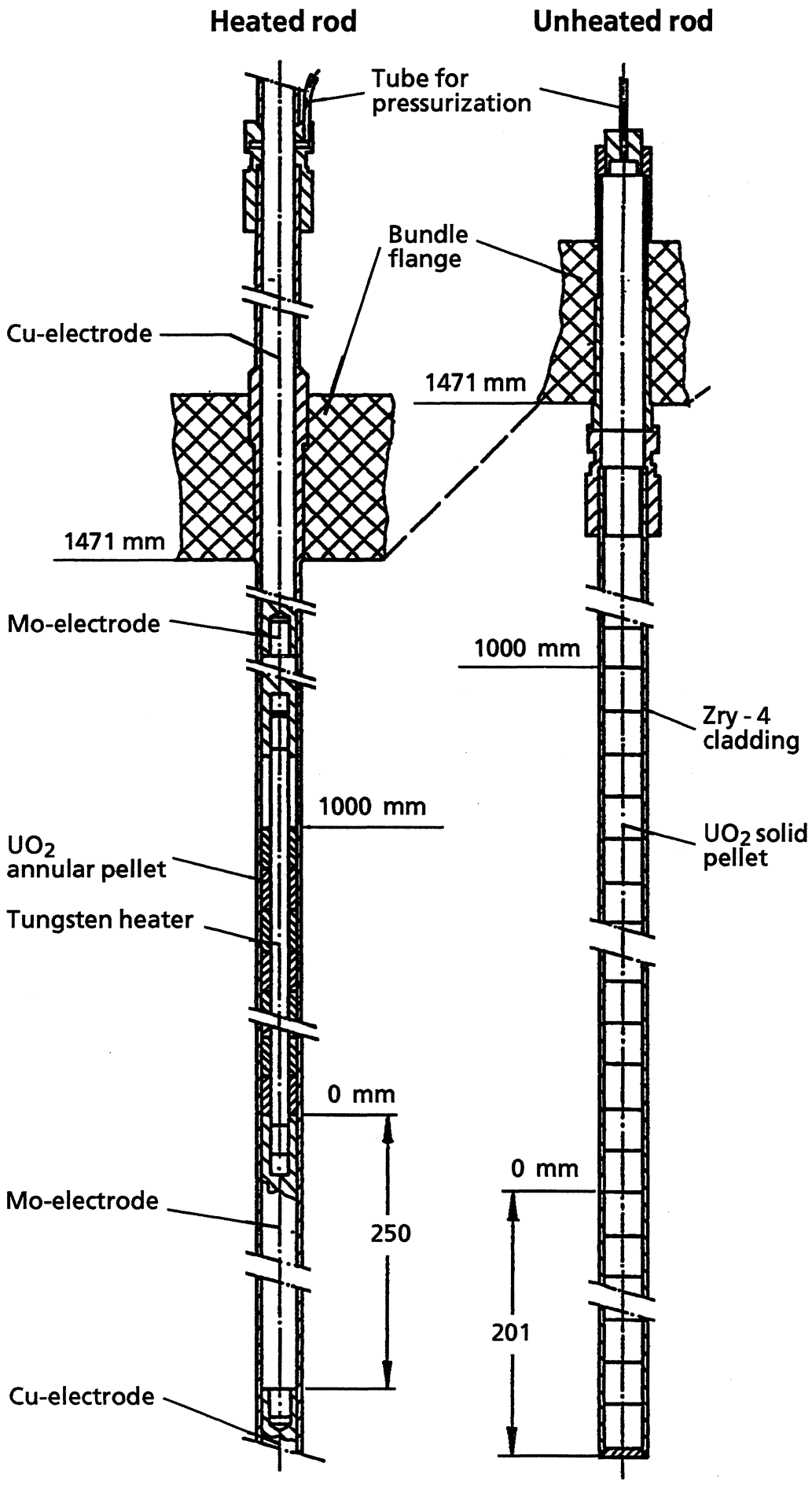

Fig. 8 Test rod design, schematic

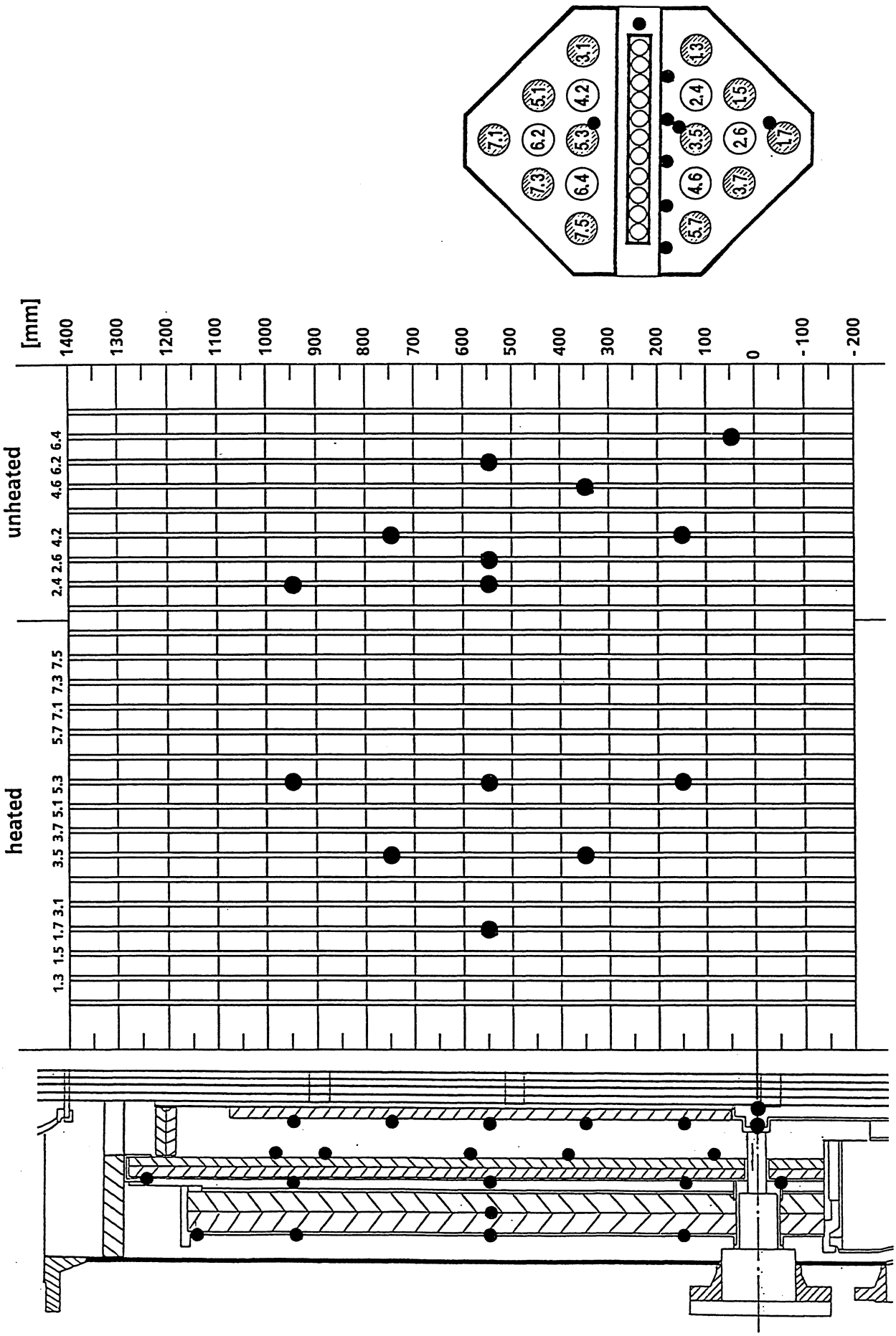

Fig. 9a Positions of thermocouples in bundle and high temperature shield (CORA-16)

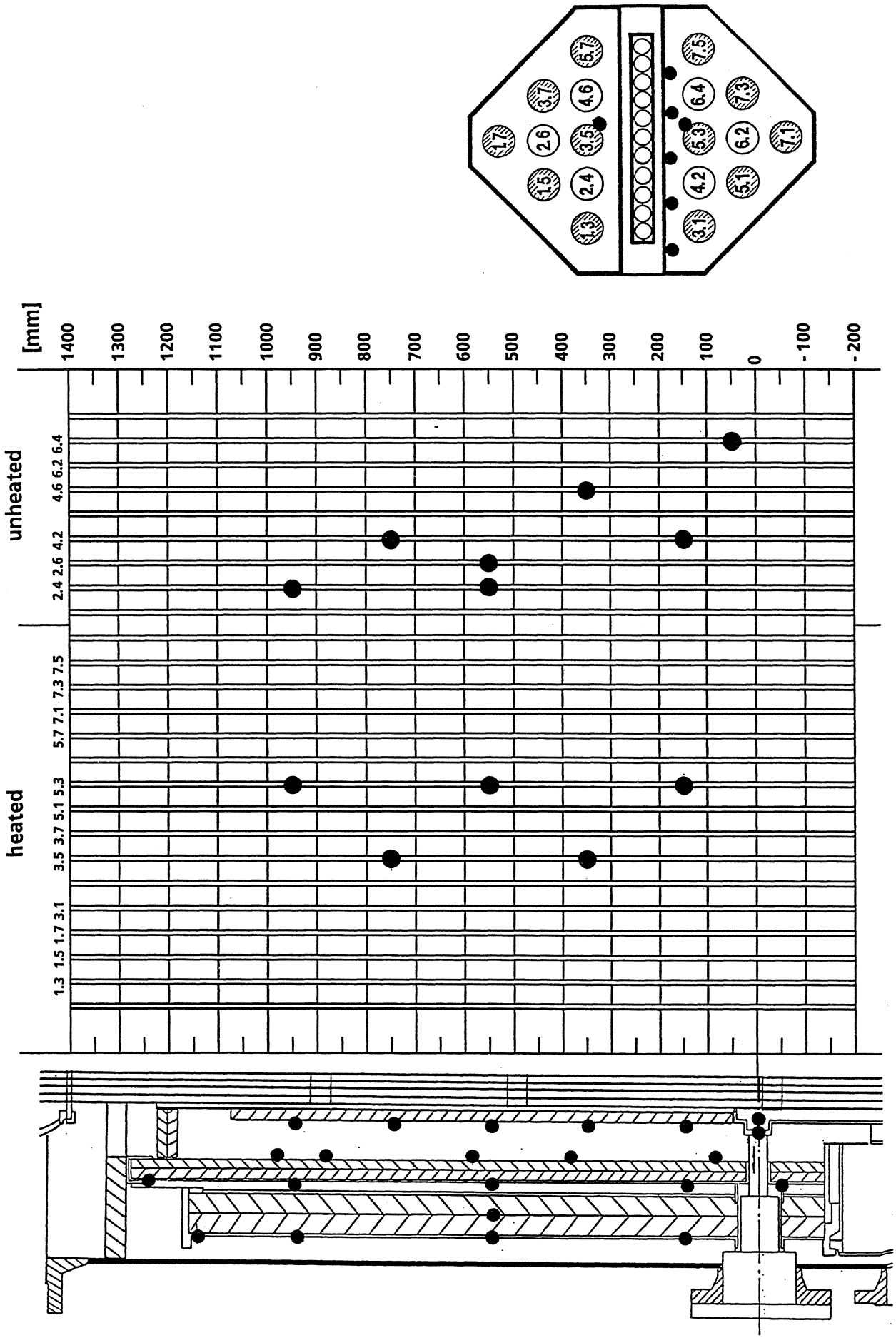

Fig. 9b Positions of thermocouples in bundle and high temperature shield of test CORA-17

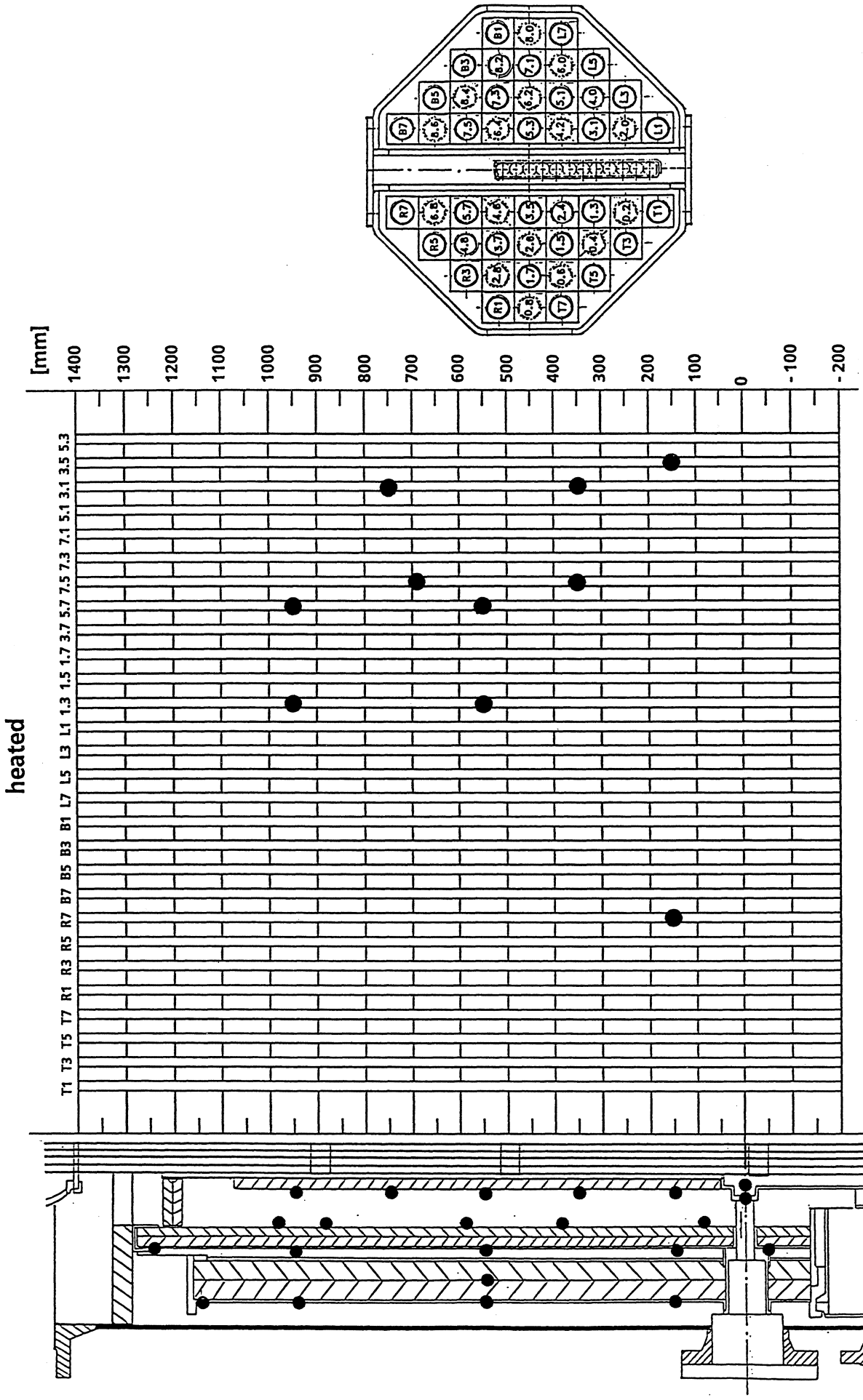

Fig. 9c Positions of thermocouples in bundle and high temperature shield of test CORA-18 (heated rods)

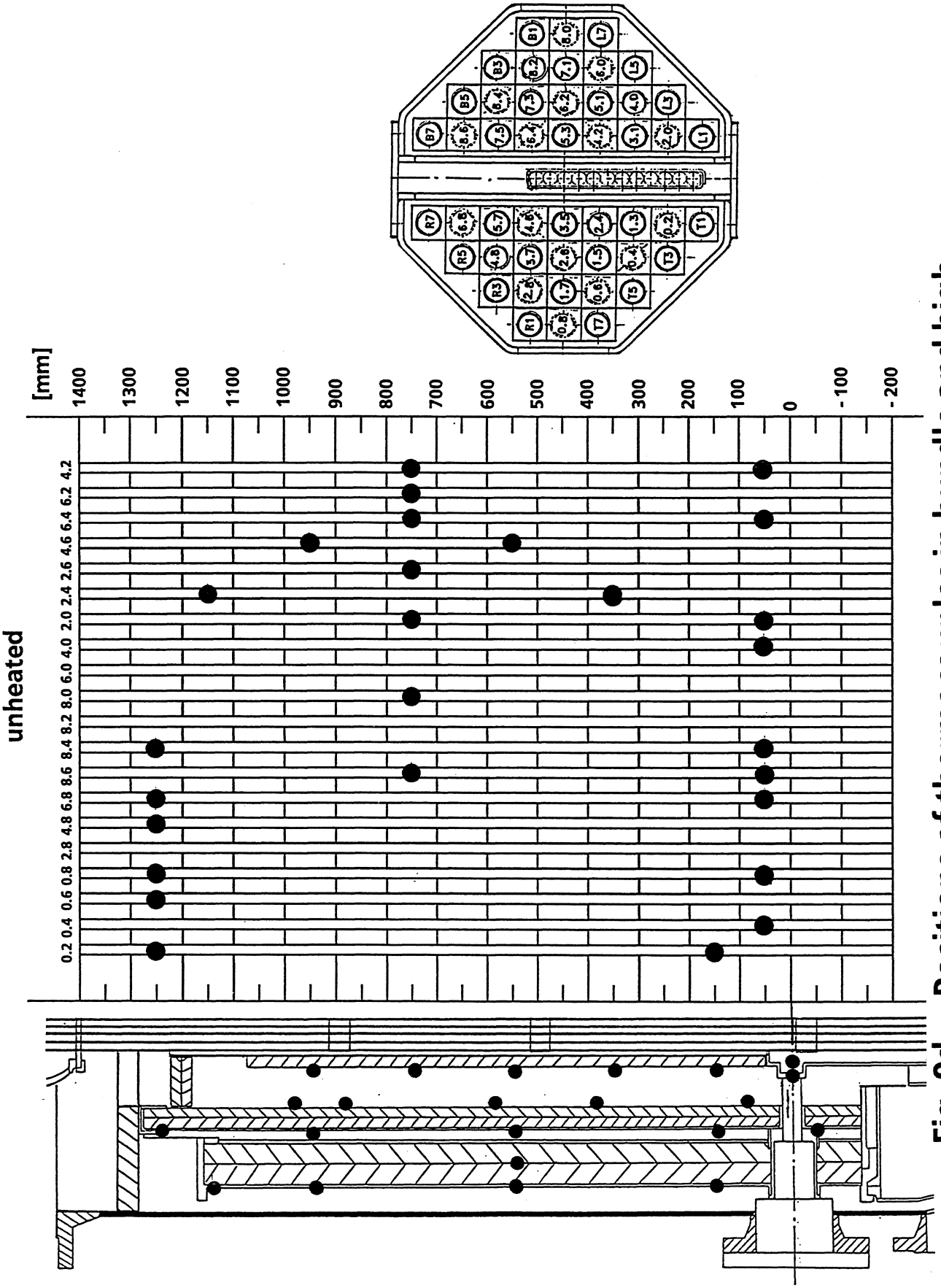

Fig. 9d Positions of thermocouples in bundle and high temperature shield of test CORA-18 (unheated rods)

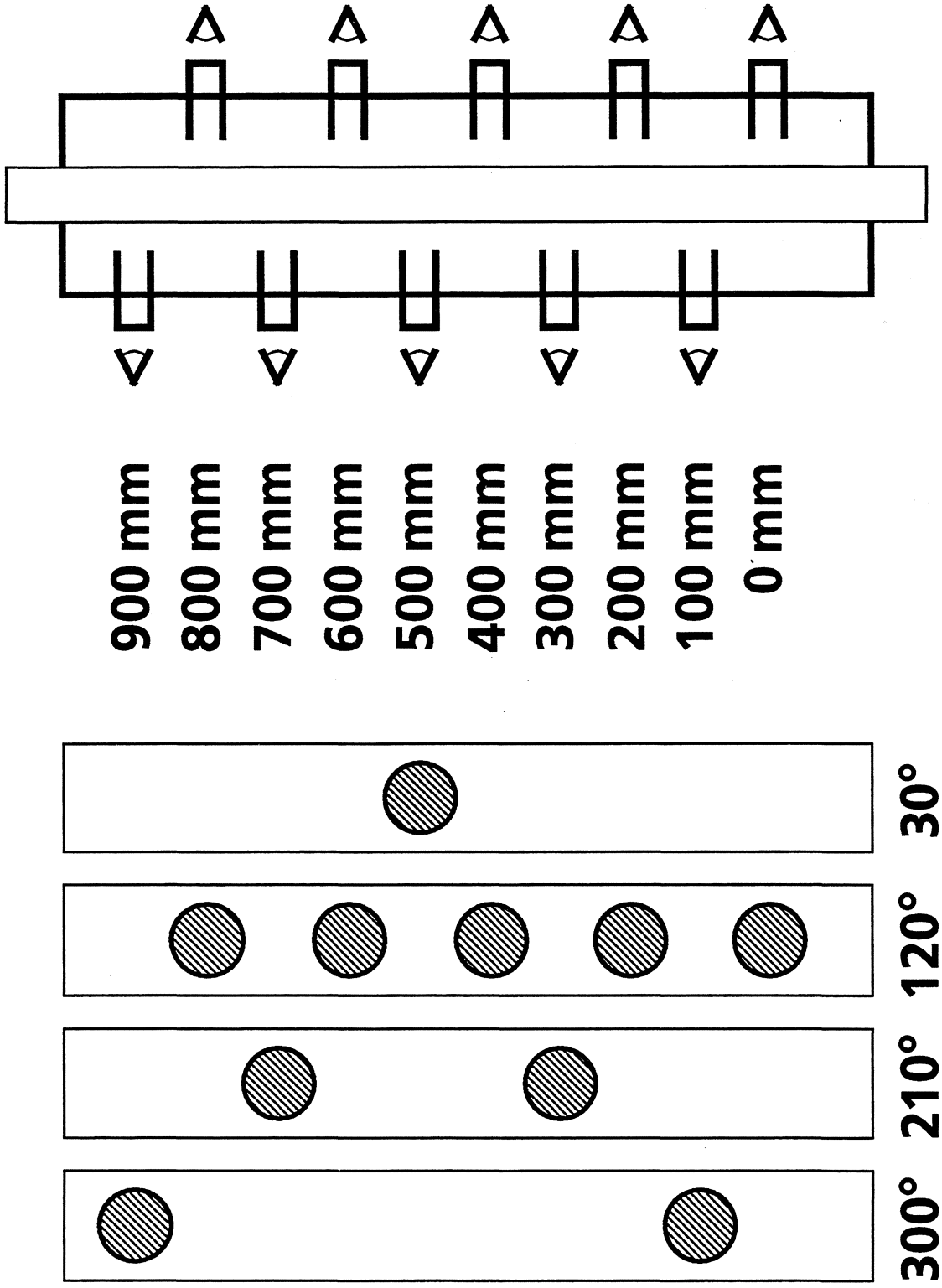

Fig. 10a Videoscope positions of bundle CORA-16

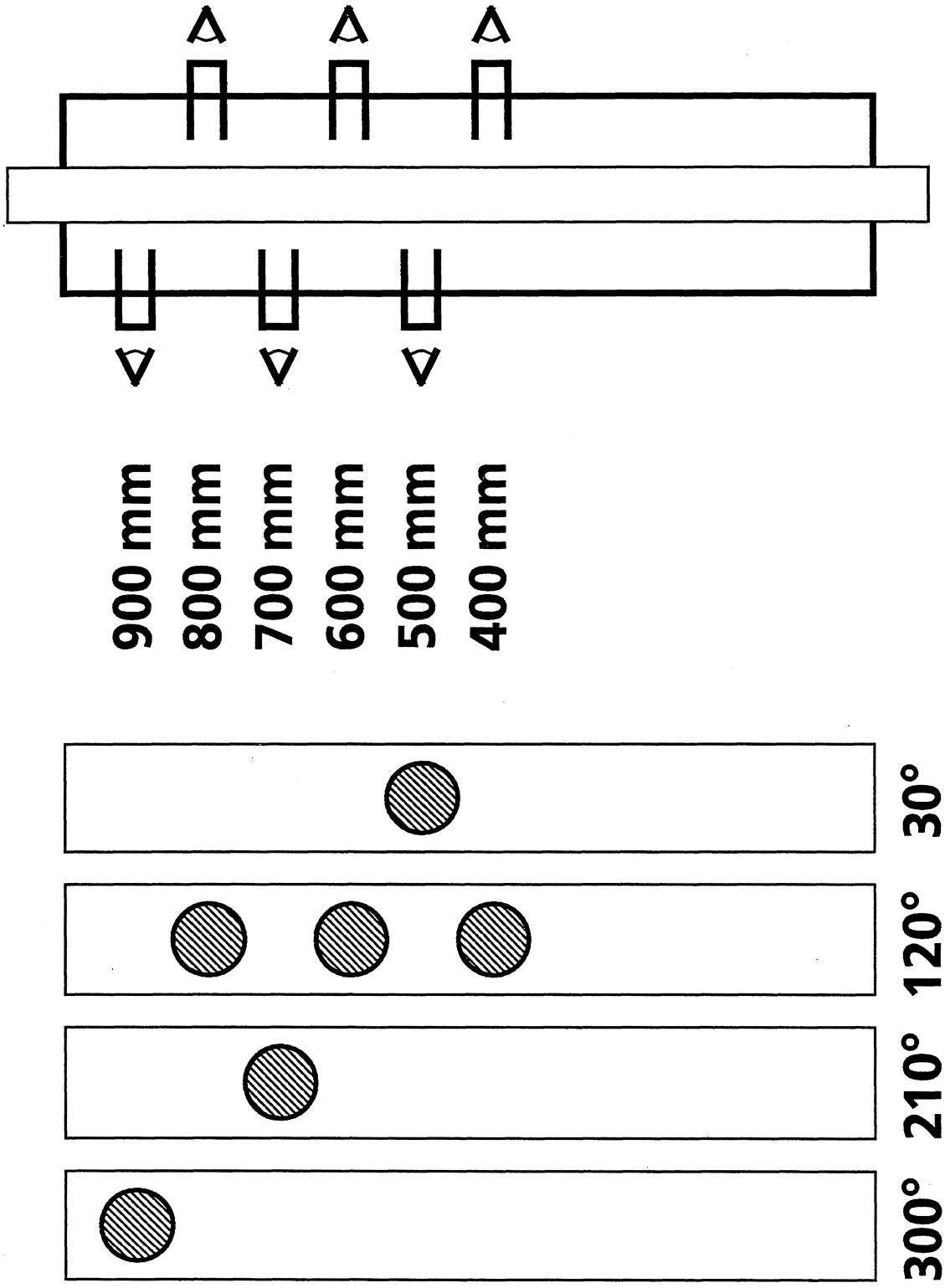

Fig. 10b Videoscope positions of bundles CORA-17 and CORA-18

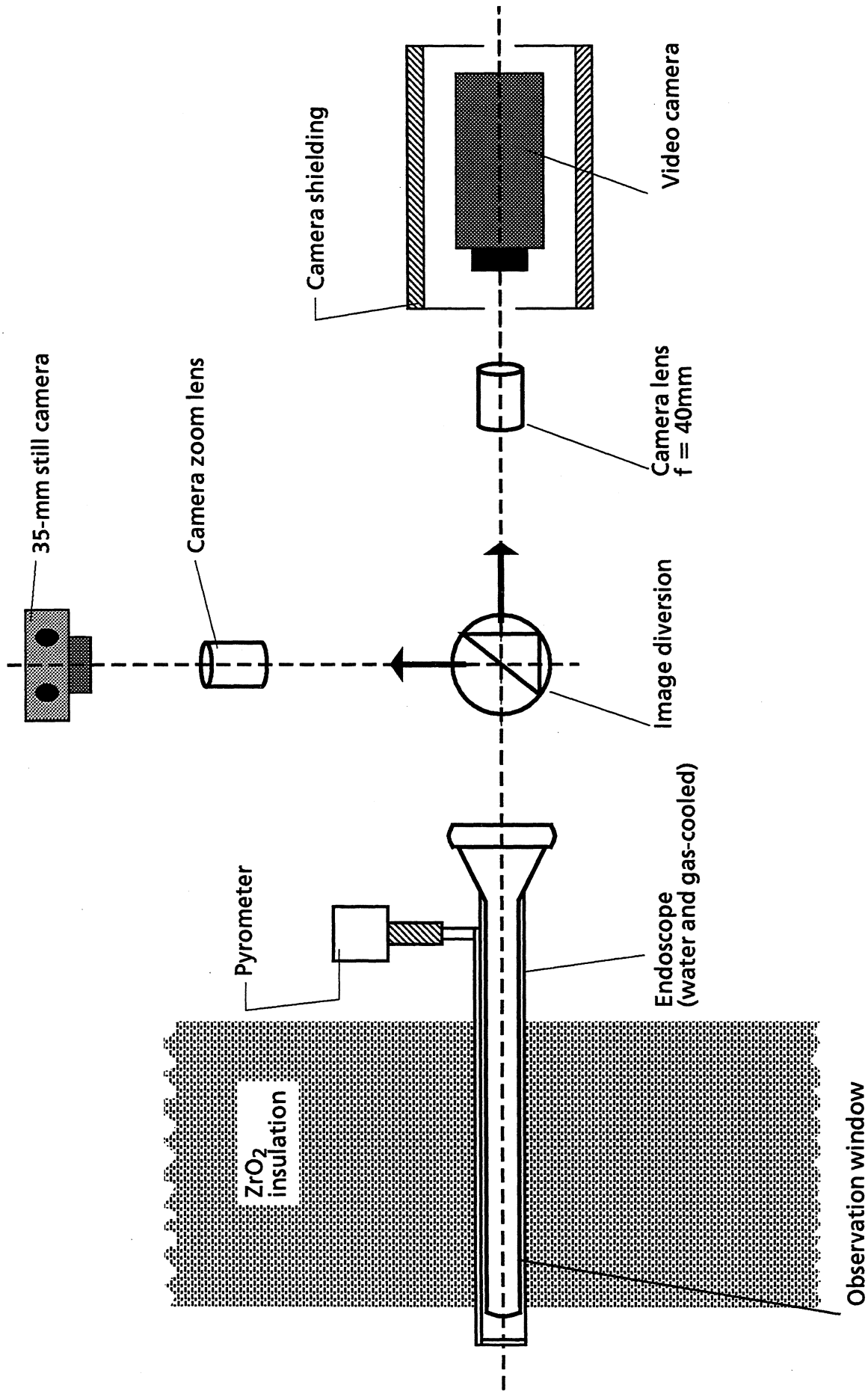

Fig. 11 Videoscope system for the CORA test bundle

(a)

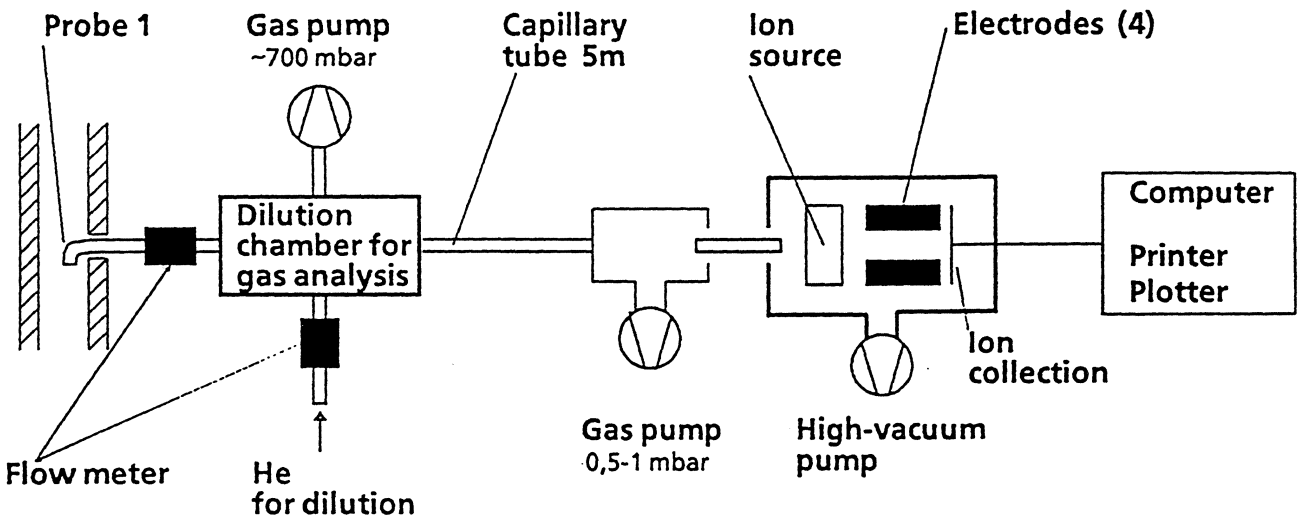

(b)

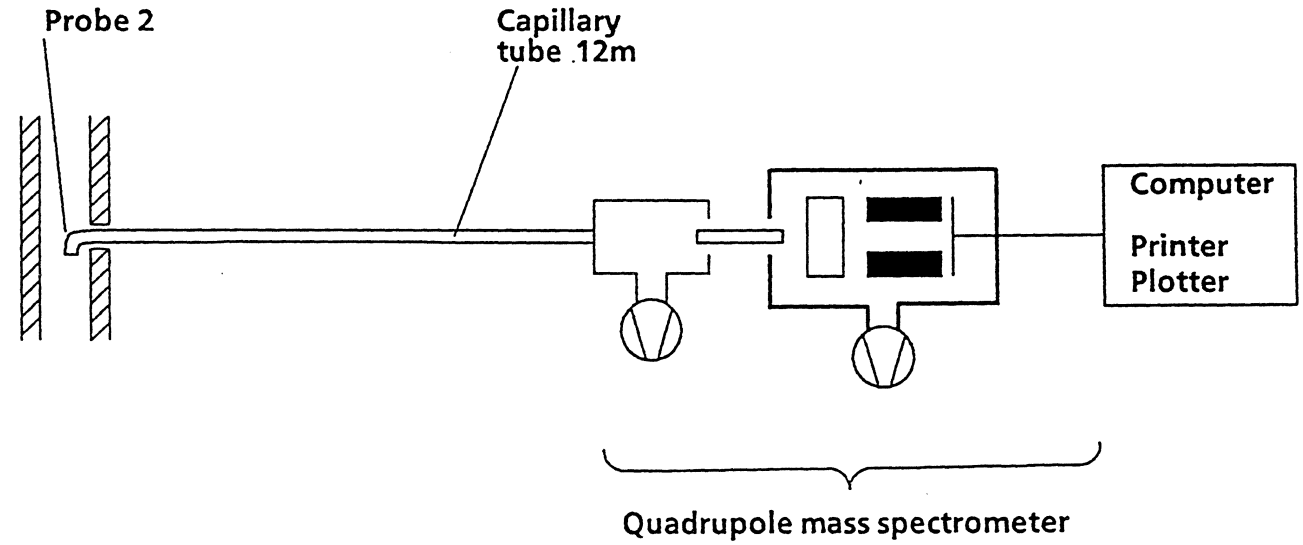

Location (a) : Outlet of test section

Location (b) : Mixing chamber

Fig. 12 Hydrogen measurement

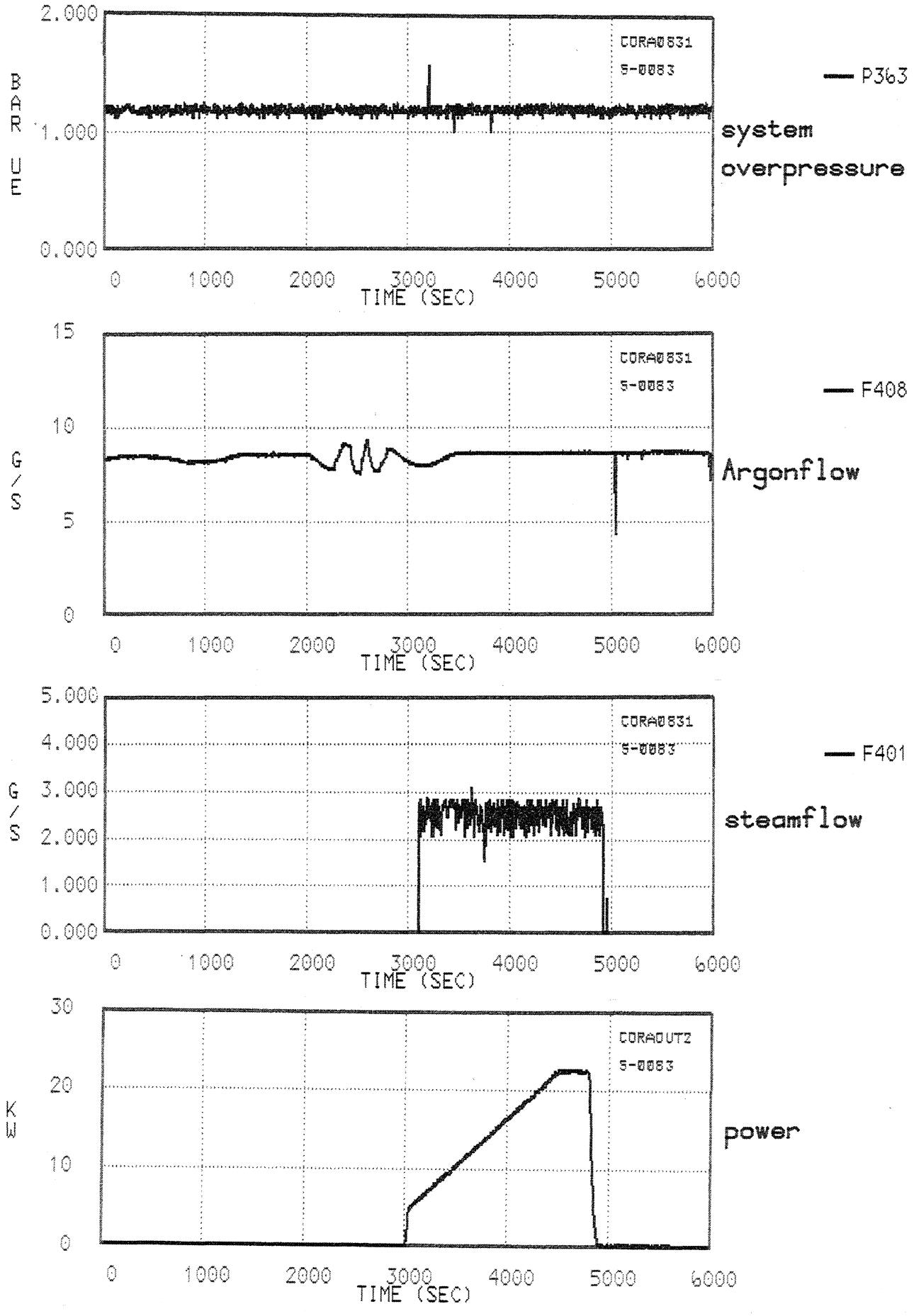

Fig. 13 System pressure, argon flow, steam flow and electric power during test CORA-16

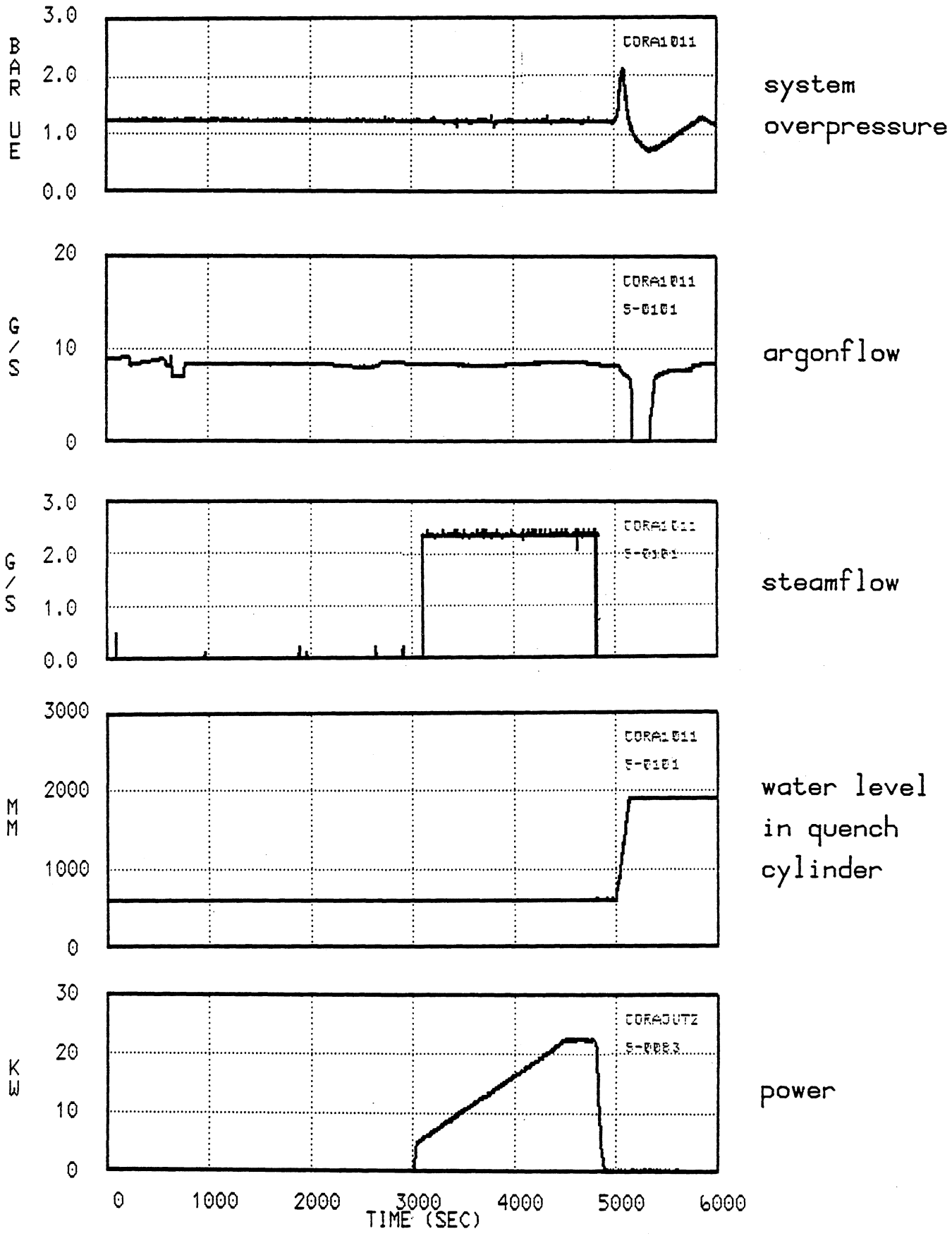

Fig. 14 System pressure, argon flow, steam flow, water level in the quench cylinder and electric power during test CORA-17

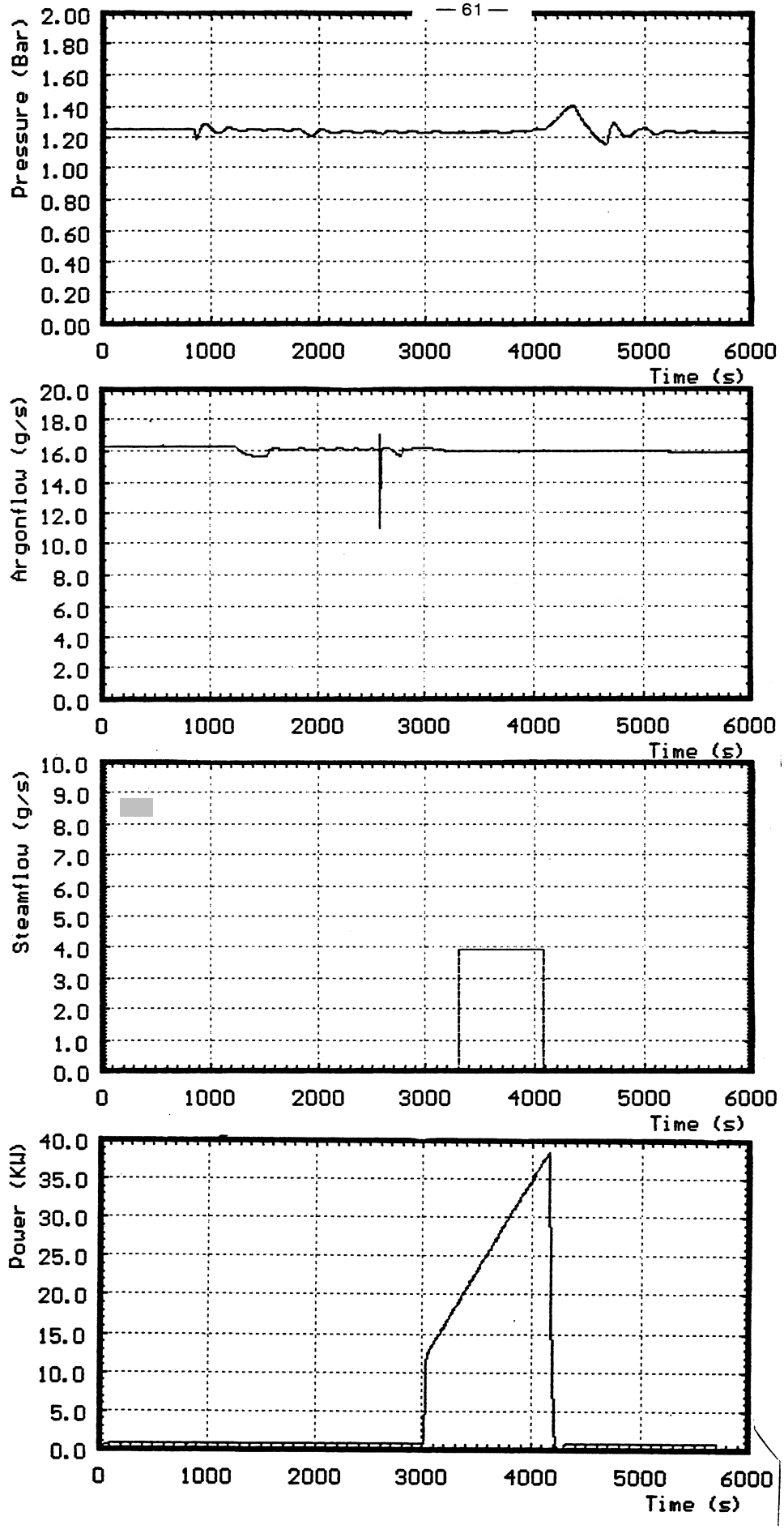

Fig. 15 System pressure, argon flow, steam flow and electric power during CORA-18

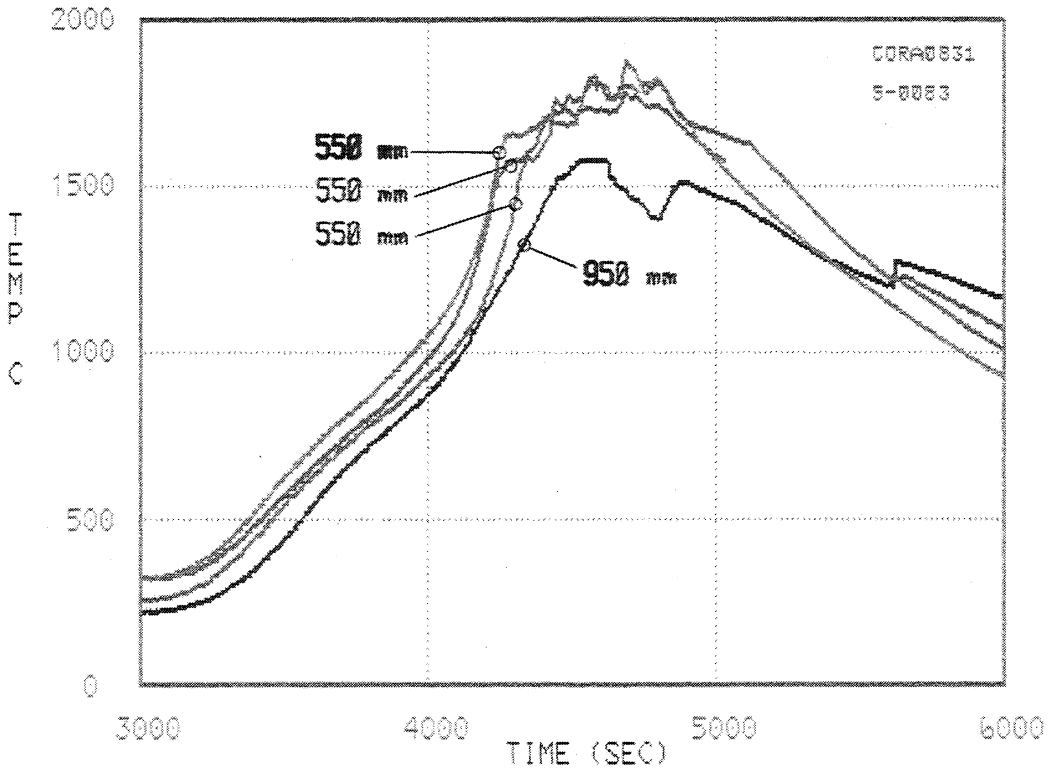

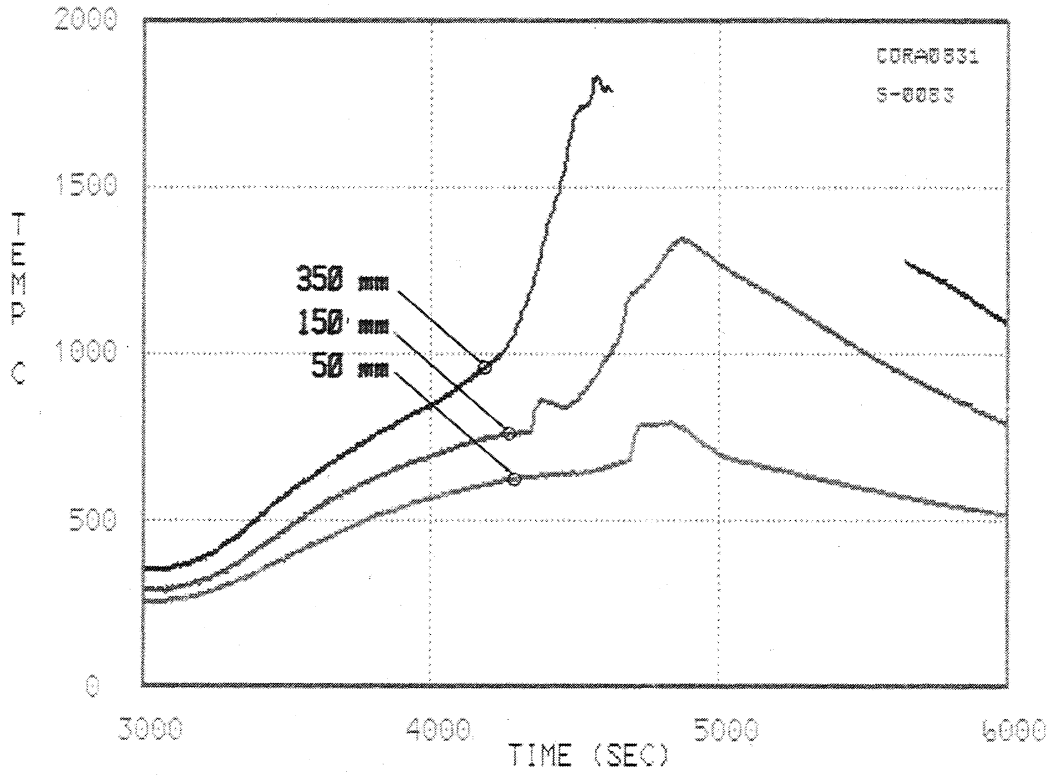

Fig. 16: CORA-16; Temperatures of unhheated rods

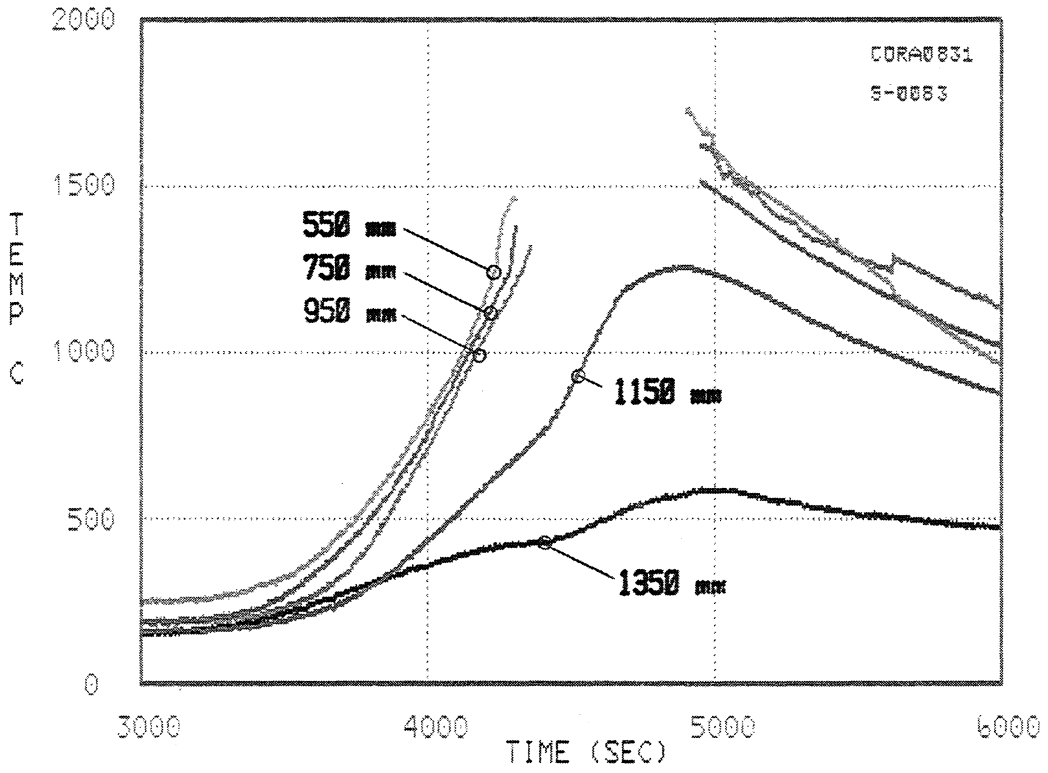

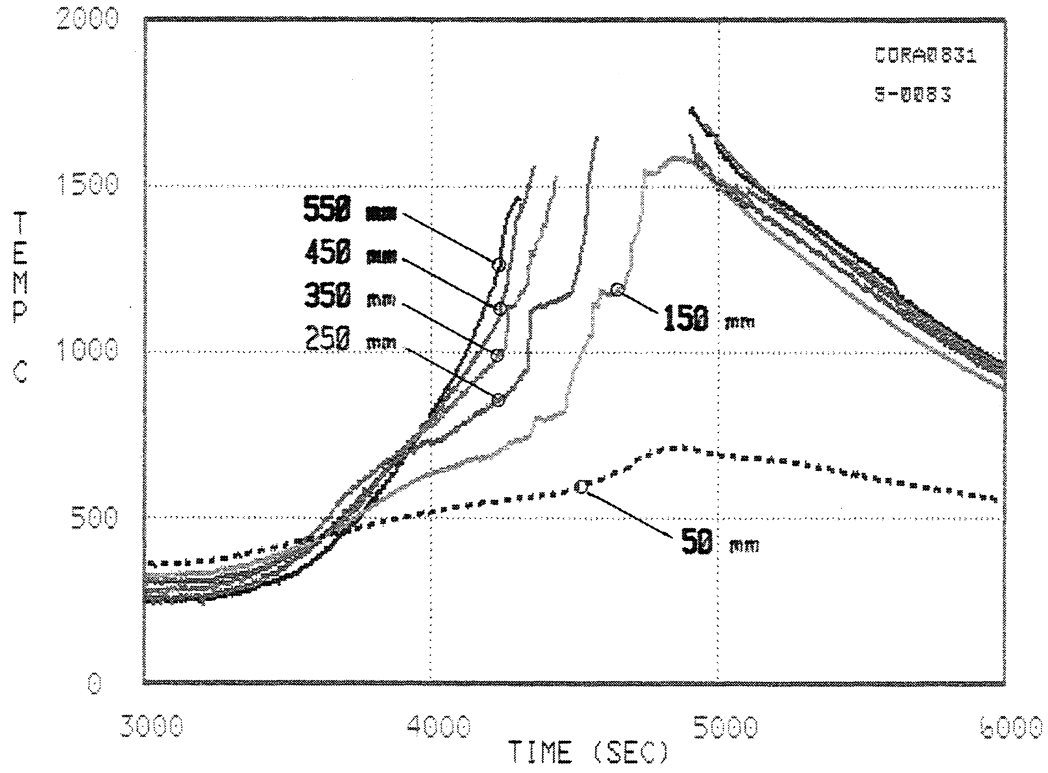

Fig. 17: CORA-16; Temperatures of the absorber blade

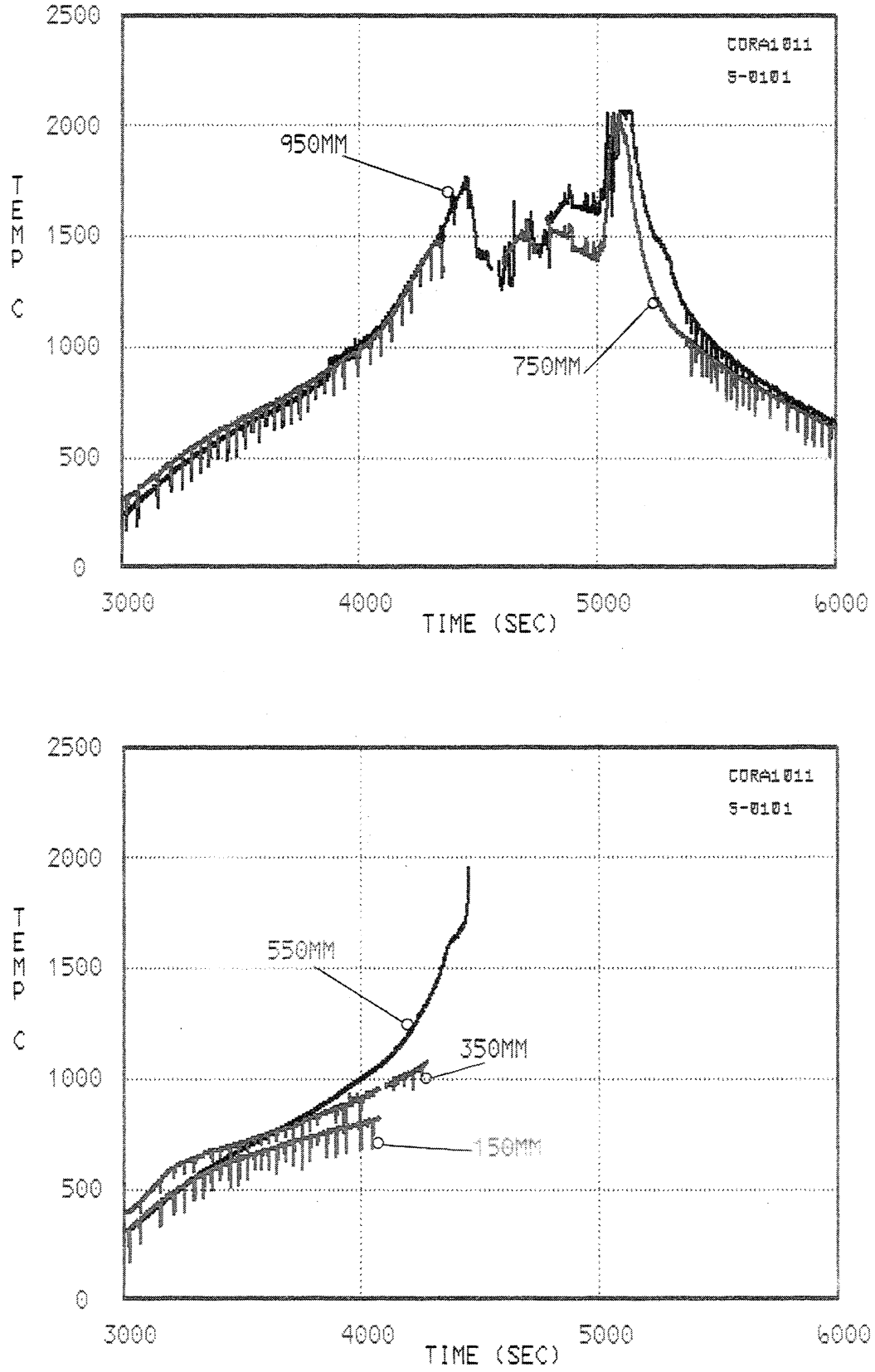

Fig. 18 CORA-17; Temperatures of unheated rods

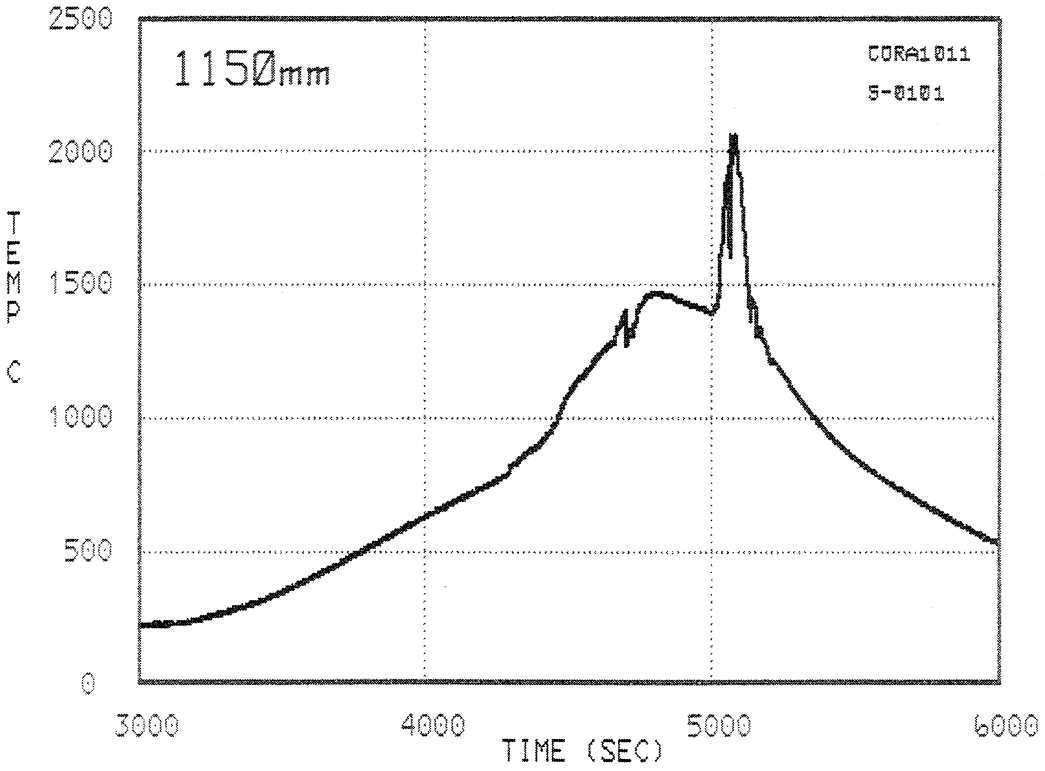

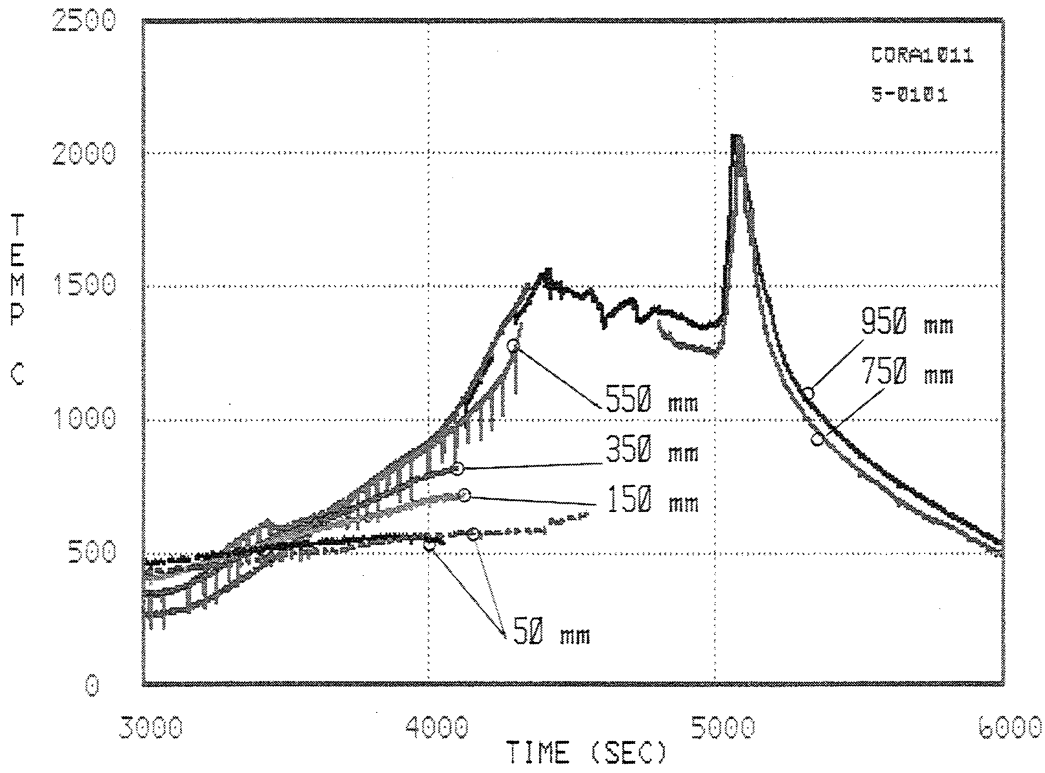

Fig. 19 CORA-17; Temperatures of the channel box walls

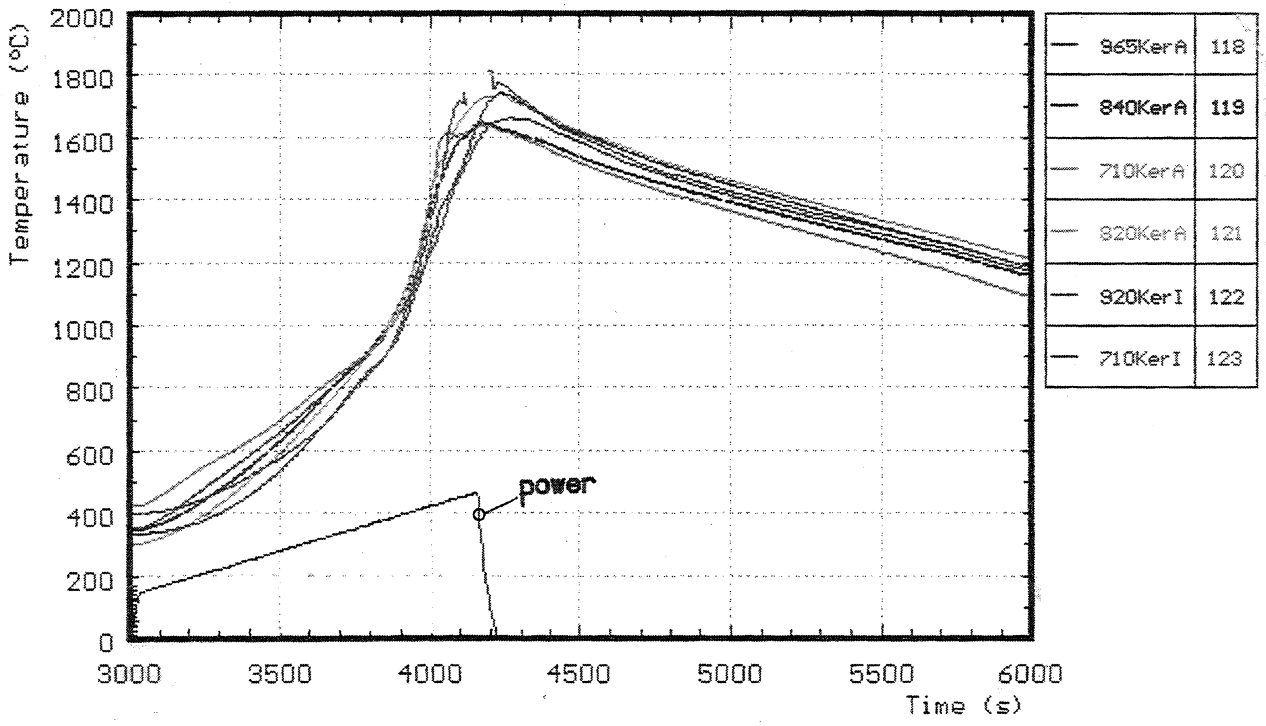

Fig. 20 CORA-18; Bundle temperatures (coolant channel) measured with ceramic protected thermocouples, 710 mm - 965 mm elevation

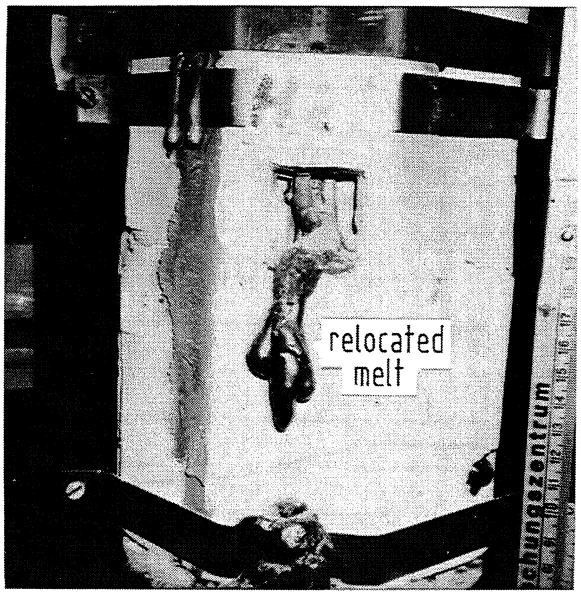

CORA 16-103
200mm elevation
120°

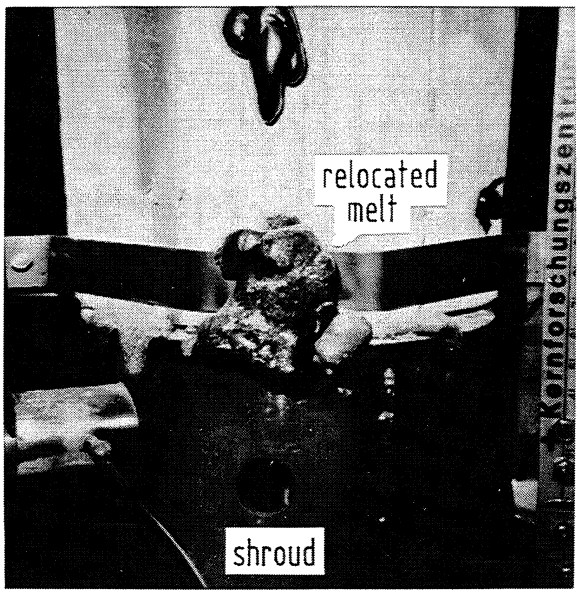

CORA 16-104
70mm elevation
120°

Fig. 21 **Absorber/steel melt that exited the observation windows during test CORA-16 (posttest view)**

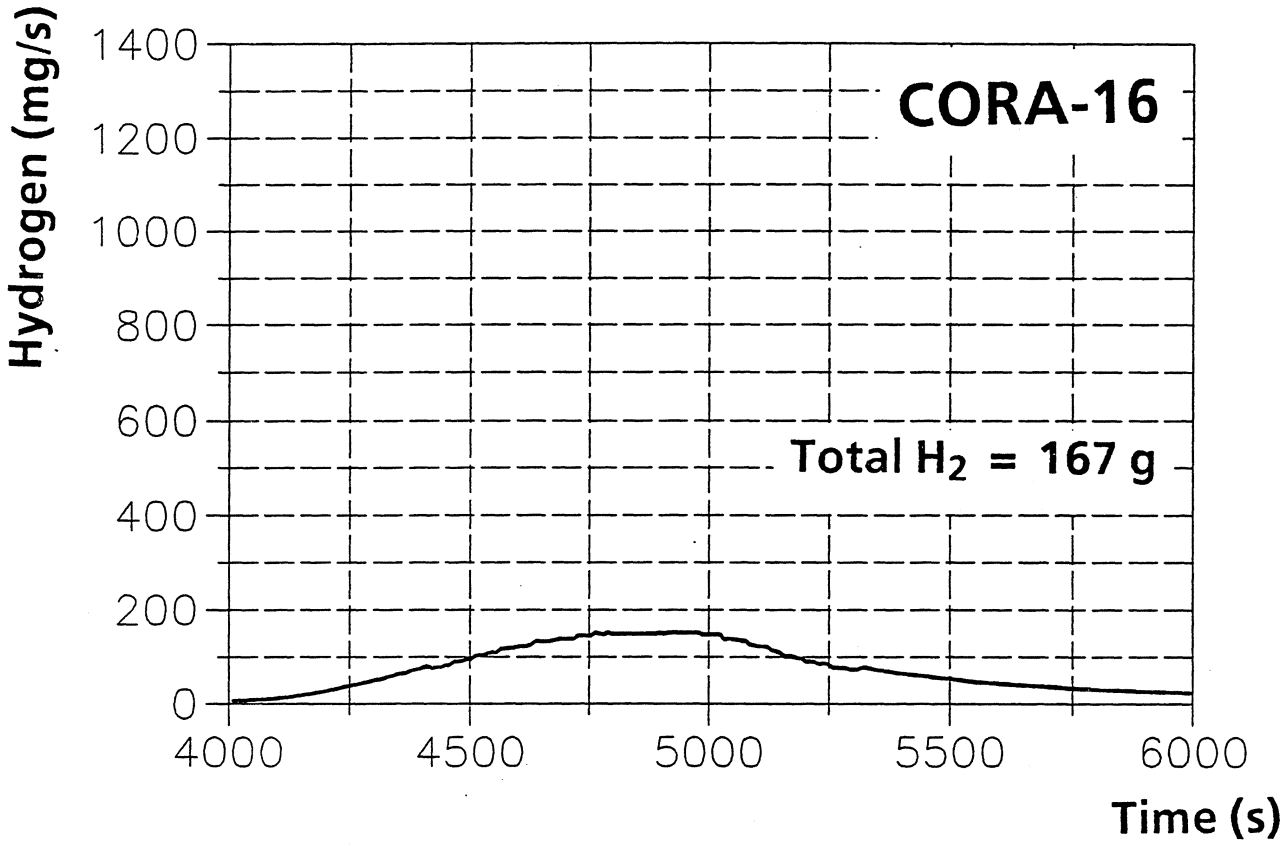

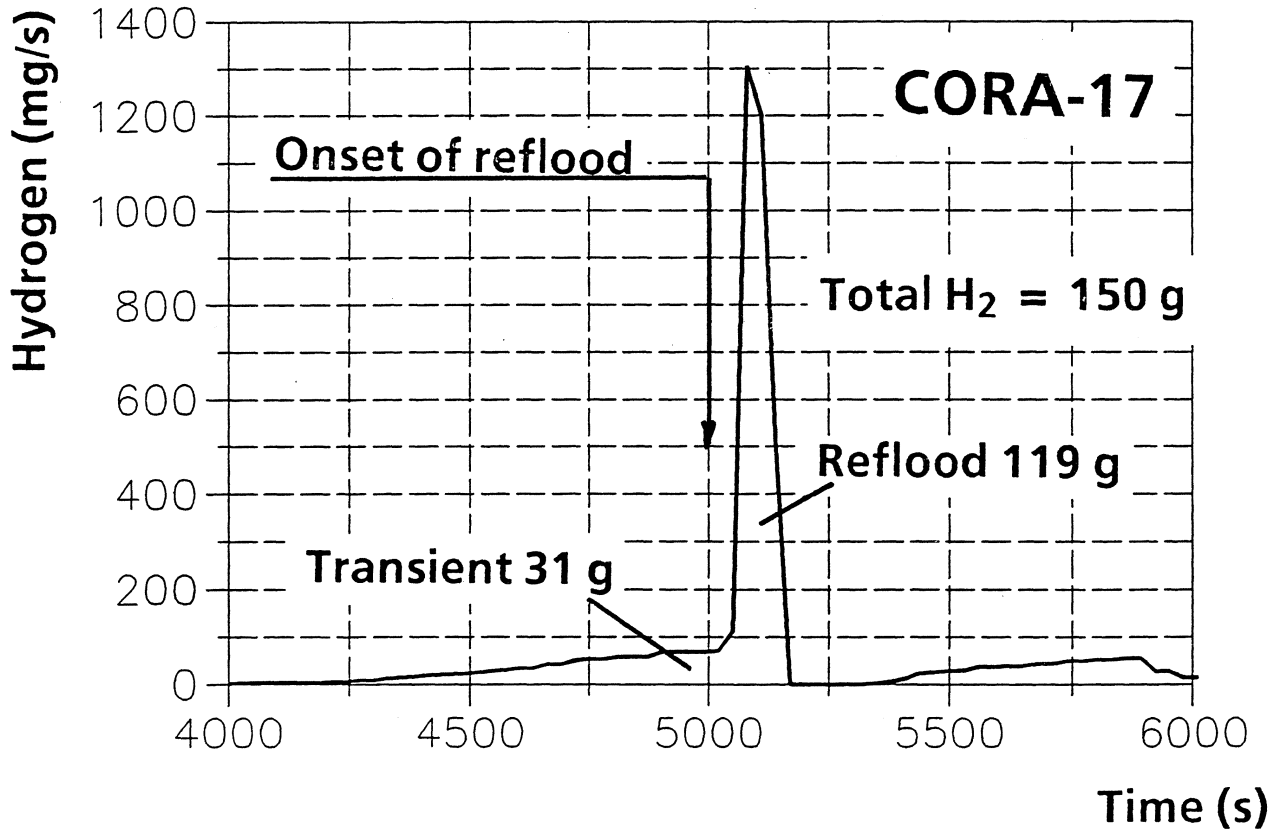

Fig. 22 Hydrogen production during tests CORA-16 (Slow cooldown) and CORA-17 (Reflood)

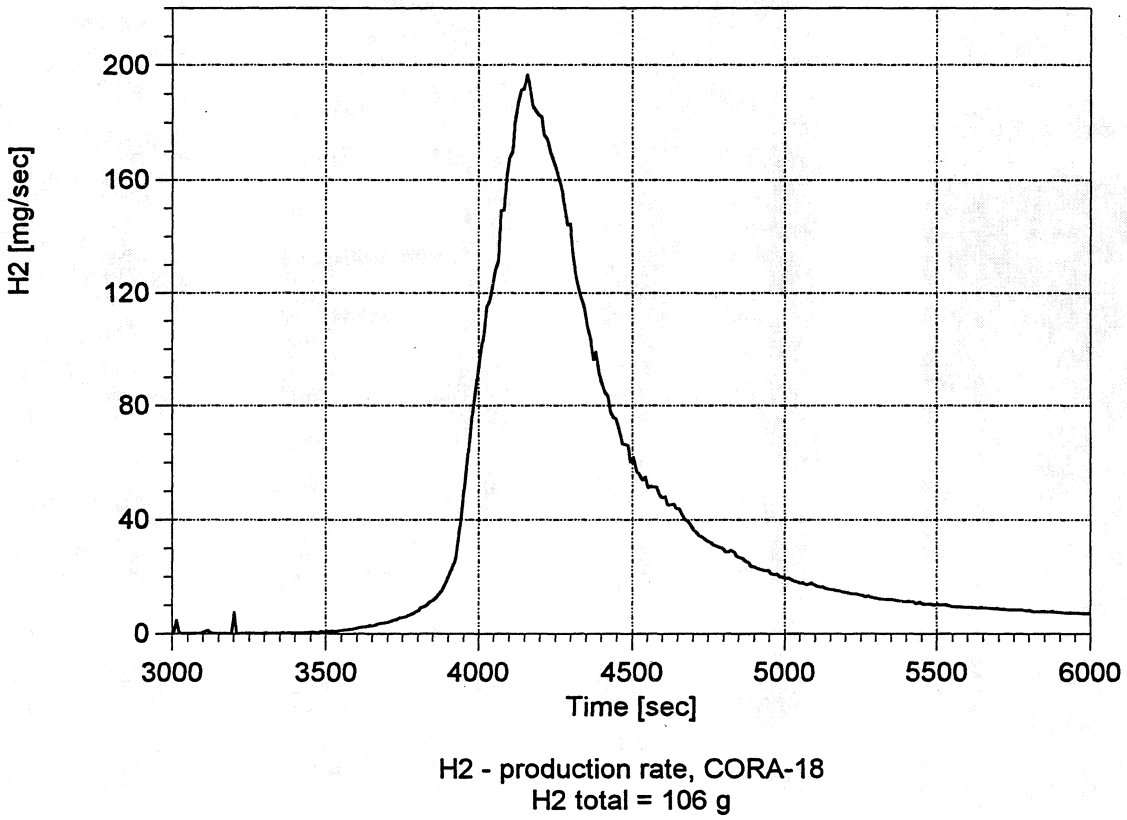

Fig. 23 Hydrogen production during tests CORA-18 (total H_2 = 106 g)

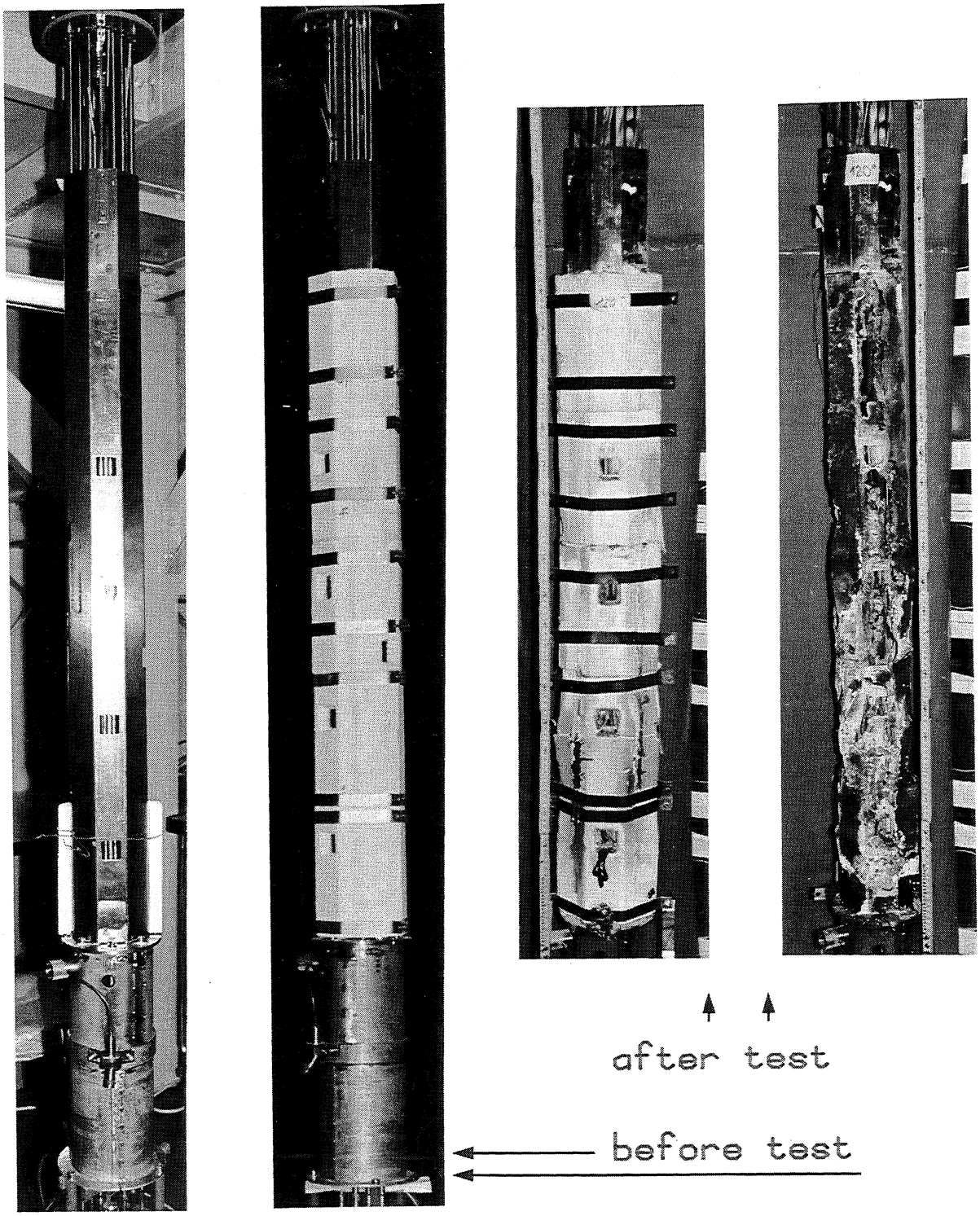

Fig. 24 Appearance of the bundle before and after test CORA-16

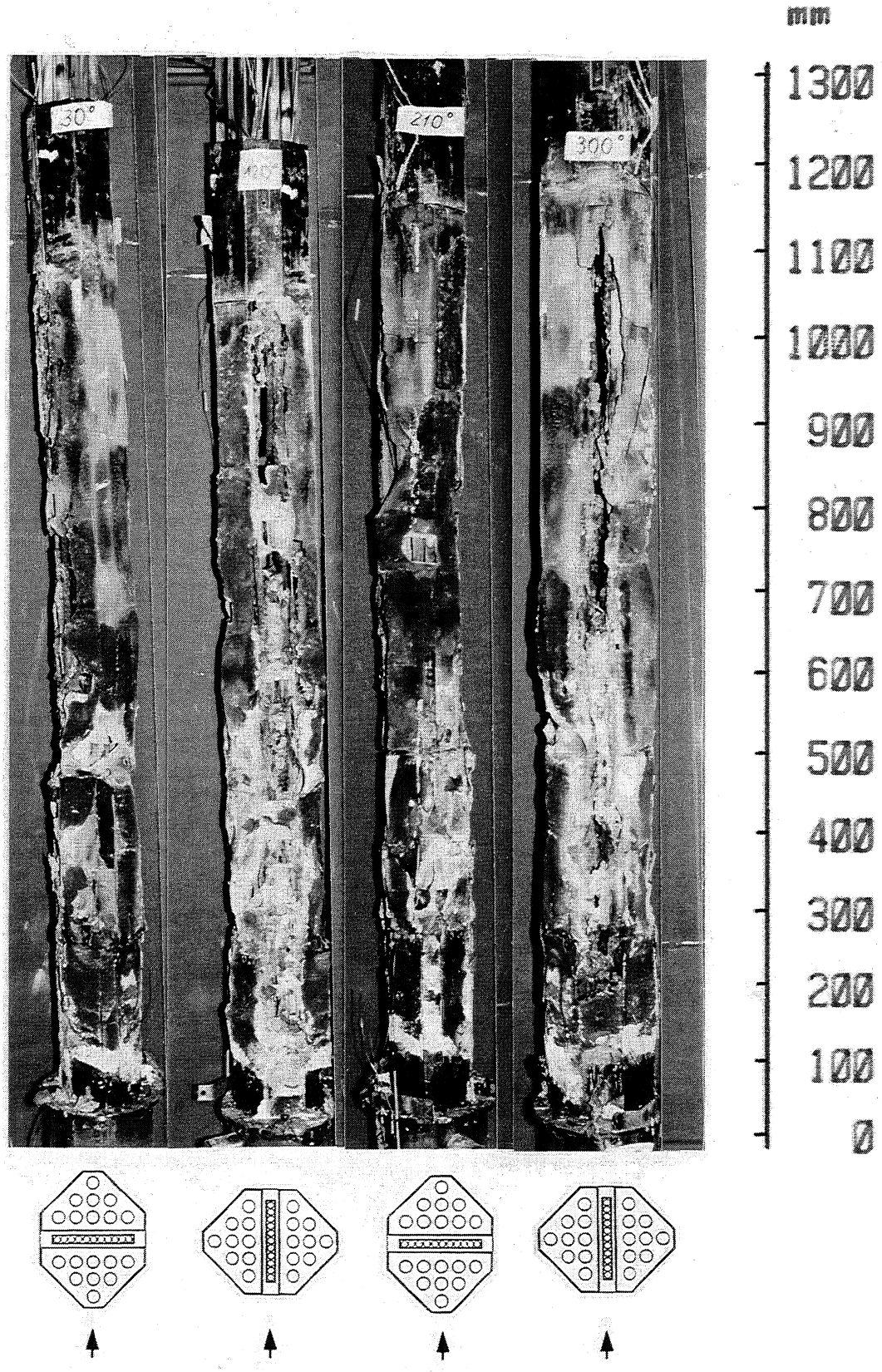

Fig. 25: CORA-16; Overall view of tested bundle before removal of the shroud

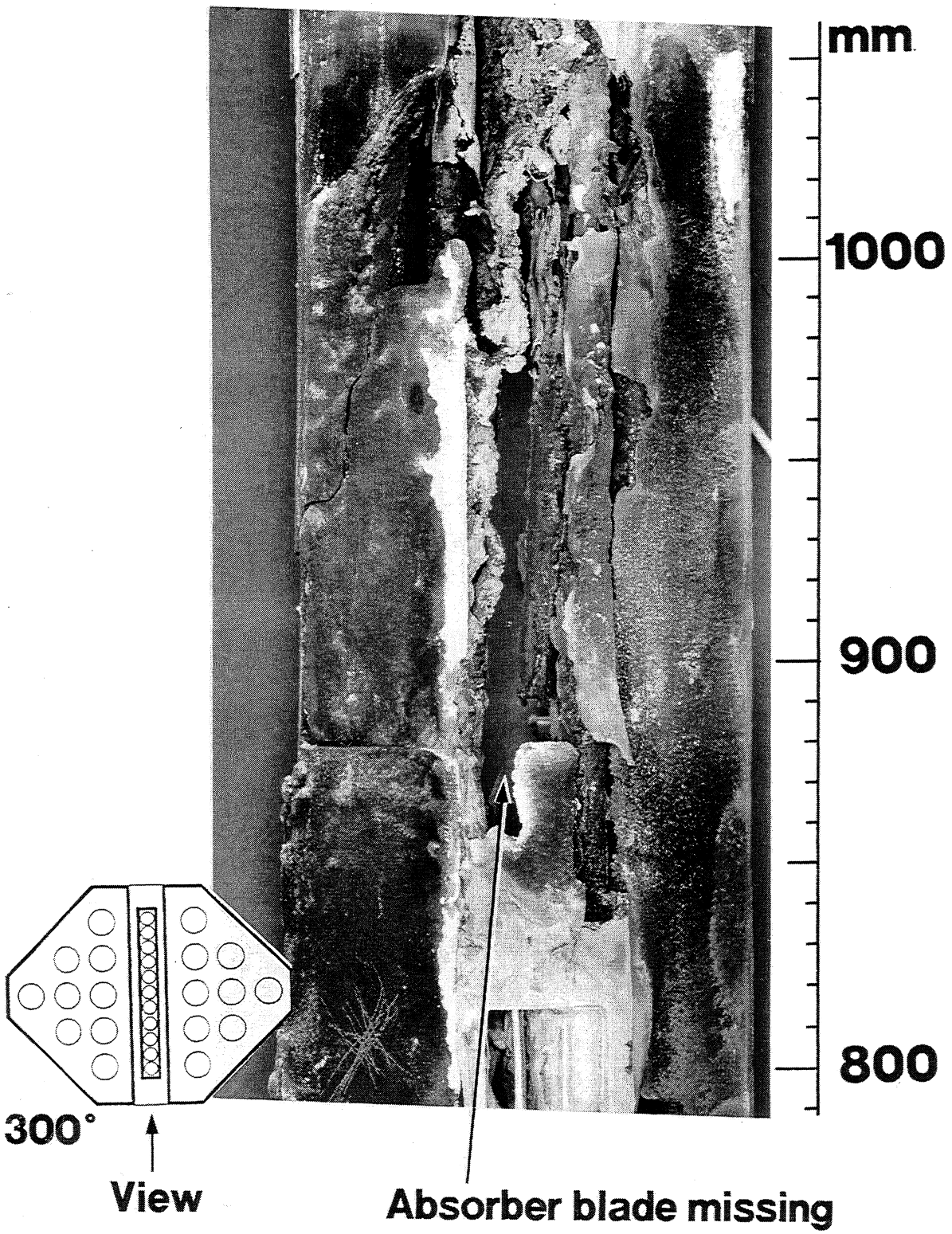

Fig. 26 CORA-16; View of the upper bundle region (300°C) demonstrating that the absorber blade is missing after the test

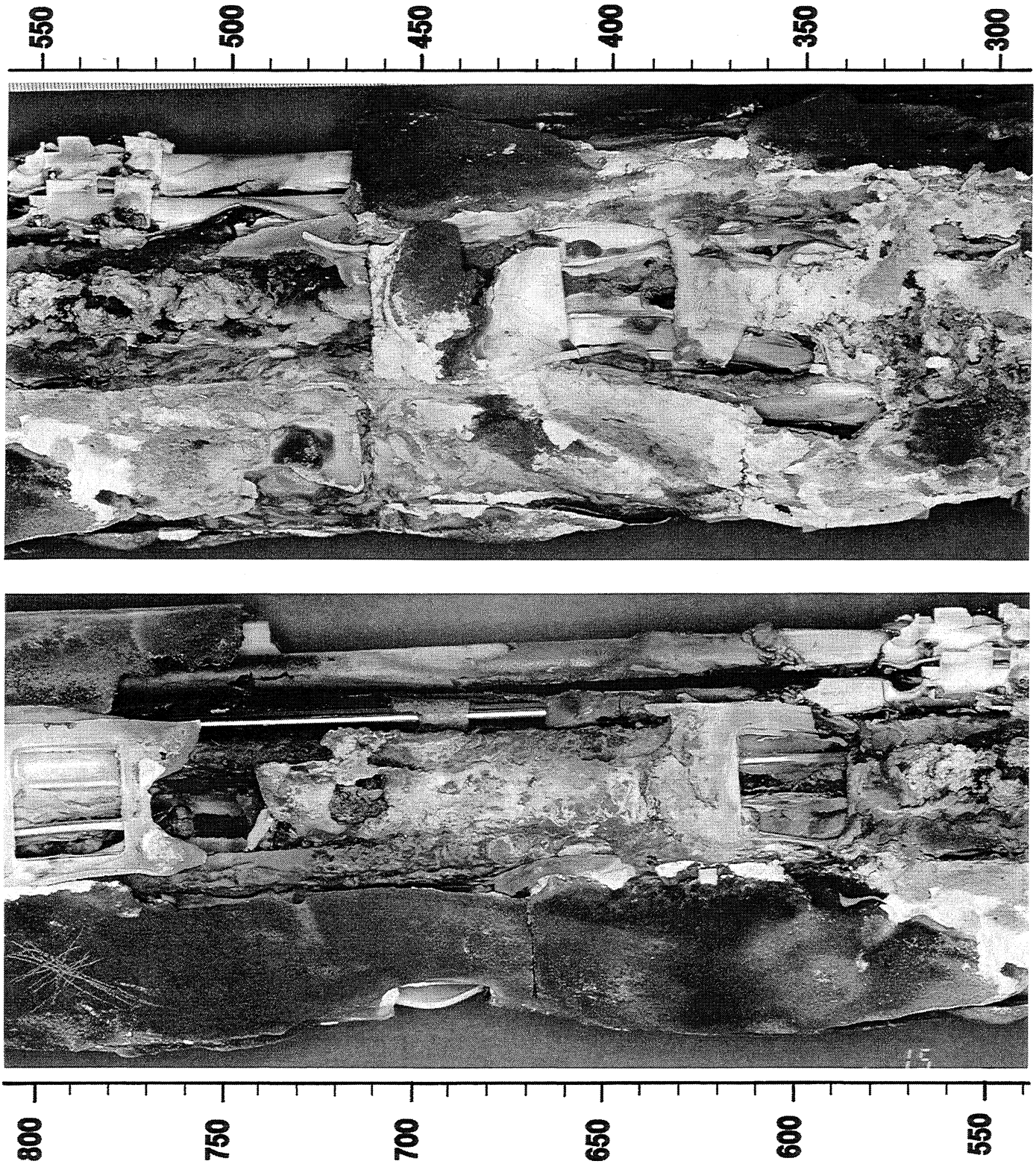

Fig. 27 Posttest appearance of bundle CORA-16, 300 mm - 800 mm, 120° orientation

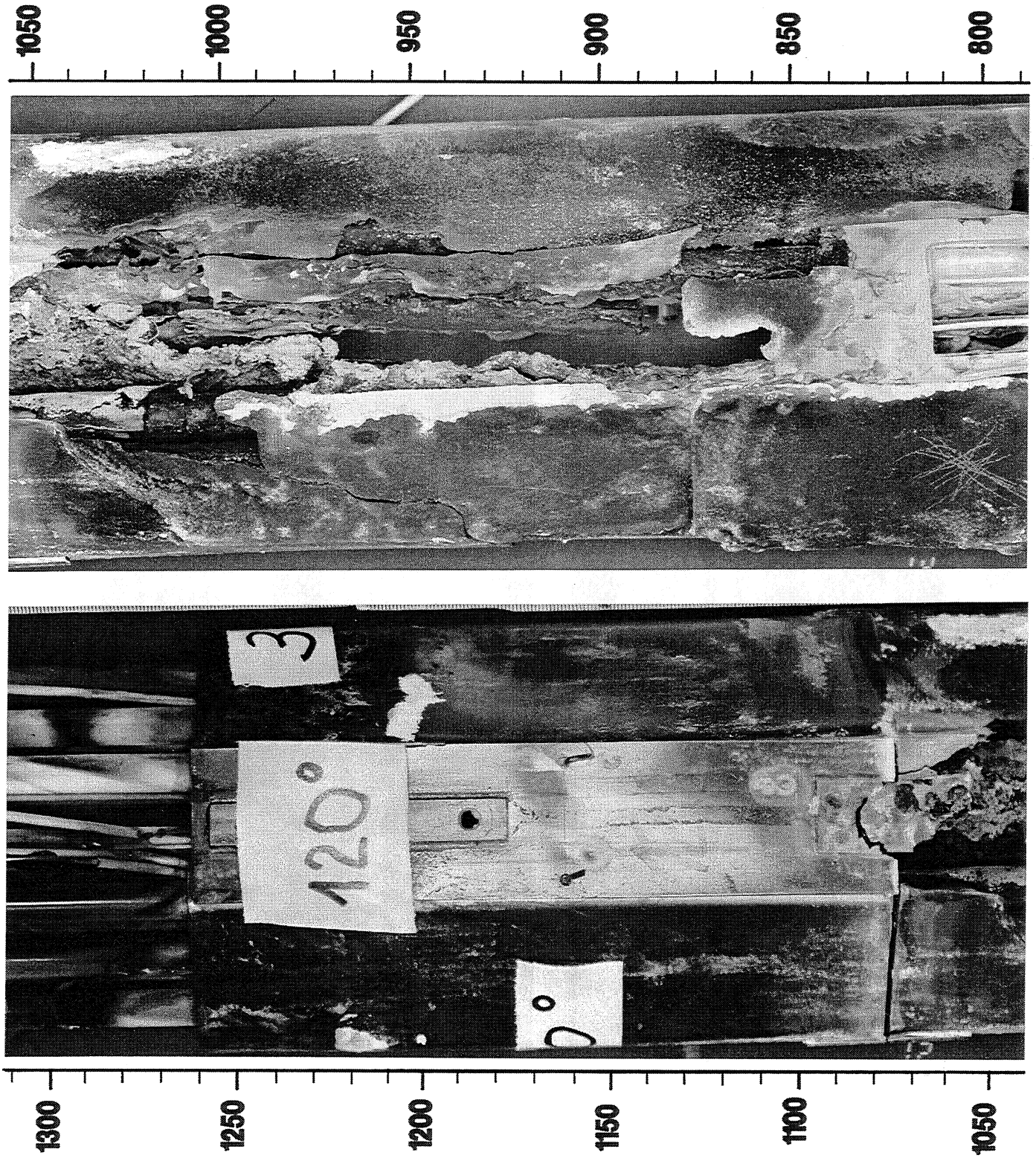

Fig. 28 Posttest appearance of bundle CORA-16, 800 mm - 1300 mm, 120° orientation

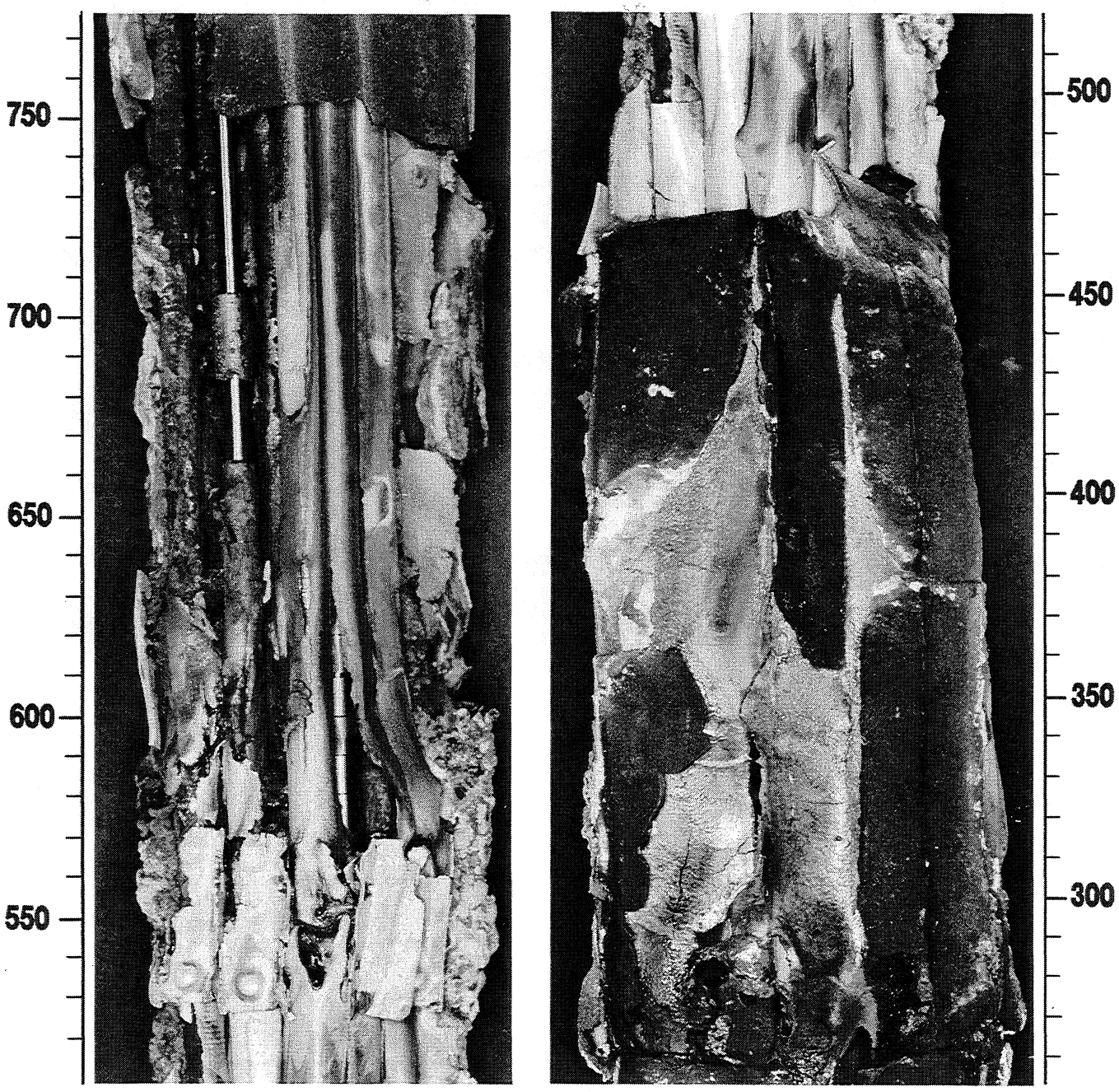

Fig. 29 Posttest appearance of bundle CORA-16, 300 mm - 750 mm, 30° orientation

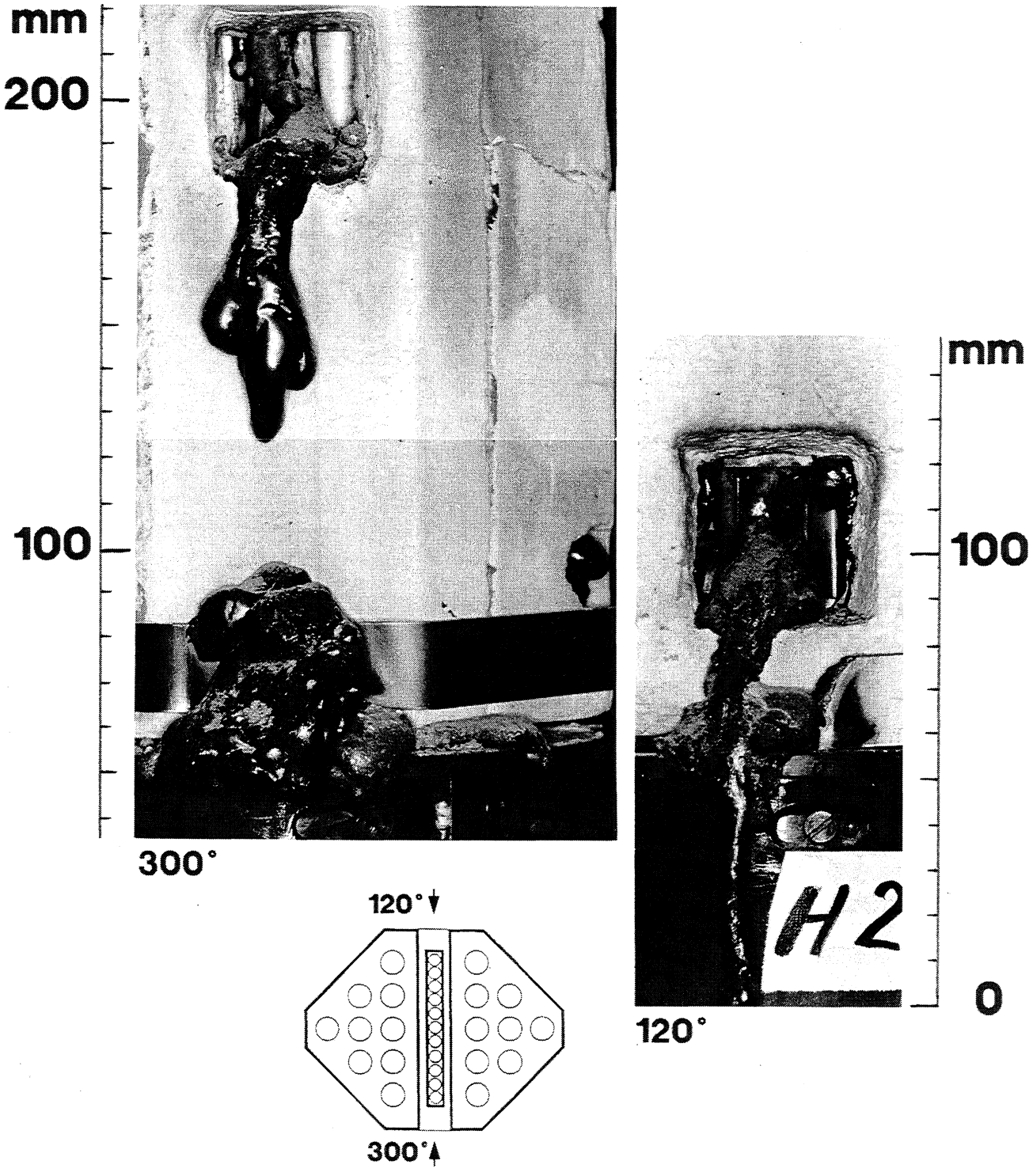

Fig. 30 Exit of absorber/steel melt at observation windows during test CORA-16, posttest view

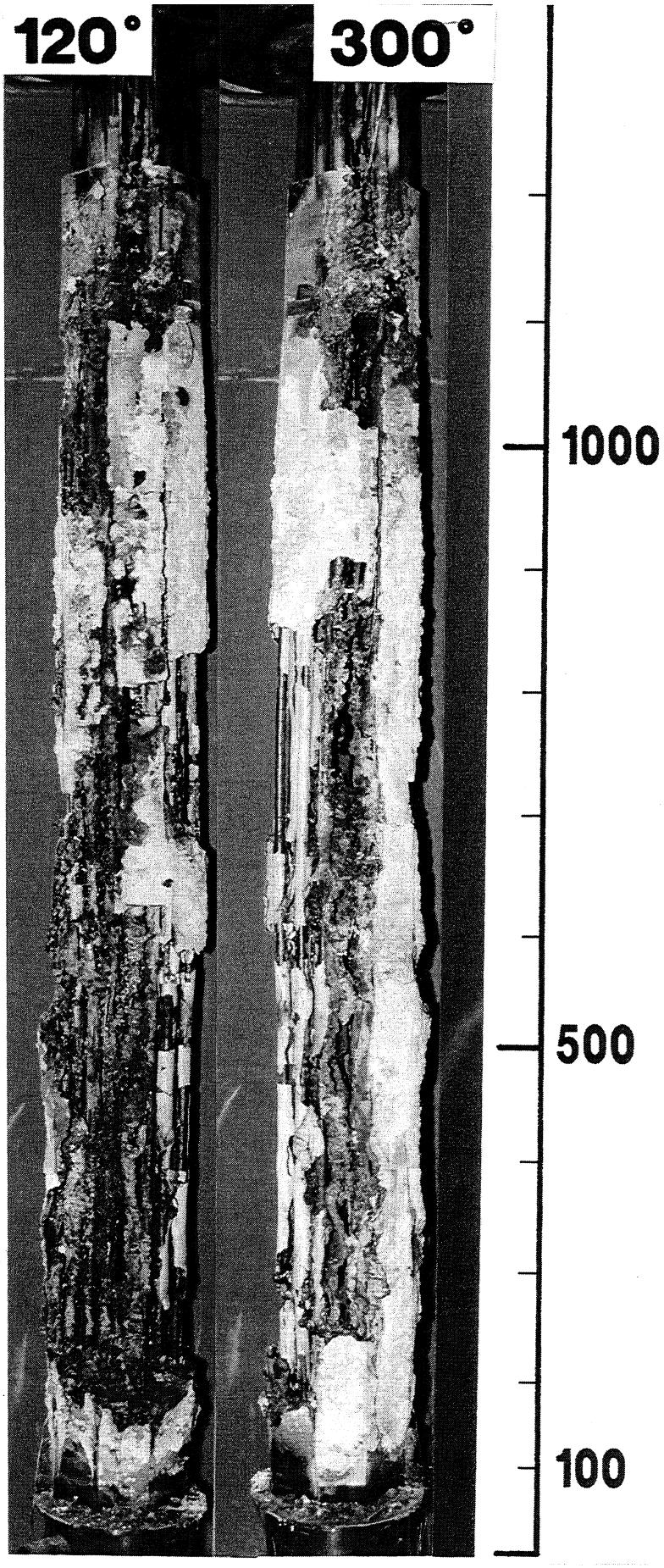

Fig. 31 CORA-17; Posttest appearance after removal of the shroud

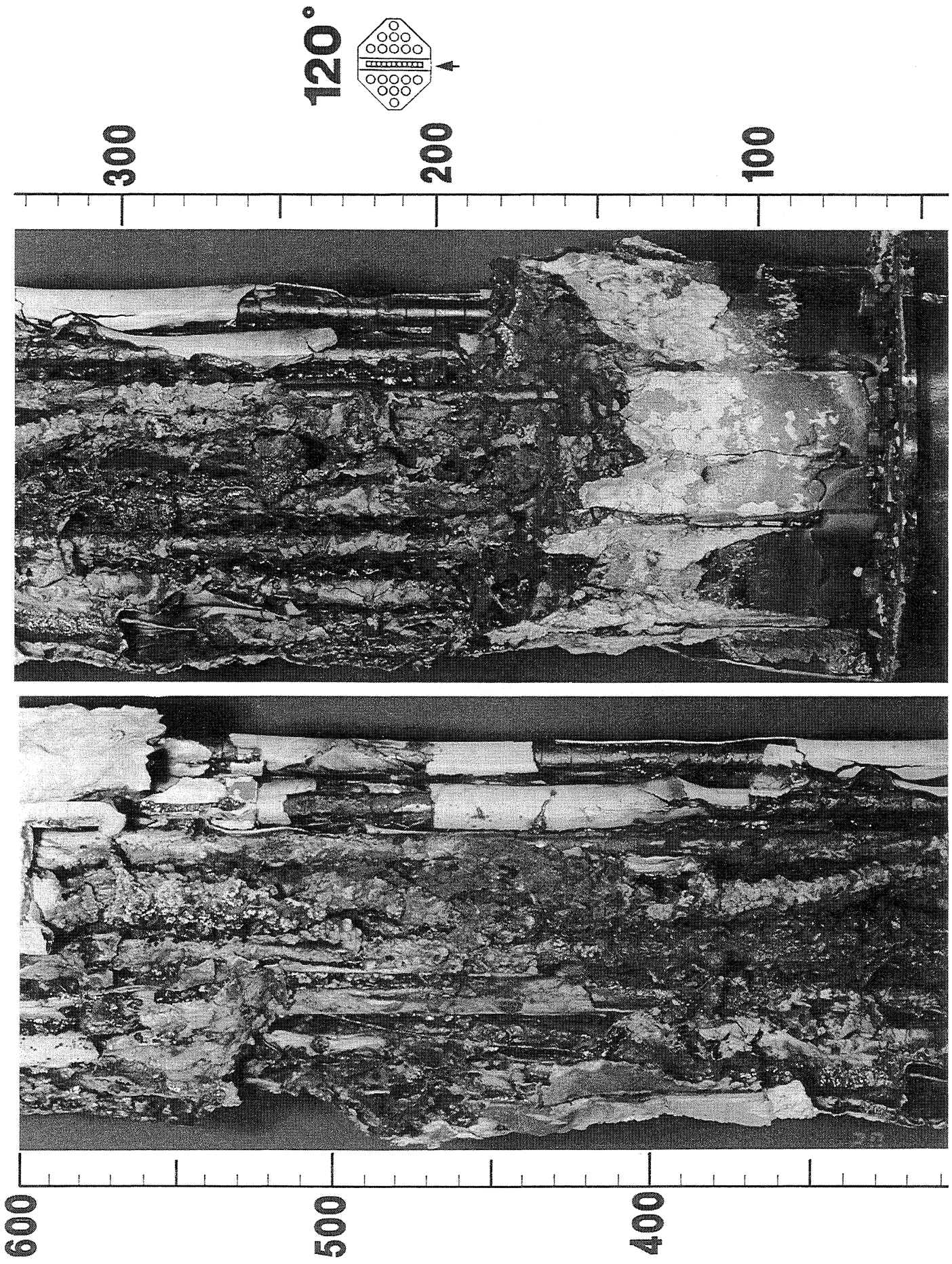

Fig. 32 CORA-17; Posttest view of the lower and central region

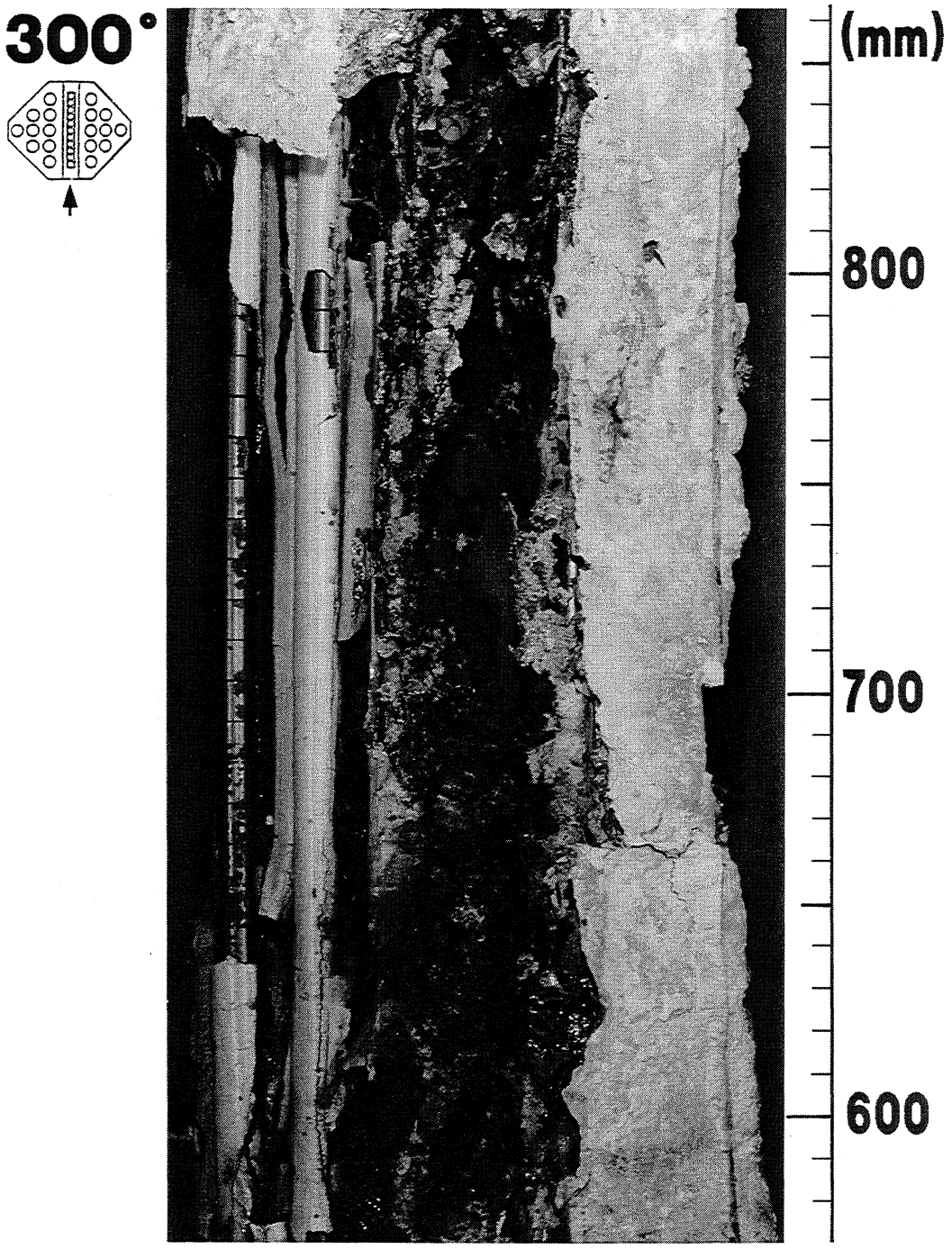

Fig. 33 CORA-17; Posttest view of the upper region

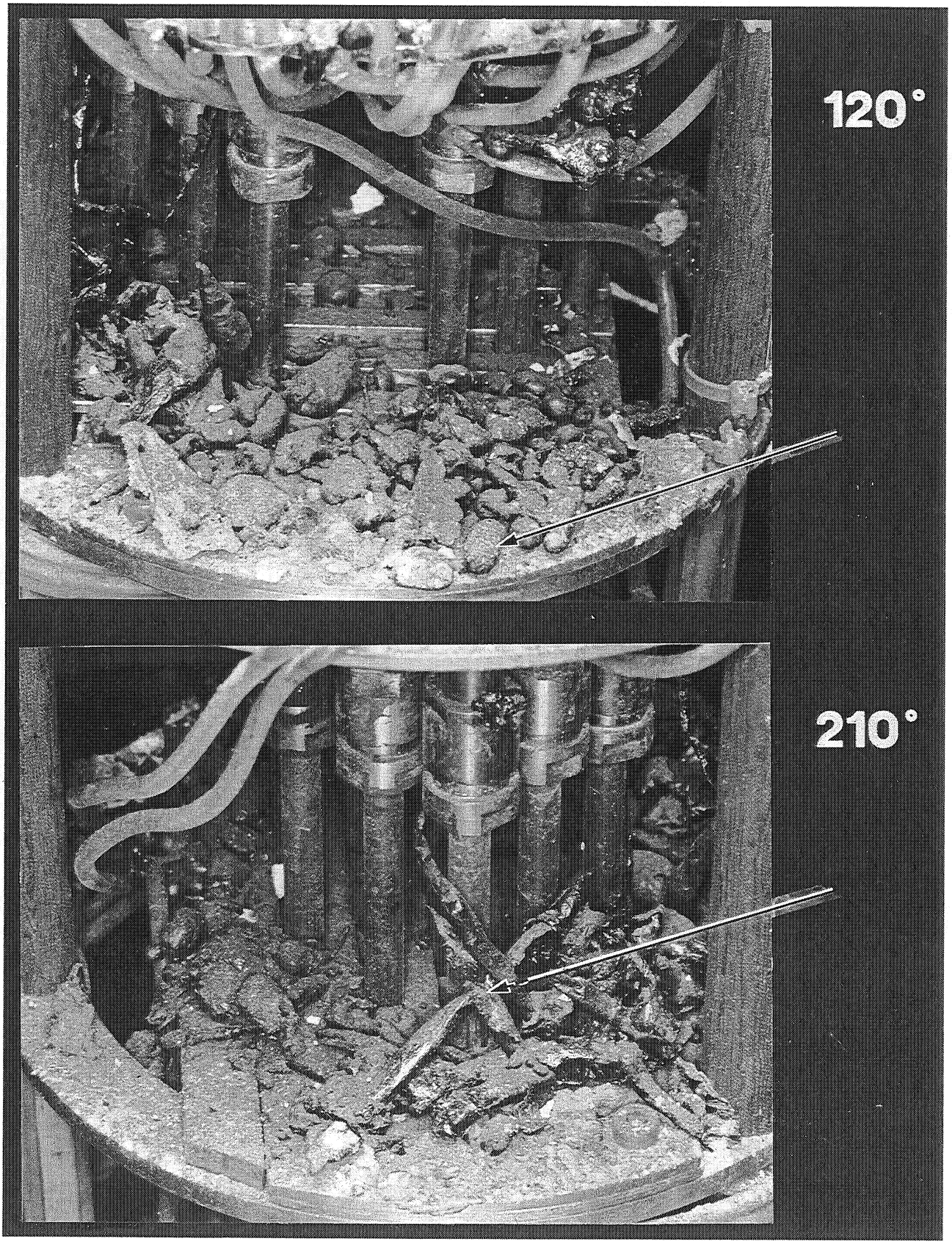

Fig. 34 CORA-17; Melt refrozen in the water of the quench cylinder

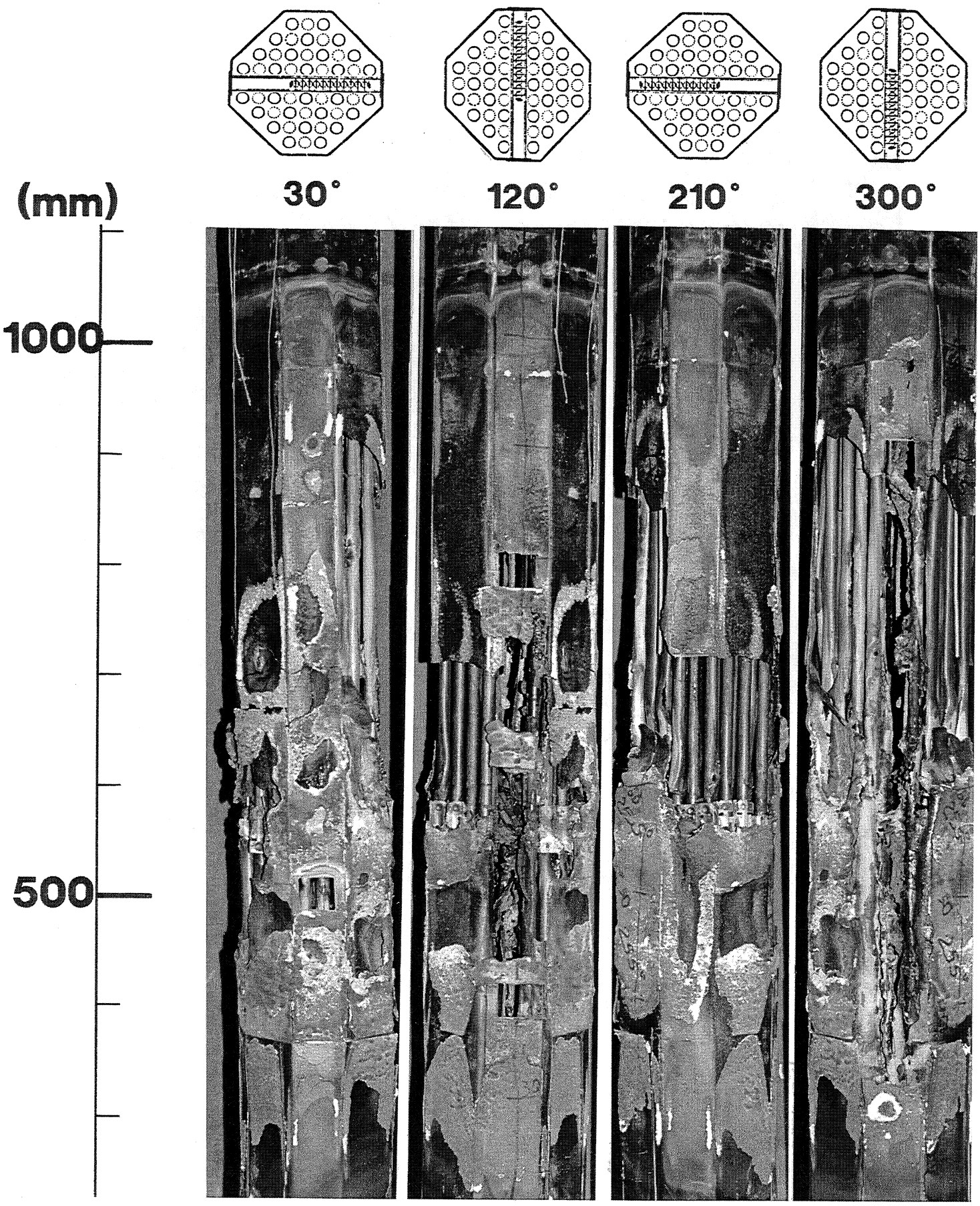

Fig. 35 CORA-18; Overall view of the bundle from four different directions

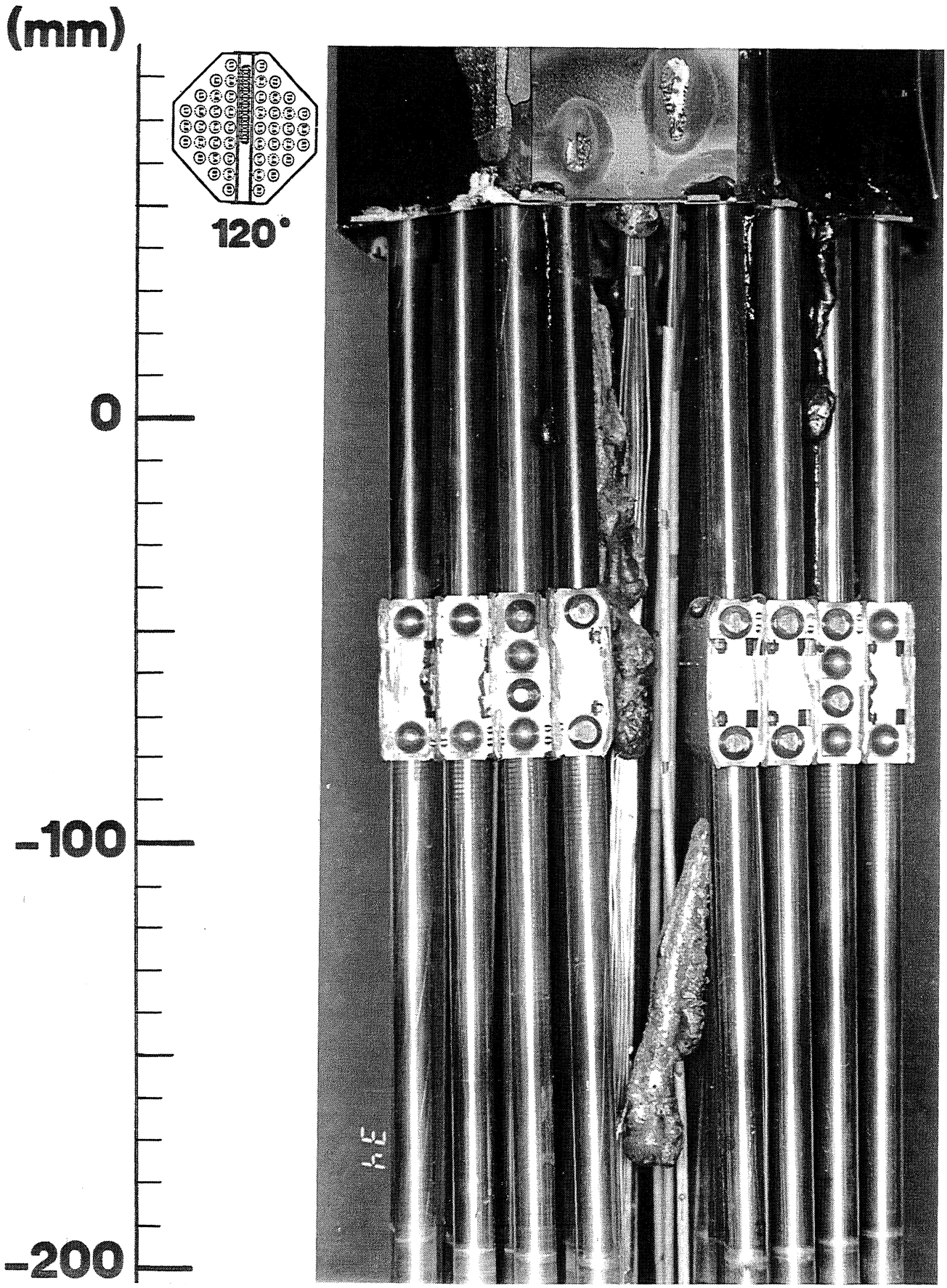

Fig. 36 Posttest appearance 7 bundle CORA-18, -200 - 80 mm, 120°

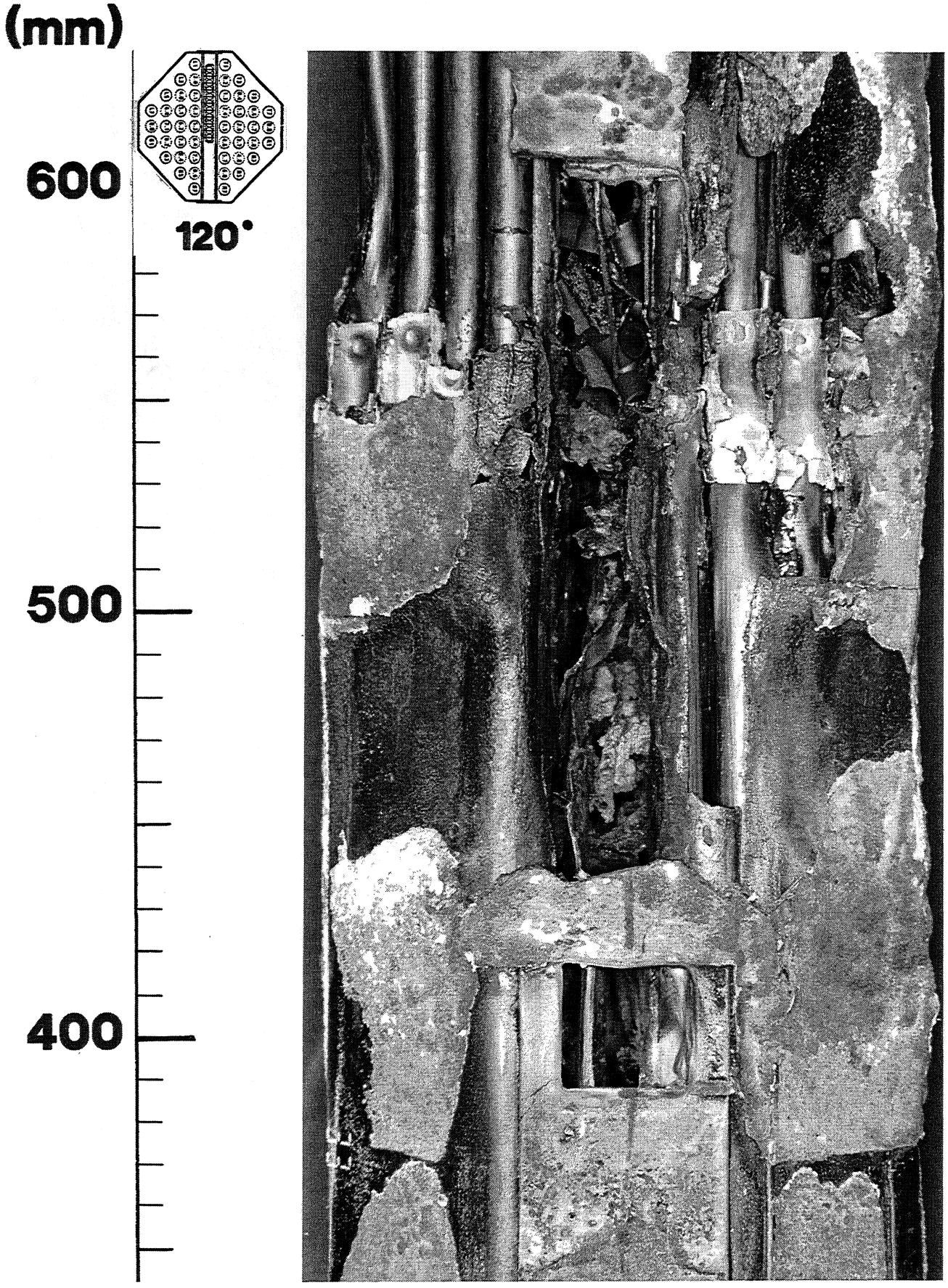

Fig. 37 Posttest appearance 7 bundle CORA-18, 350 - 600 mm, 120°

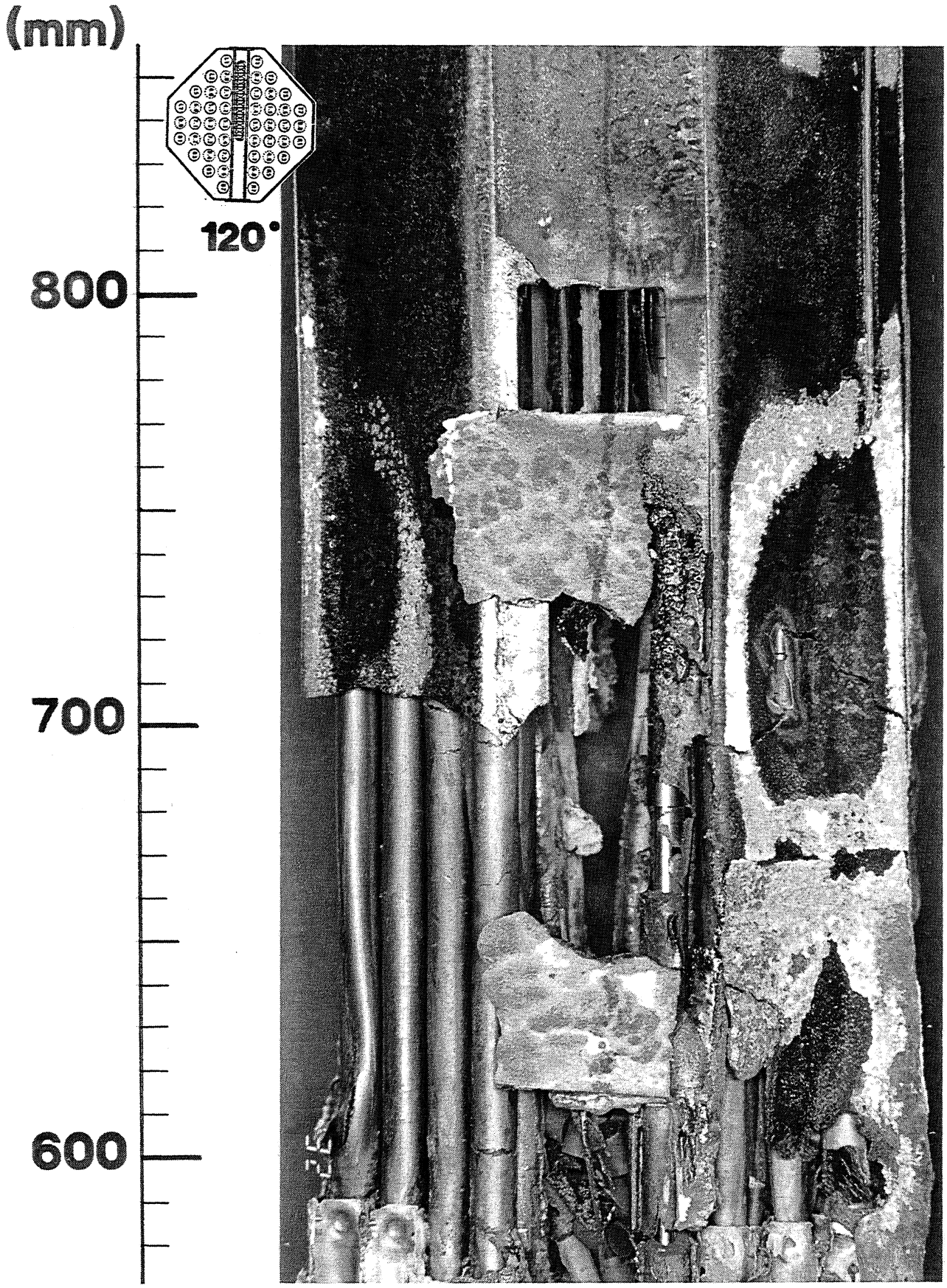

Fig. 38 Posttest appearance of bundle CORA-18, 600 - 850 mm, 120°

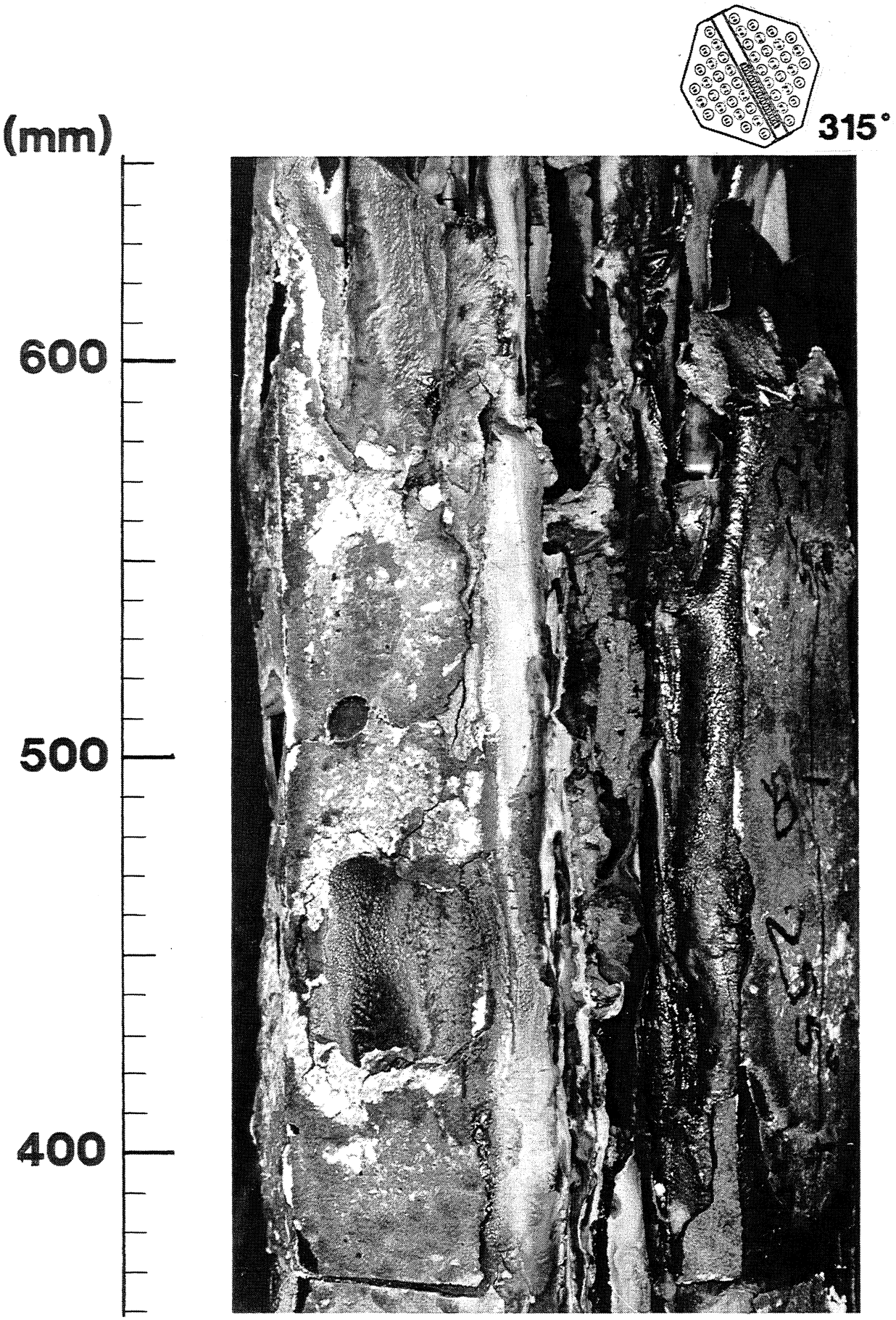

Fig. 39 Posttest appearance of bundle CORA-18, 400 - 650 mm, 315°

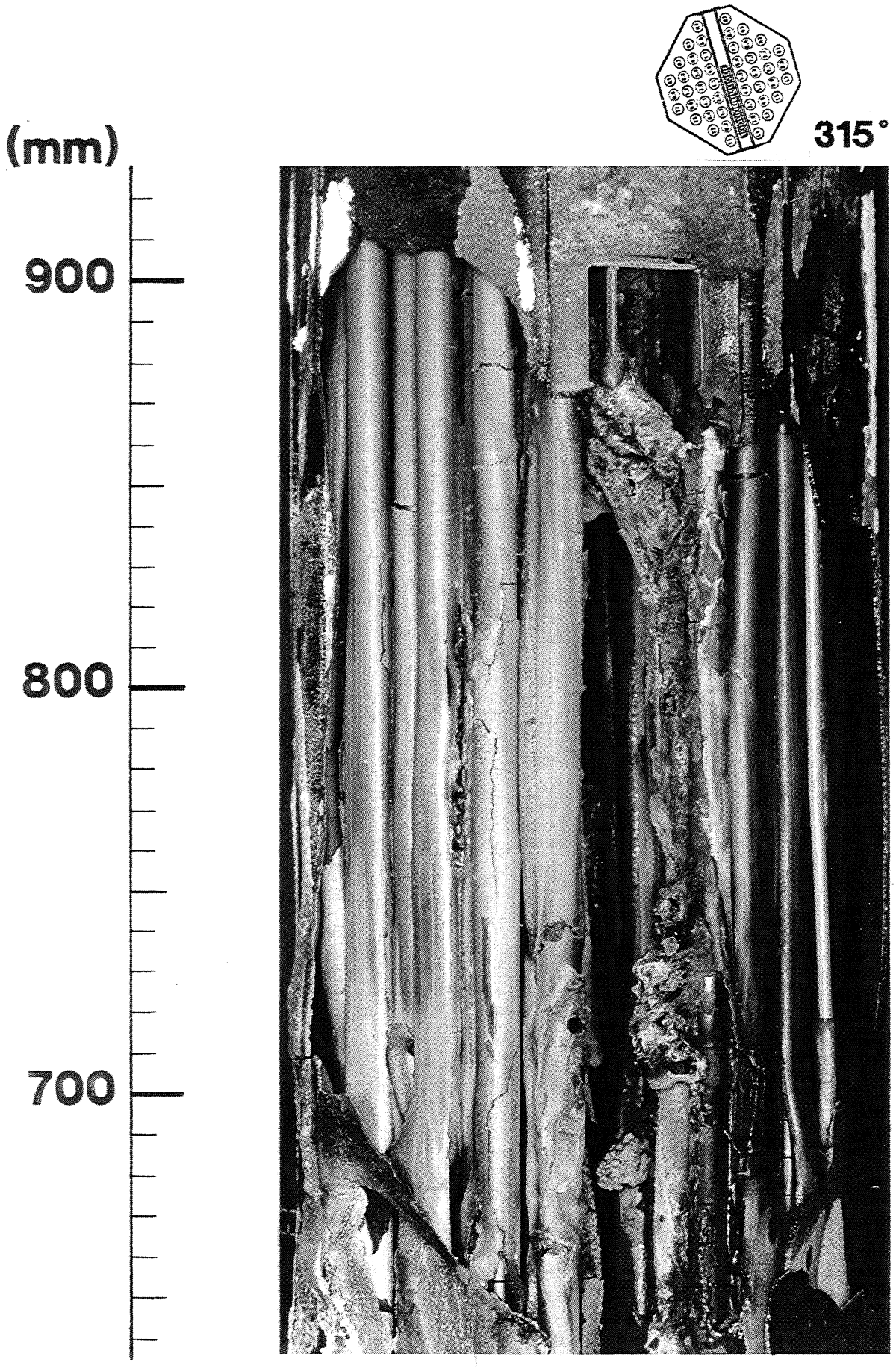

Fig. 40 Posttest appearance of bundle CORA-18, 650 - 900 mm, 315°

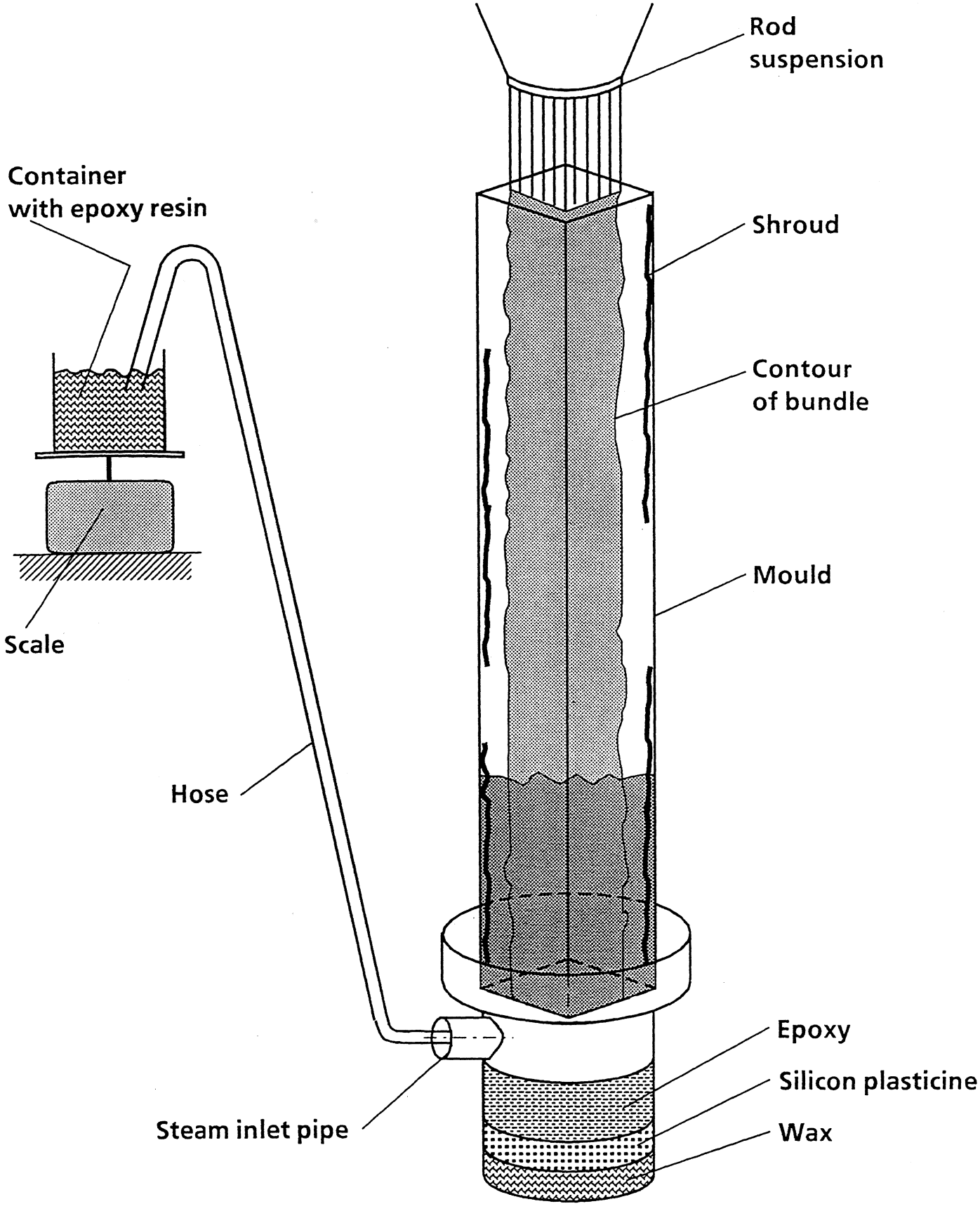

Fig. 41 Epoxying process of the tested bundle

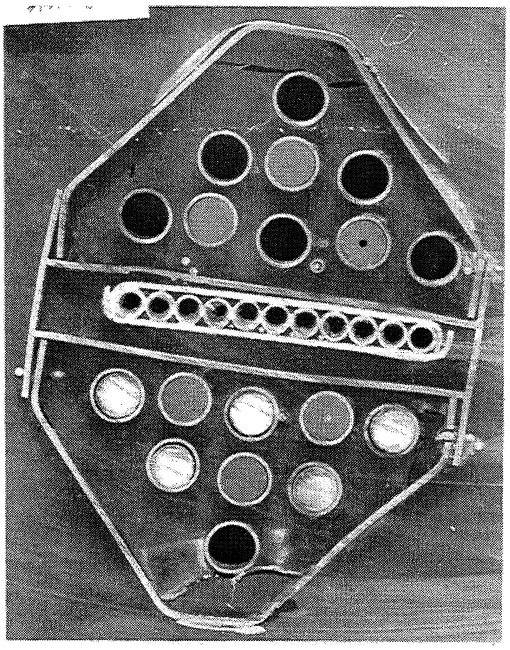

1145mm

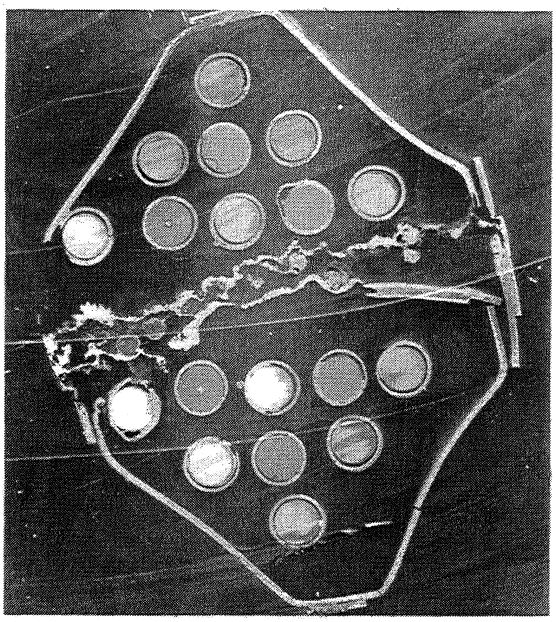

1050mm

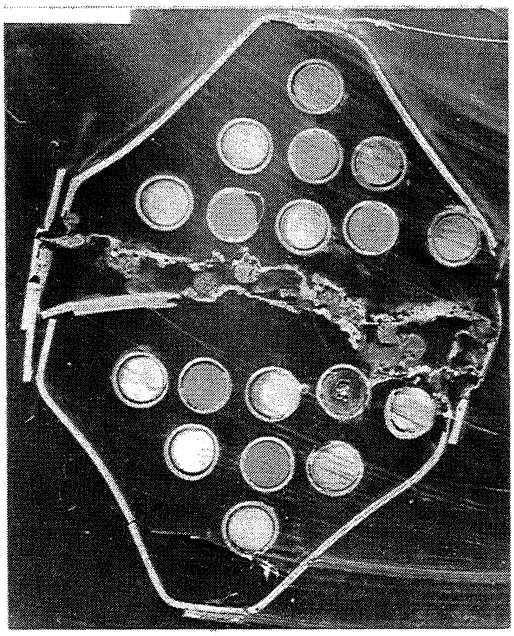

1052mm

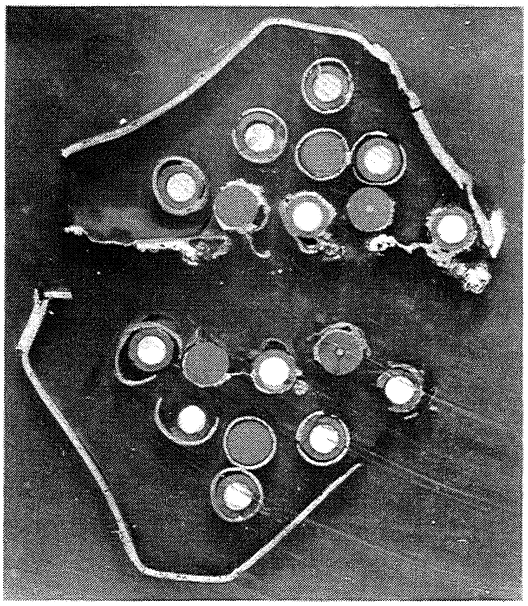

950mm

Fig. 42 Horizontal cross sections of bundle CORA-16

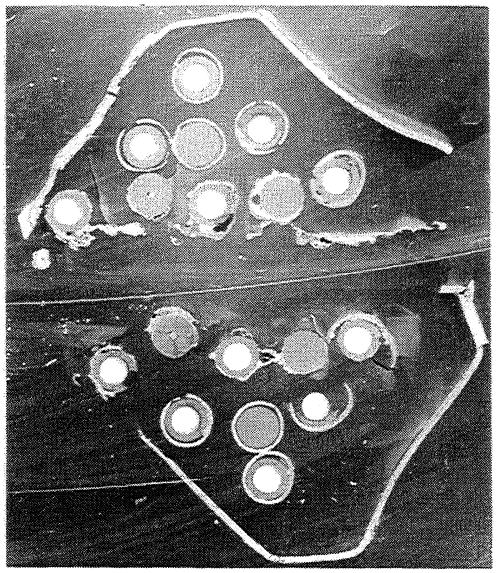

836mm

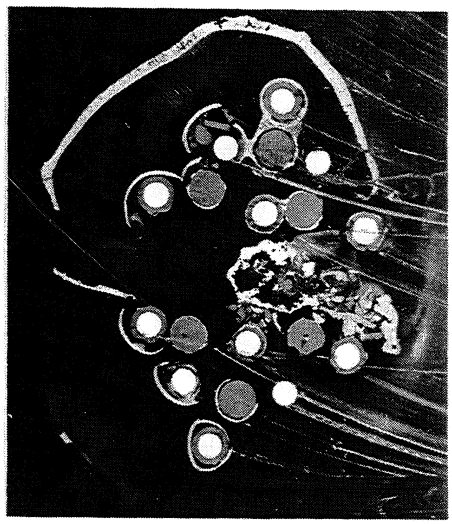

724mm

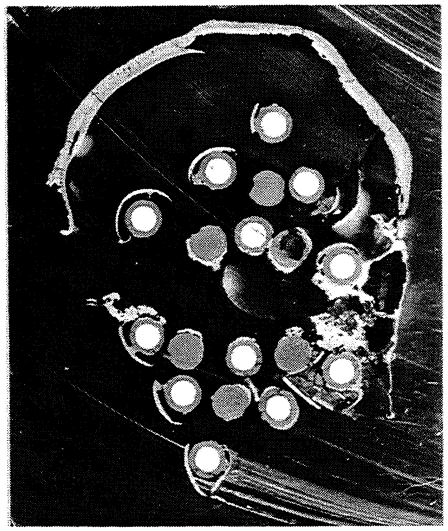

612mm

Fig. 43 Horizontal cross sections of bundle CORA-16

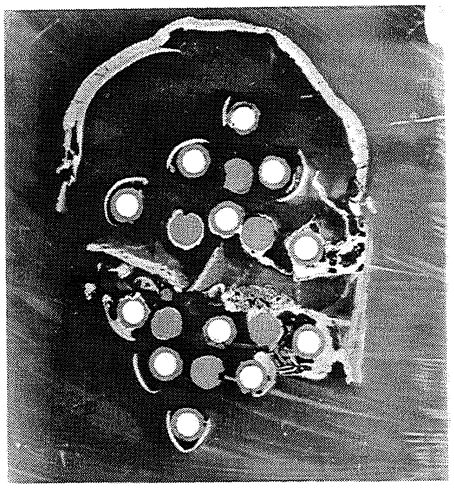

597mm

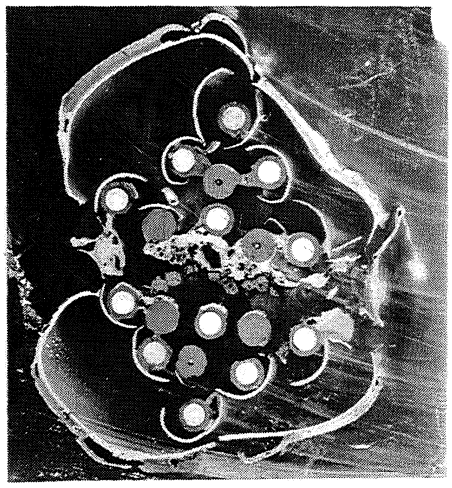

412mm

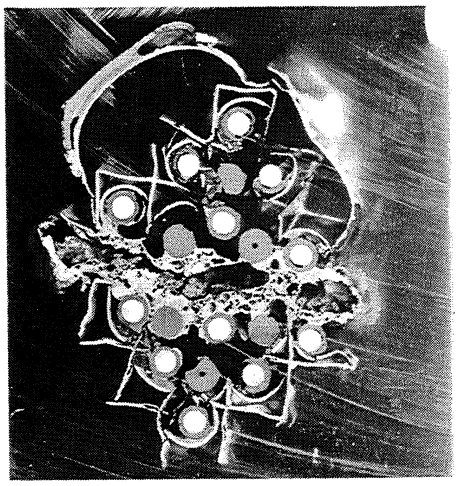

512mm

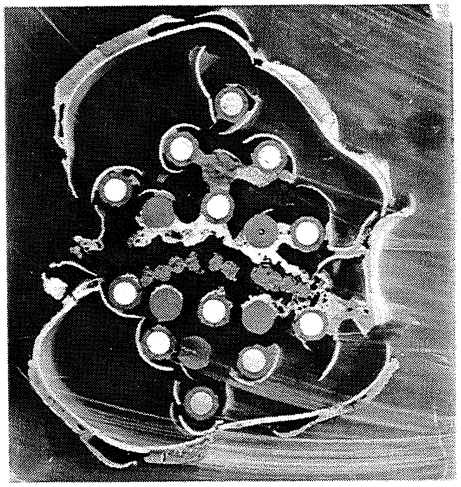

397mm

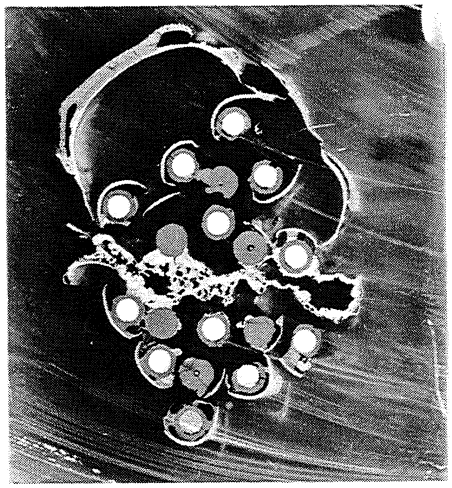

497mm

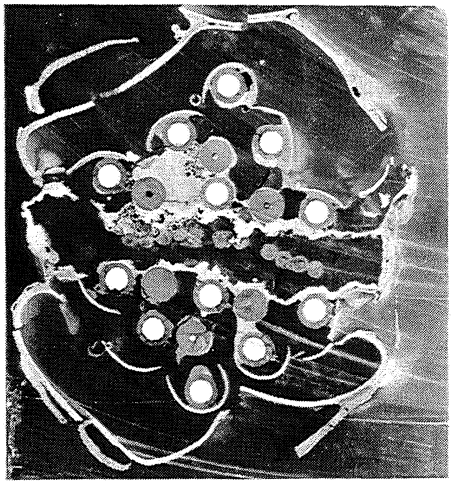

312mm

Fig. 44 Horizontal cross sections of bundle CORA-16

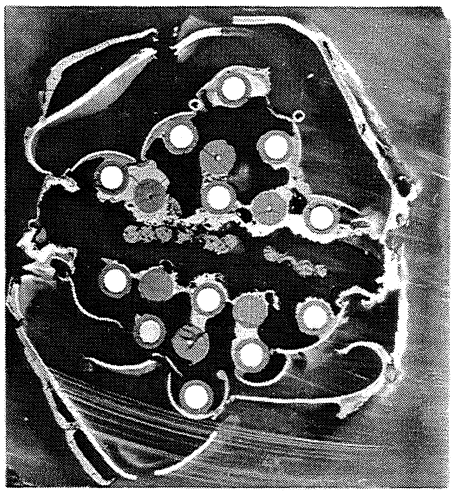

297mm

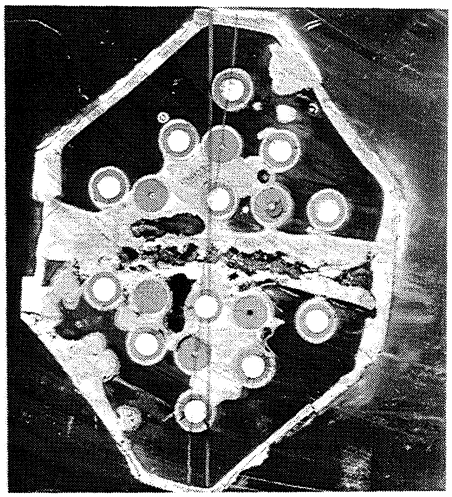

112mm

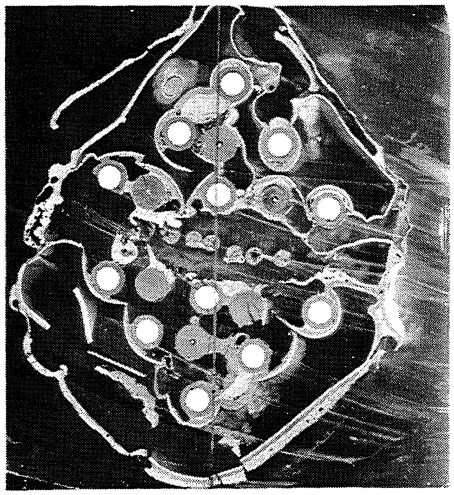

212mm

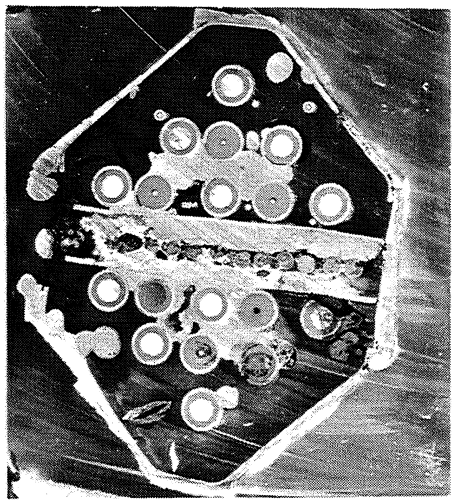

97mm

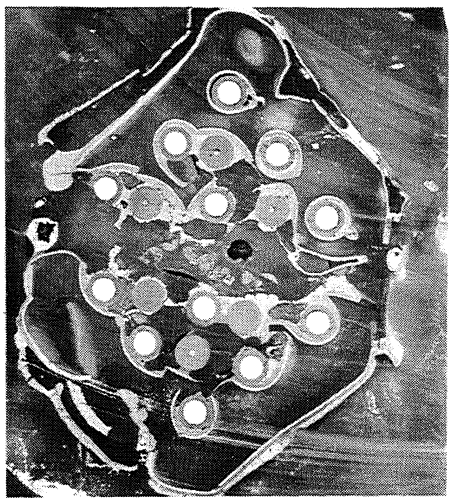

197mm

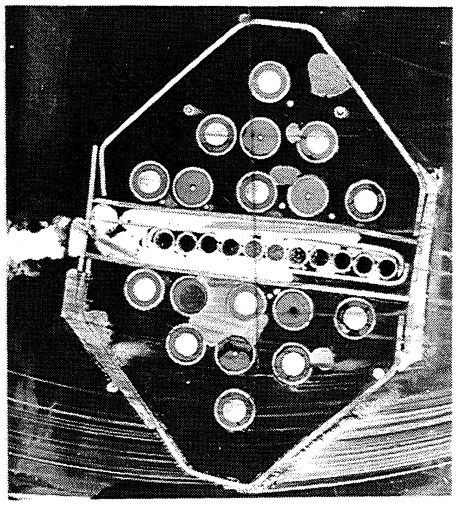

65mm

Fig. 45 Horizontal cross sections of bundle CORA-16

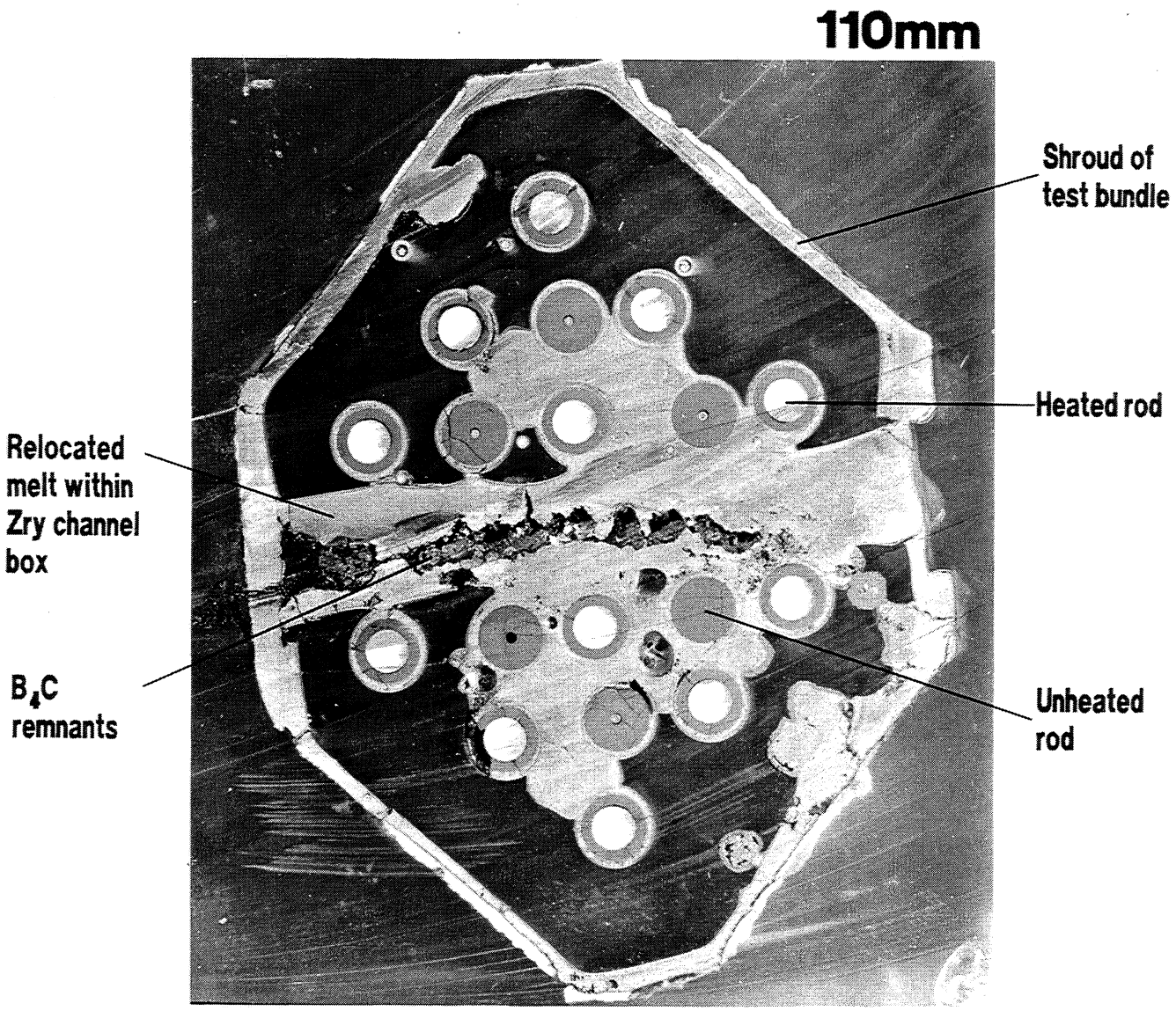

Fig. 46 Cross section of bundle CORA-16 at 110 mm

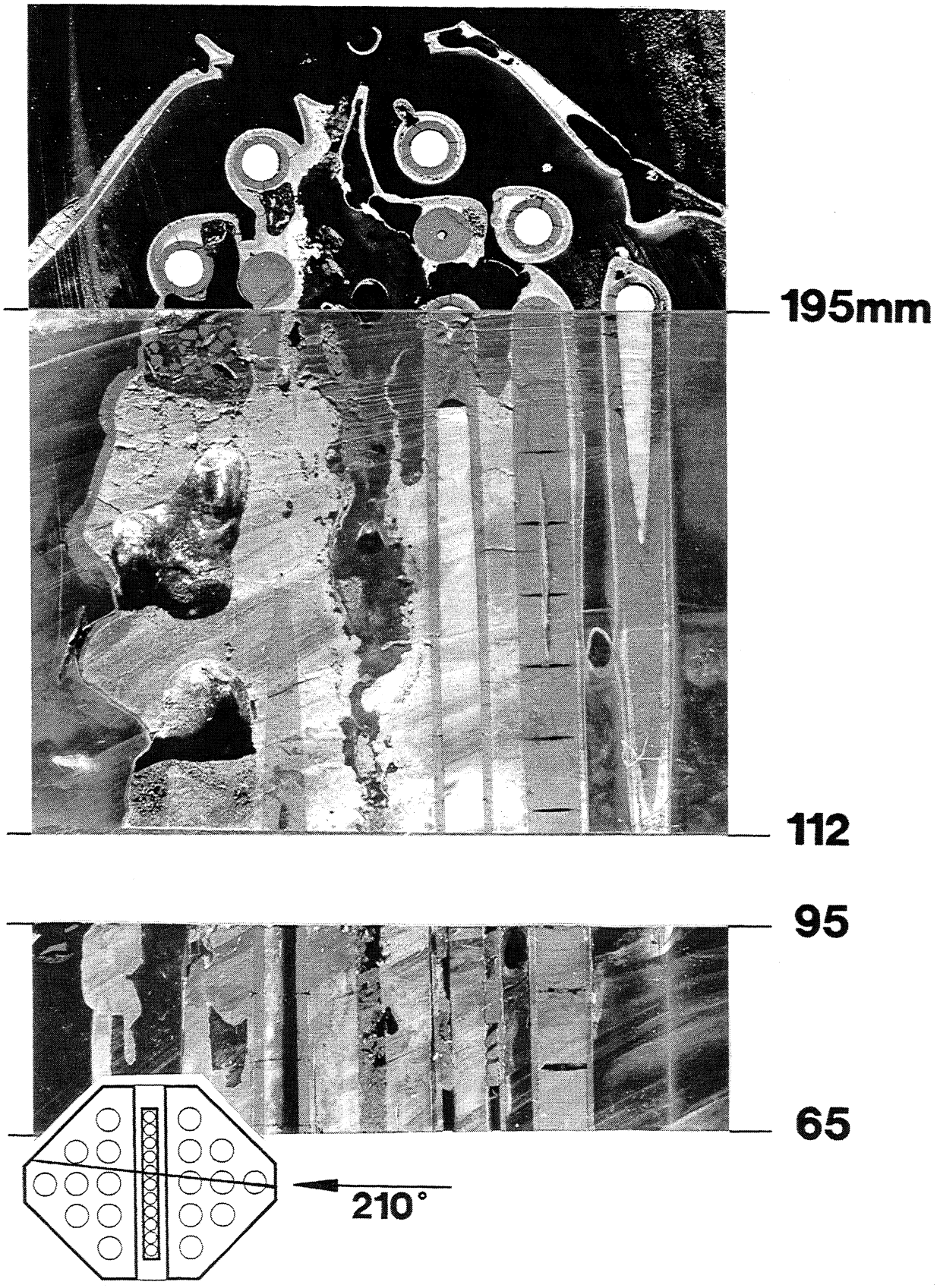

Fig. 47 Vertical cross section of the lower region of bundle CORA-16

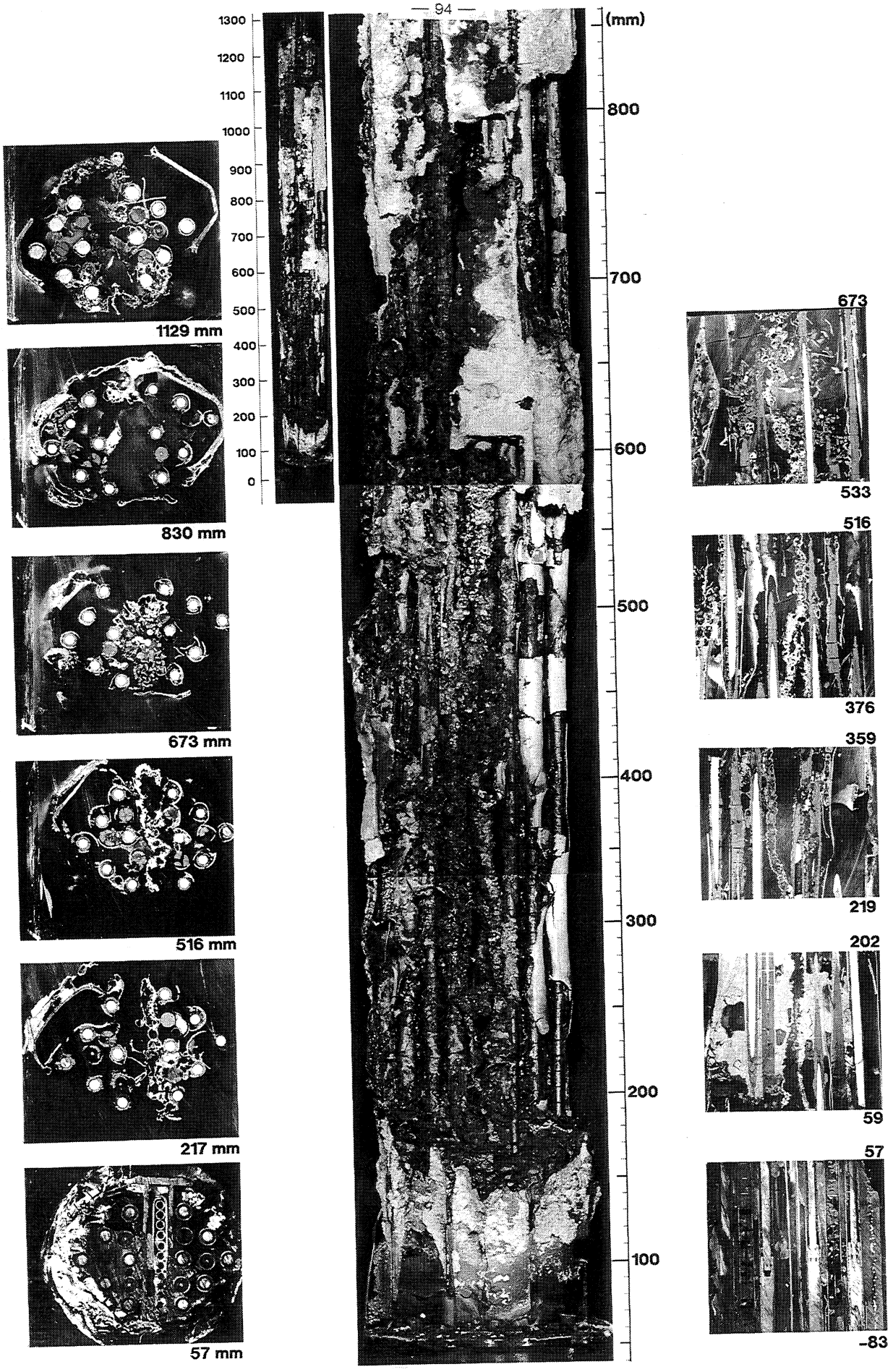

Fig. 48 Posttest view and cross sections of bundle CORA-17

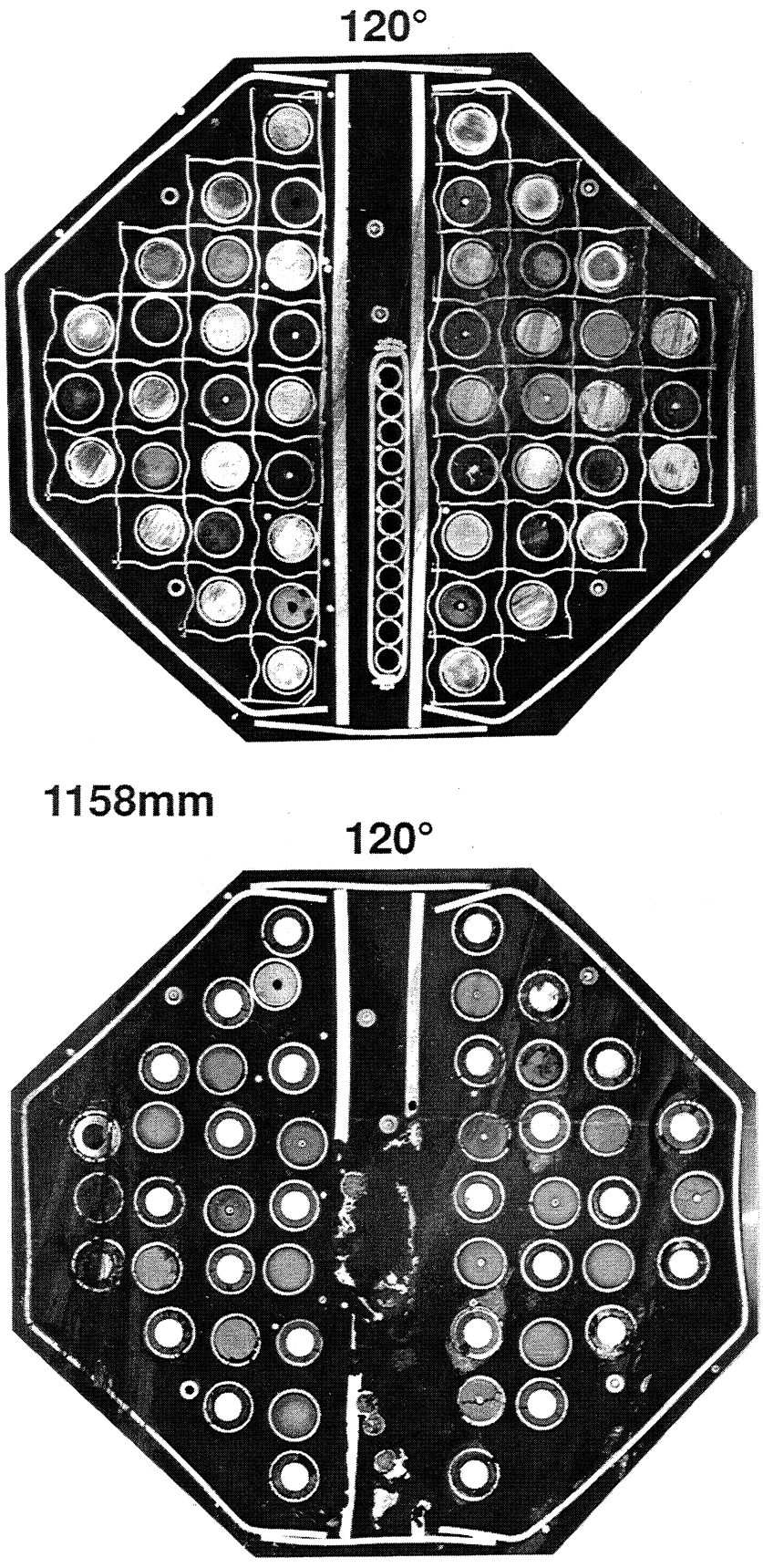

Fig. 49 Horizontal cross sections of bundle CORA-18

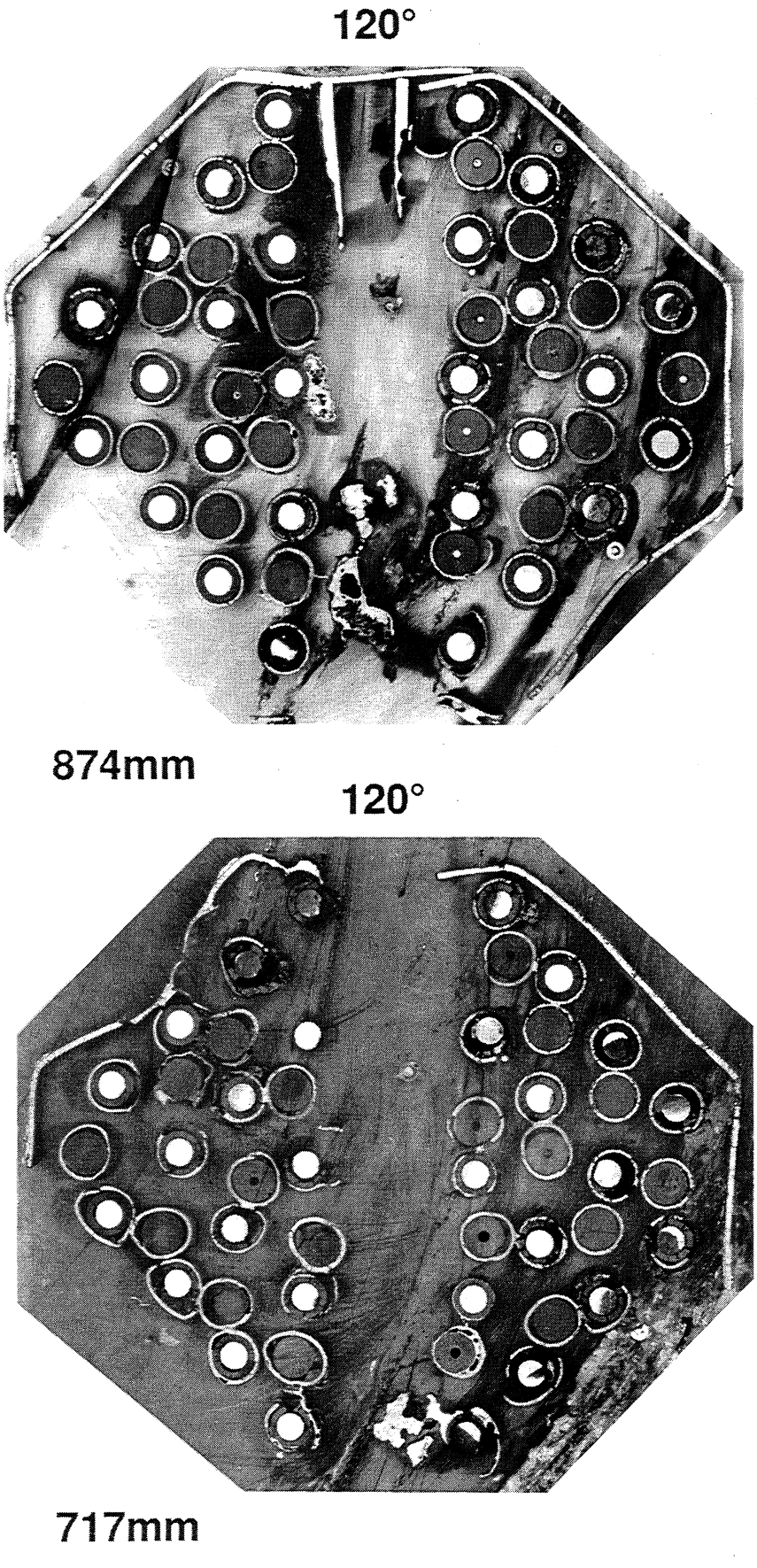

Fig. 50 Horizontal cross sections of bundle CORA-18

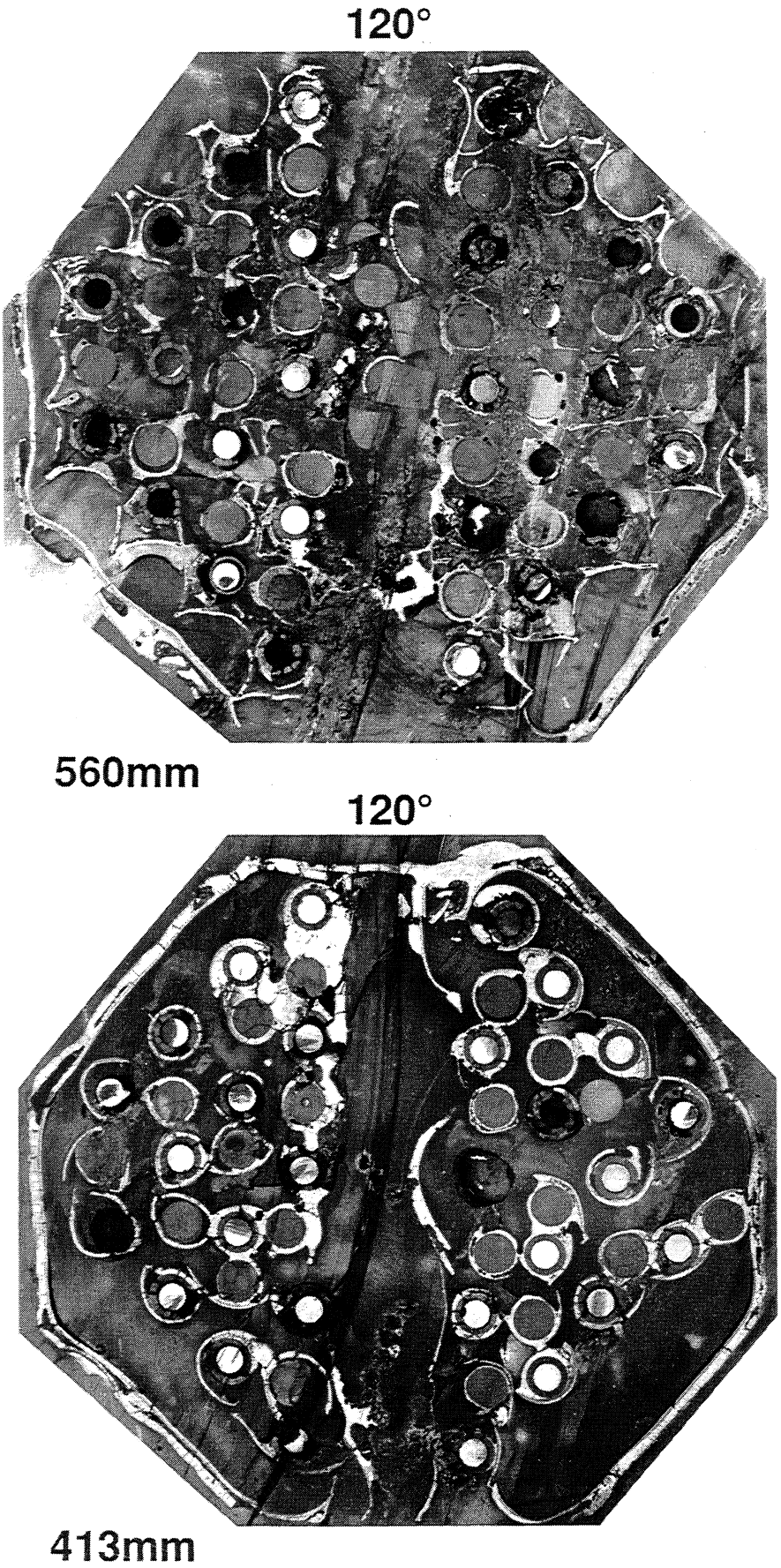

Fig. 51 Horizontal cross sections of bundle CORA-18

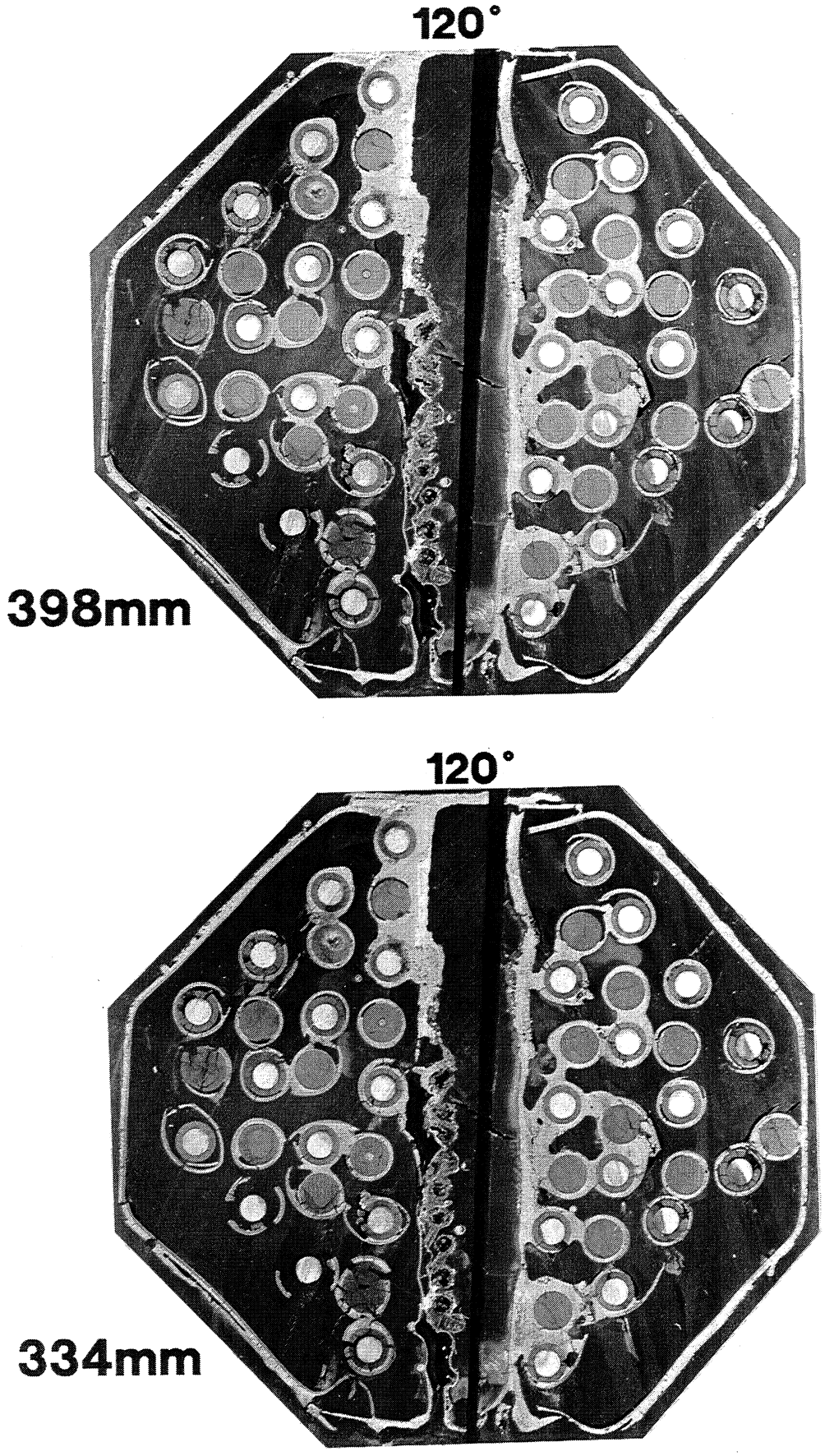

Fig. 52 Horizontal cross sections of bundle CORA-18

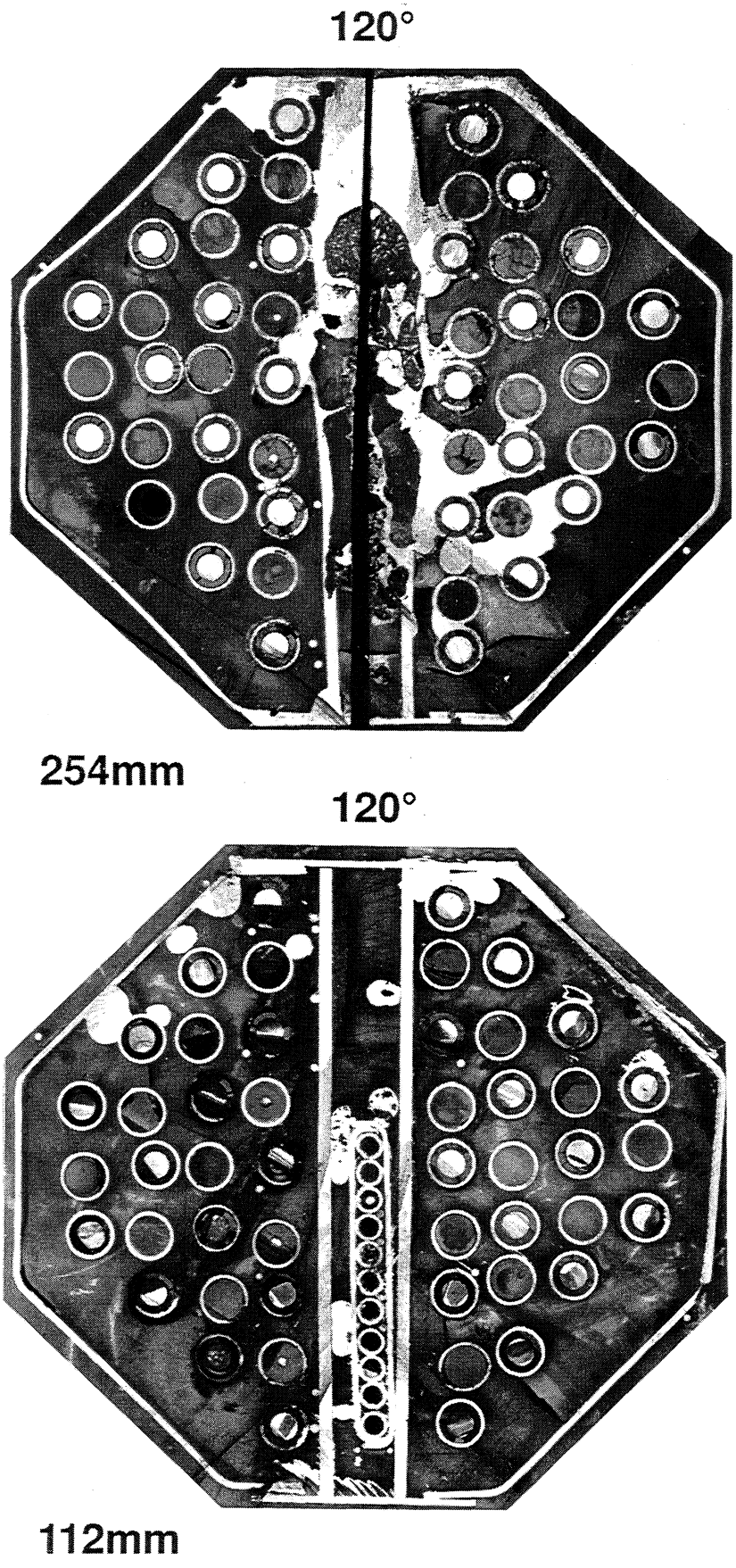

Fig. 53 Horizontal cross sections of bundle CORA-18

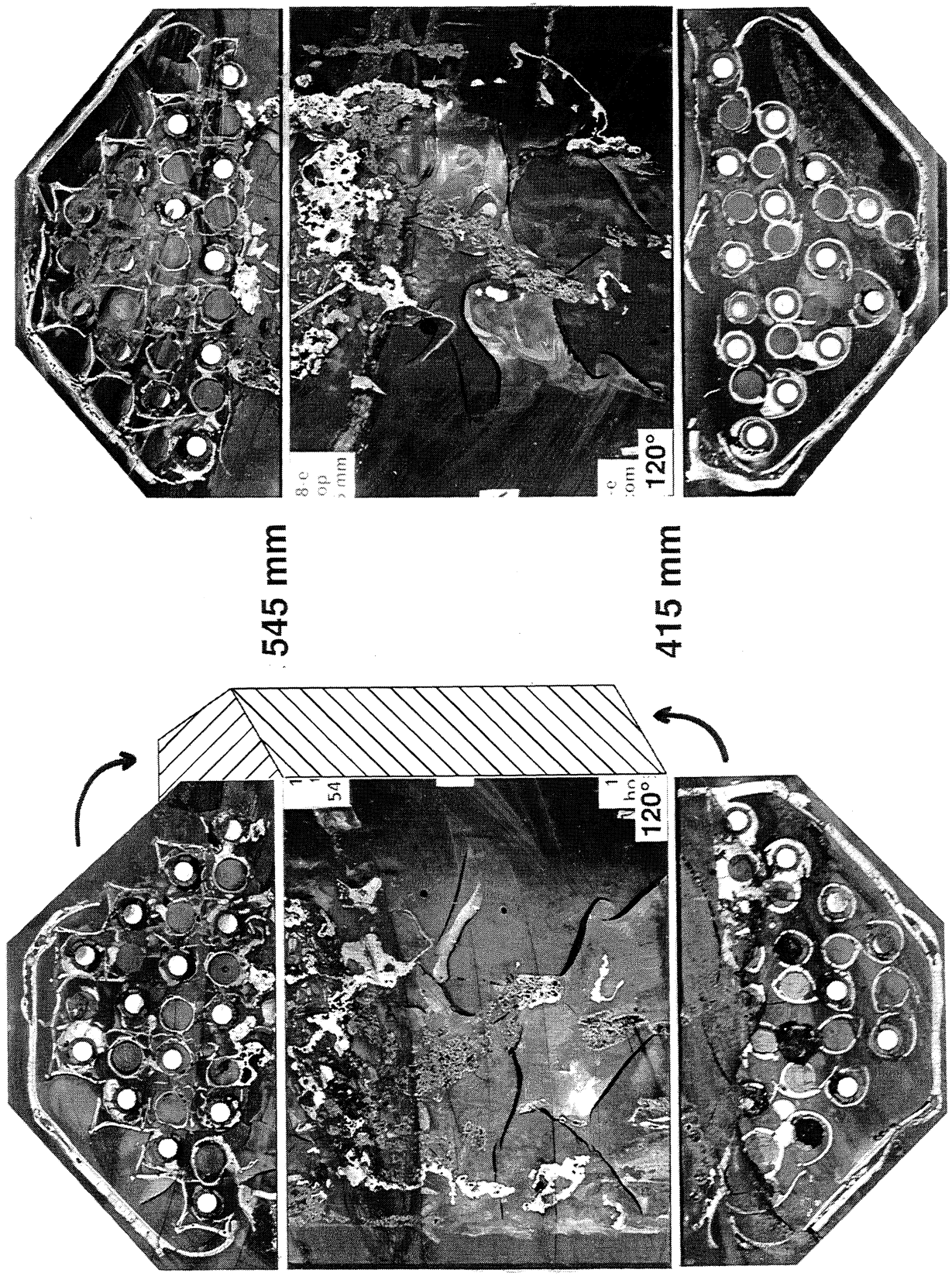

Fig. 54 Vertical sections of bundle CORA-18, 415 - 545 mm

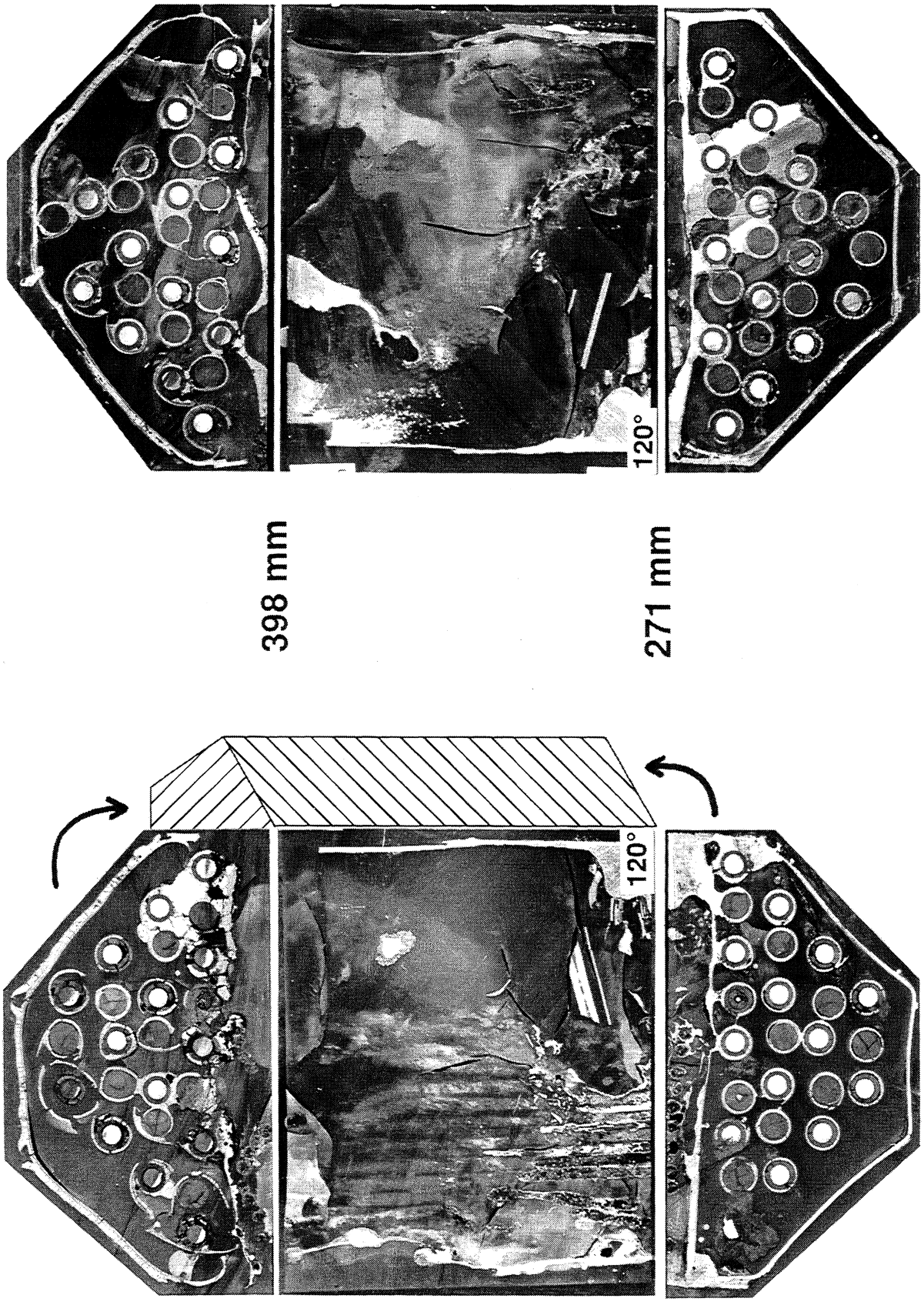

Fig. 55 Vertical sections of bundle CORA-18, 271 - 398 mm

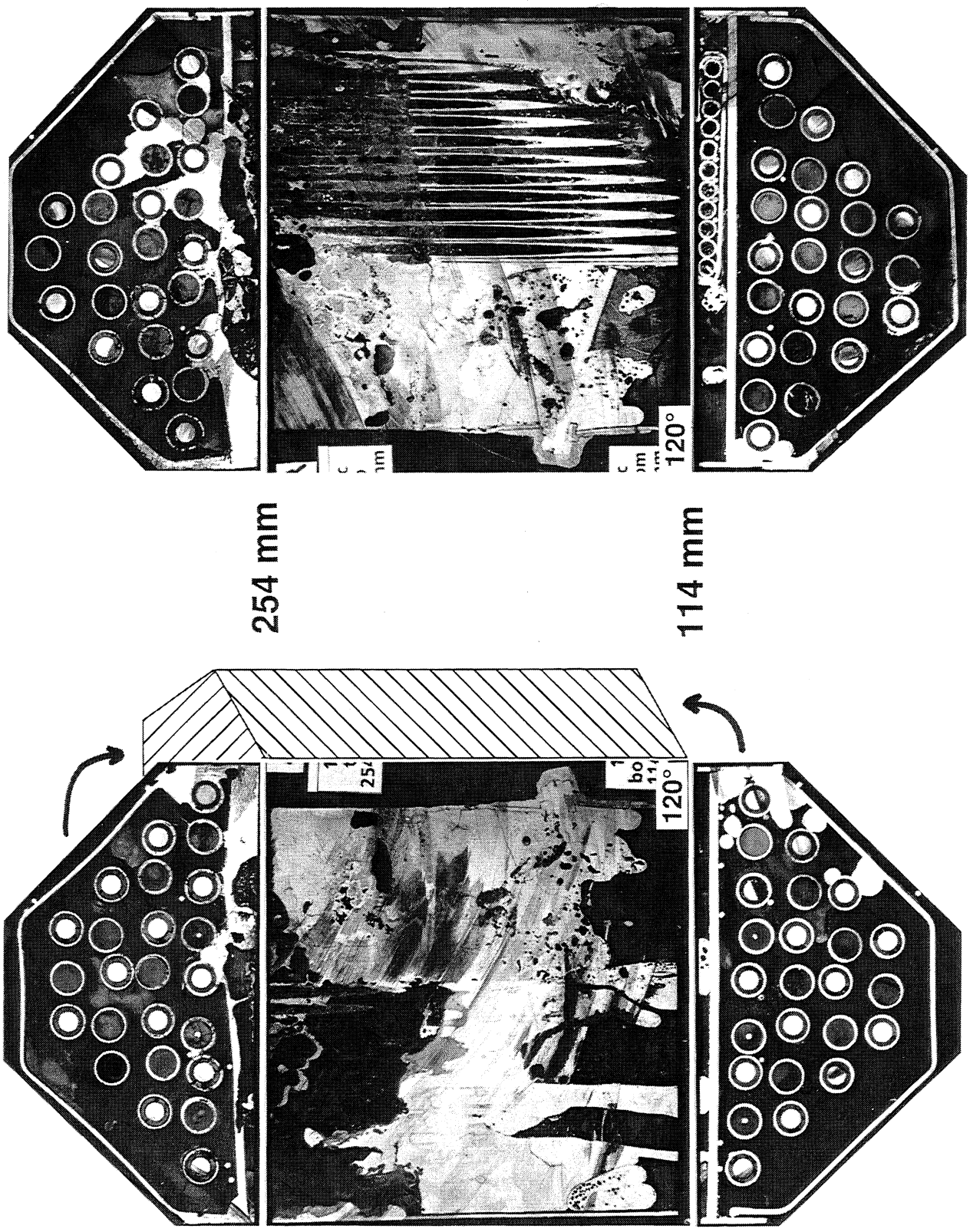

Fig. 56 Vertical sections of bundle CORA-18, 114 - 254 mm

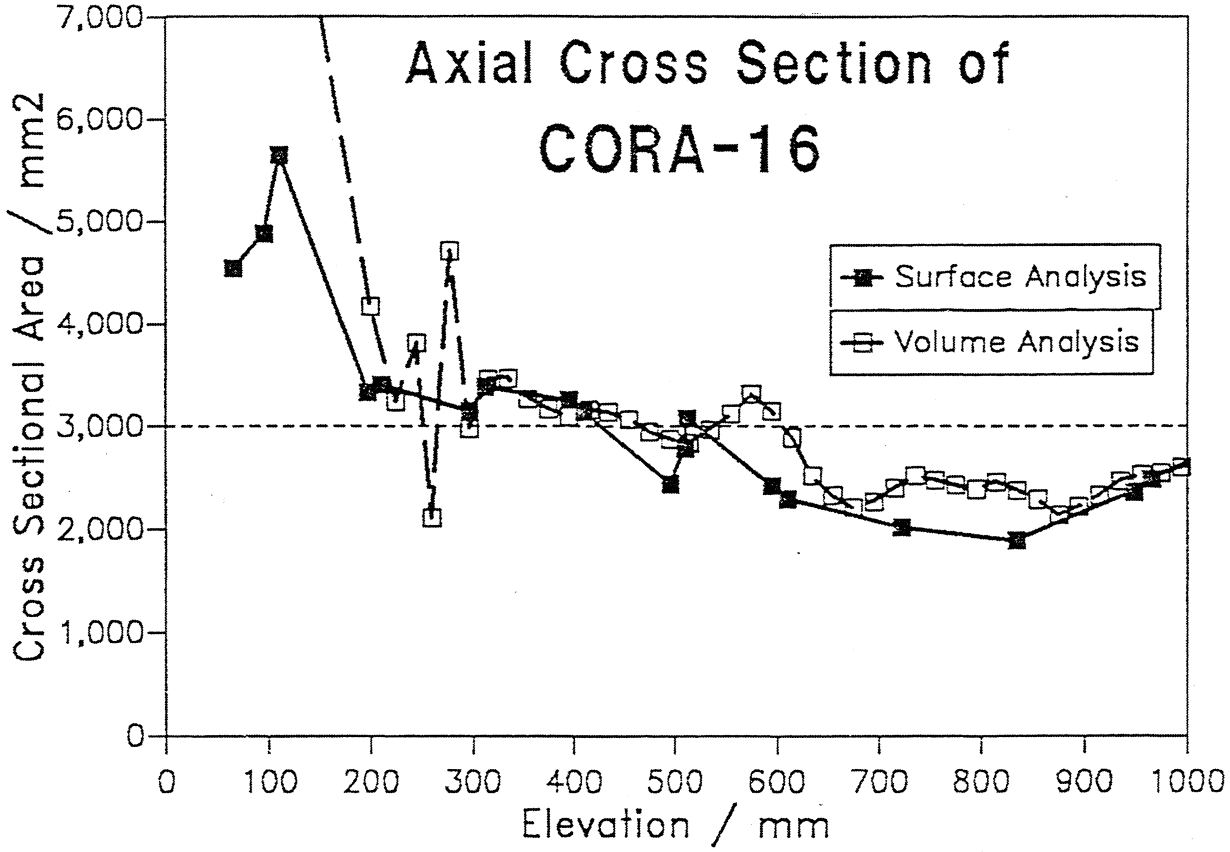

Fig. 57 Axial profile of material of bundle CORA-16

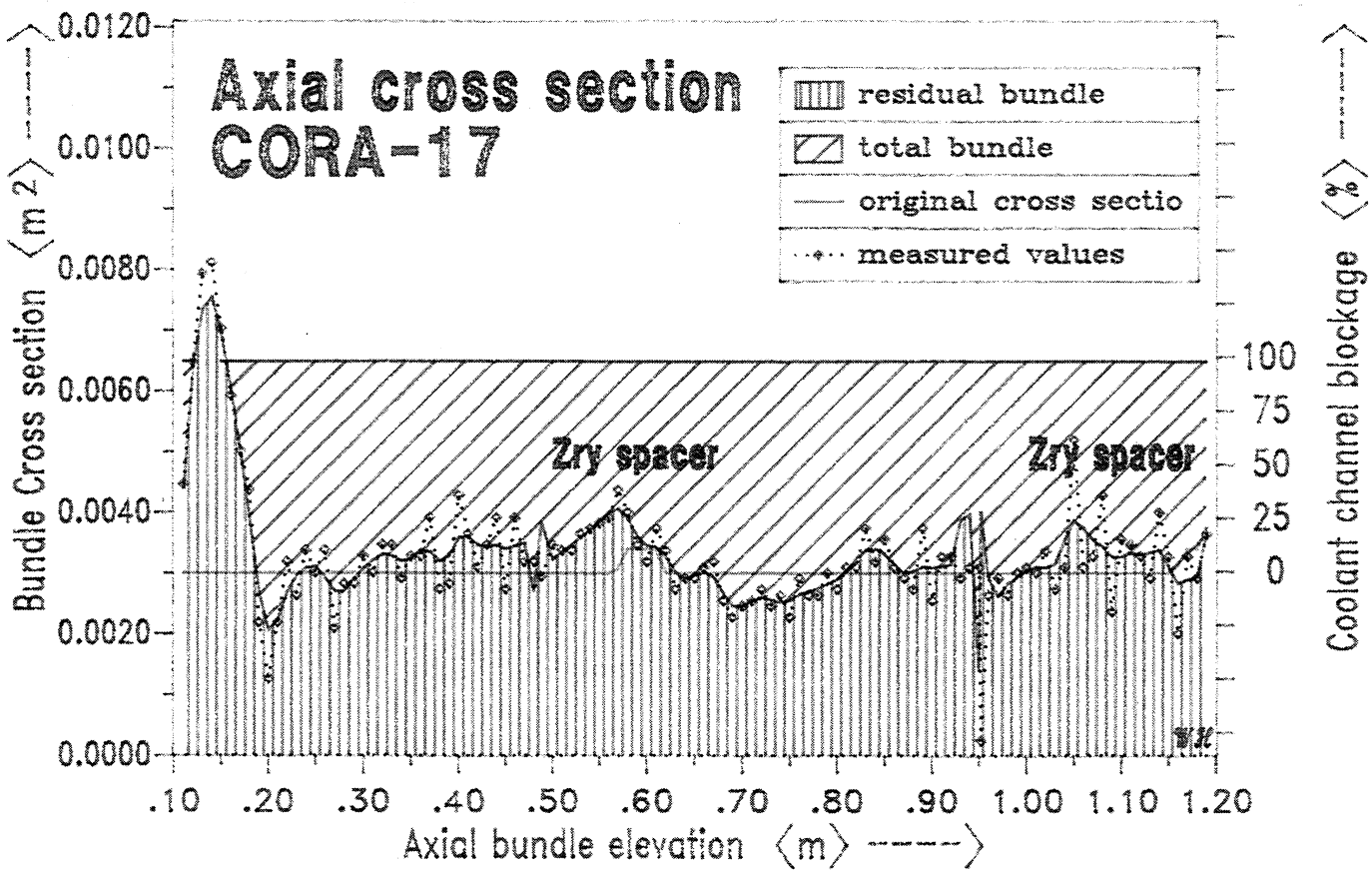

Fig. 58 Axial distribution of material of bundle CORA-17

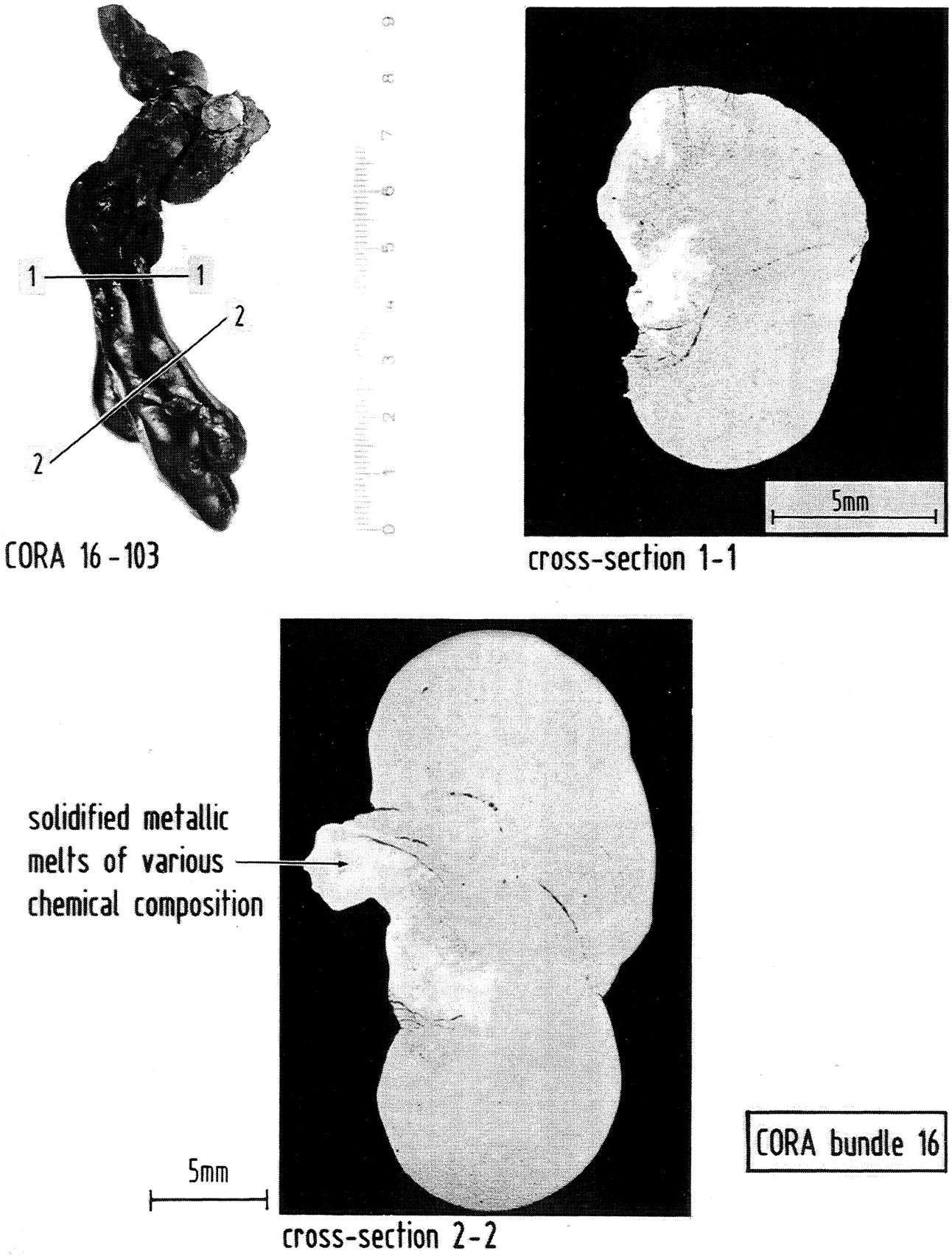

Fig. 59 Macroscopic appearance of a solidified melt nose of bundle CORA-16

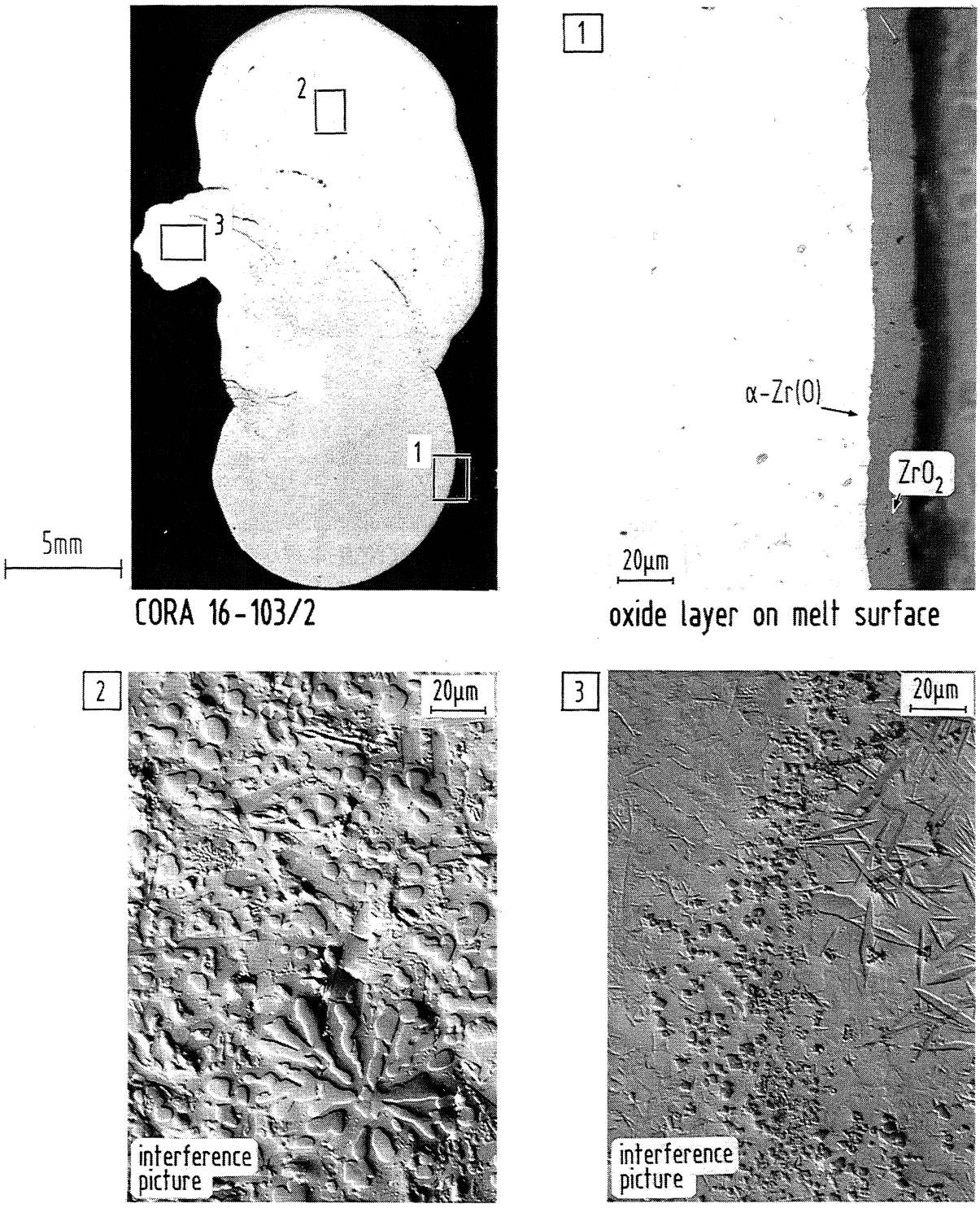

Fig. 60 **Formation of different phases of the solidified melt (CORA-16). A thin oxide layer formed on the surface of the melt.**

SEM picture

phase	Fe	Cr	Ni	Zr	Sn	U	
1	28.8	17.3	–	53.9	–	–	metallic
2	–	–	–	100	–	–	metallic
3	15.1	5.1	1.9	78	–	–	metallic
4+5	15.5	3.8	2.2	78.5	–	–	oxide
6	5.6	–	–	77	17.4	–	metallic
7	15.8	1.5	3.9	77.1	–	1.7	oxide
8	–	–	–	97.2	2.8	–	metallic
integral	12.4	3.5	1.6	80.9	1.6		+ (O,C)

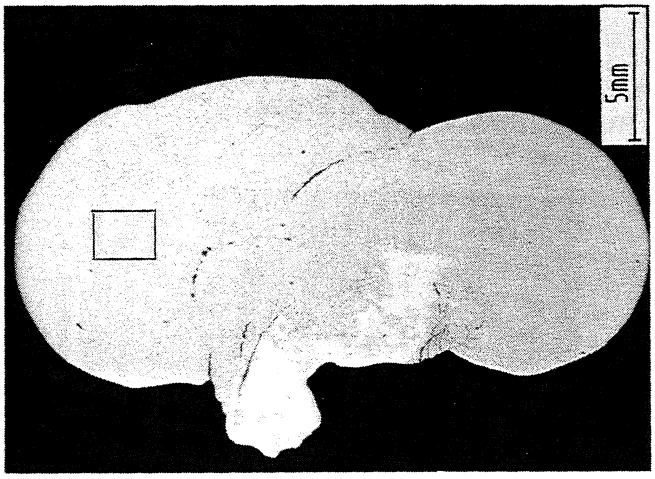

cross-section CORA 16-103/2

solidified metallic melts of various chemical composition

Fig. 61 Chemical analysis of the phases formed during solidification (CORA-16)

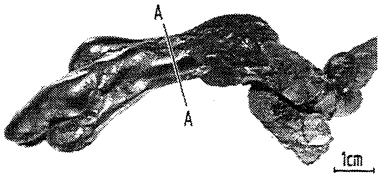

CORA 16-103; relocated melt

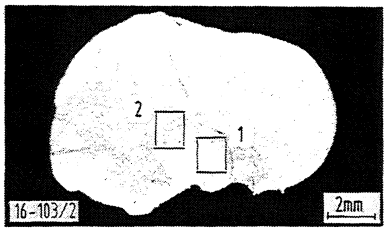

cross-section A-A; ≈ 0.5 wt.% U

1

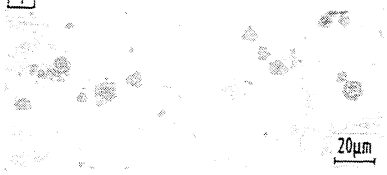

microstructure of solidified metallic melt

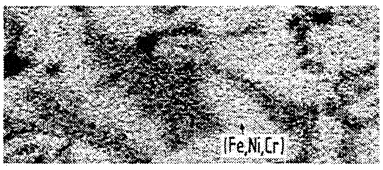

Fe map

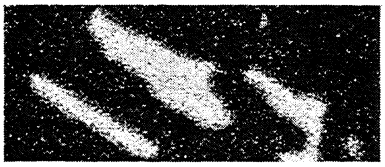

Cr map

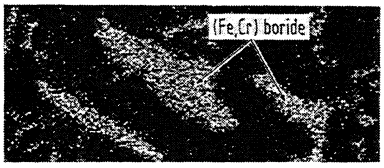

B map

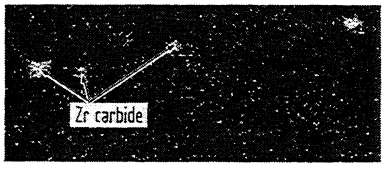

C map 5µm

2

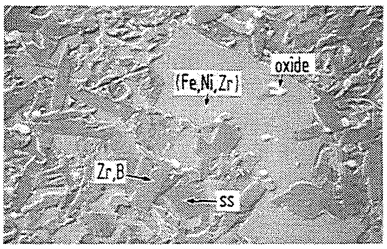

SEM photograph

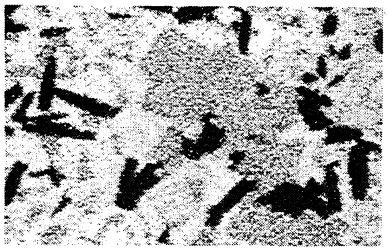

Fe map

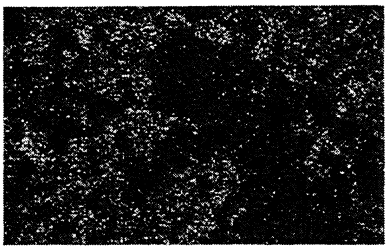

Cr map

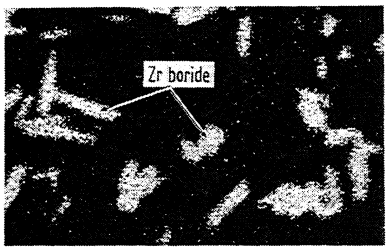

B map

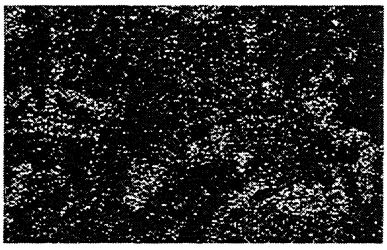

Zr map 5µm

the matrix consists of Fe,Cr,Ni,Zr which contains boride and carbide precipitates

Fig. 62 Distribution of elements at two positions of the solidified melt

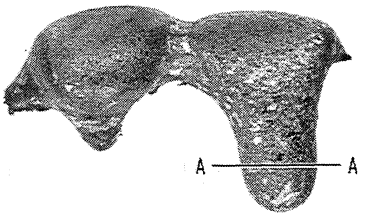

CORA 16-104; relocated melt

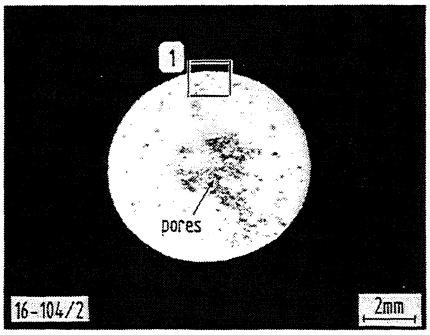

cross-section A-A, no U

1

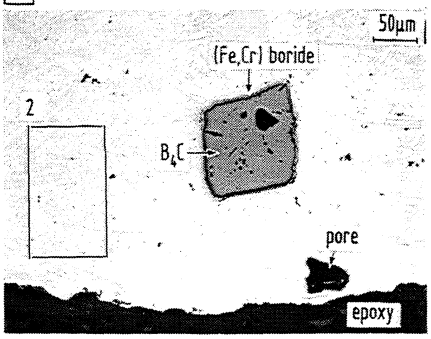

microstructure of solidified metallic melt

2

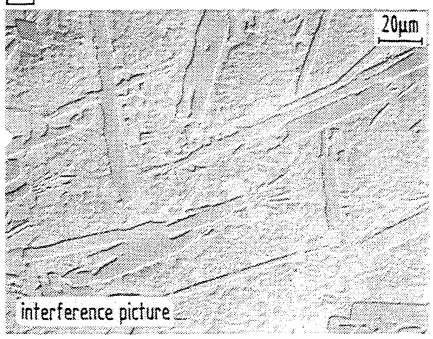

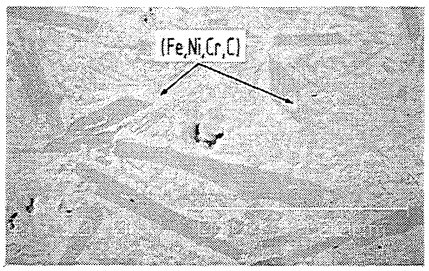

SEM photograph

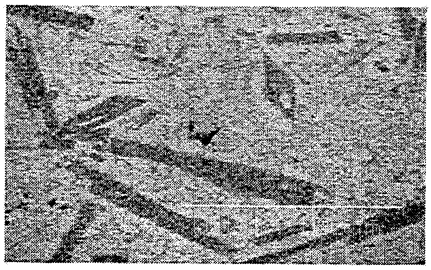

Fe map

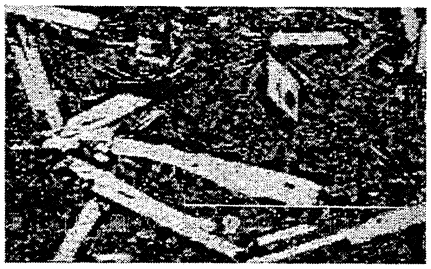

Cr map

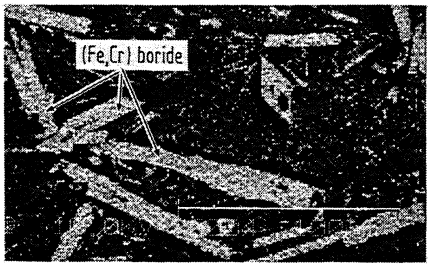

B map

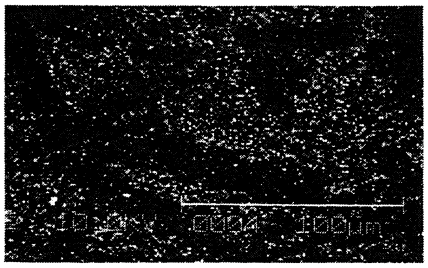

C map 20µm

the matrix consists of Fe,Cr,Ni,Zr which contains (Fe,Cr) boride precipitates

Fig. 63 Distribution of elements of melt solidified outside the bundle

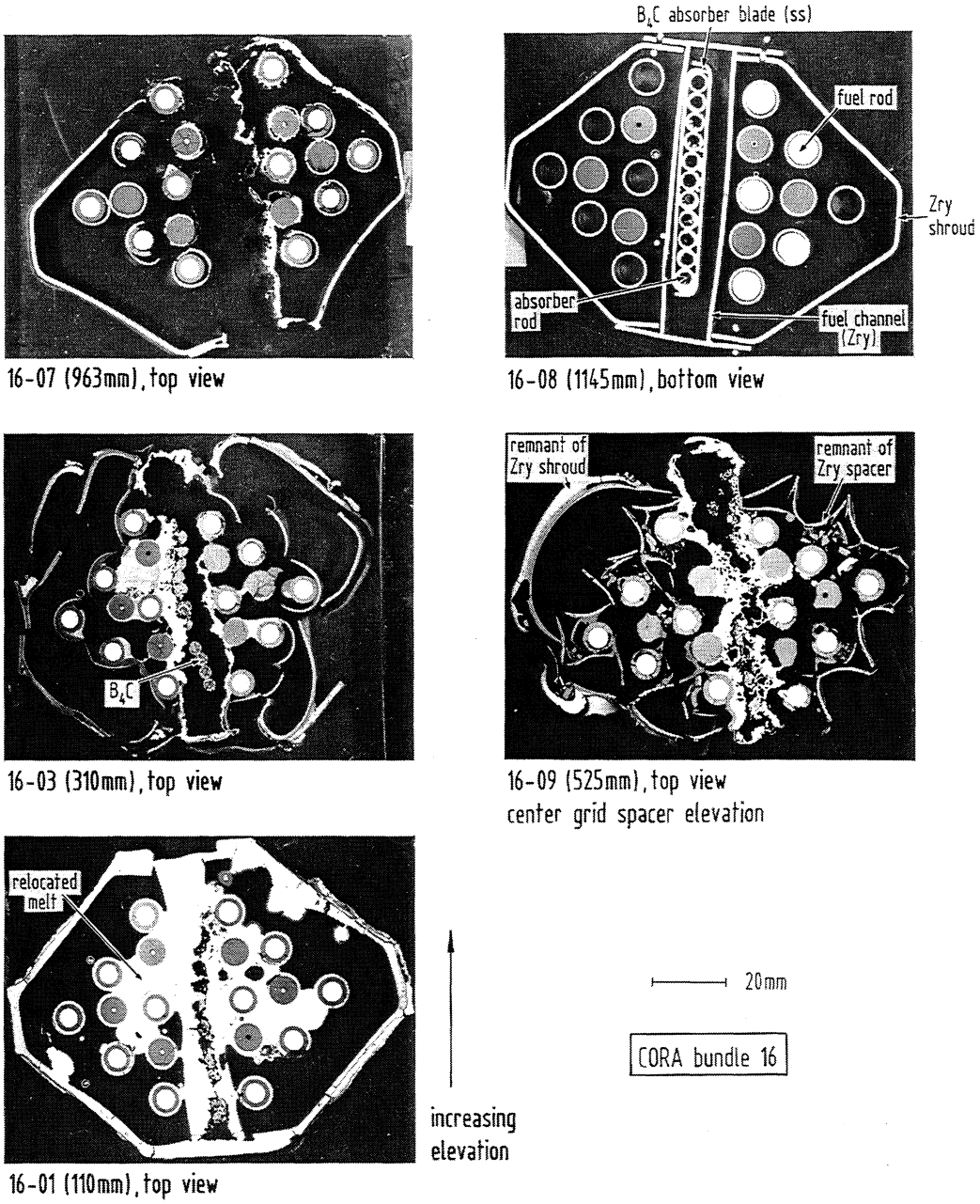

16-07 (963mm), top view

16-08 (1145mm), bottom view

16-03 (310mm), top view

16-09 (525mm), top view
center grid spacer elevation

16-01 (110mm), top view

Fig. 64 Horizontal cross section of bundle CORA-16. Formation of a flow channel blockage at 110 mm elevation

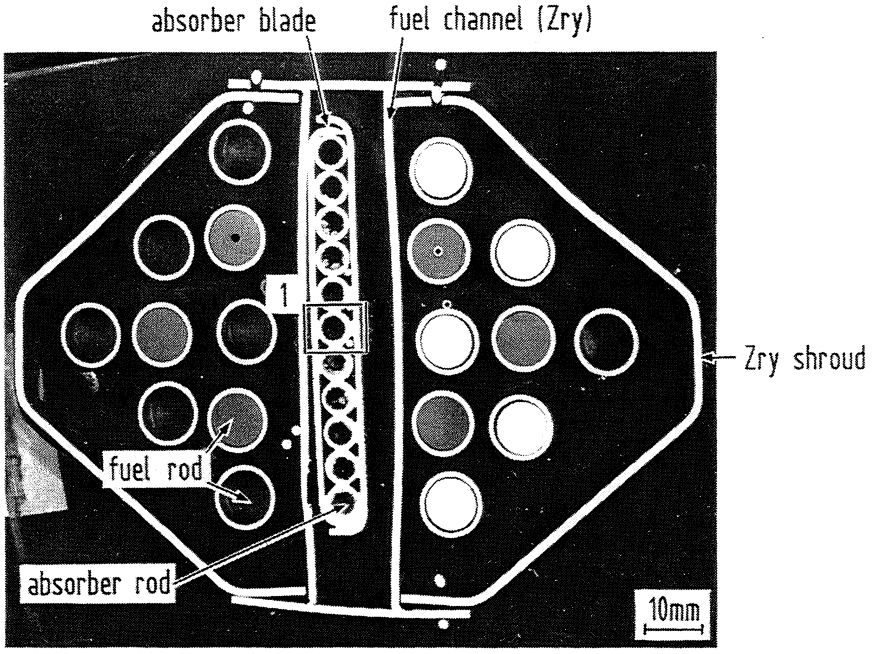

cross-section CORA 16-08 (1145mm)

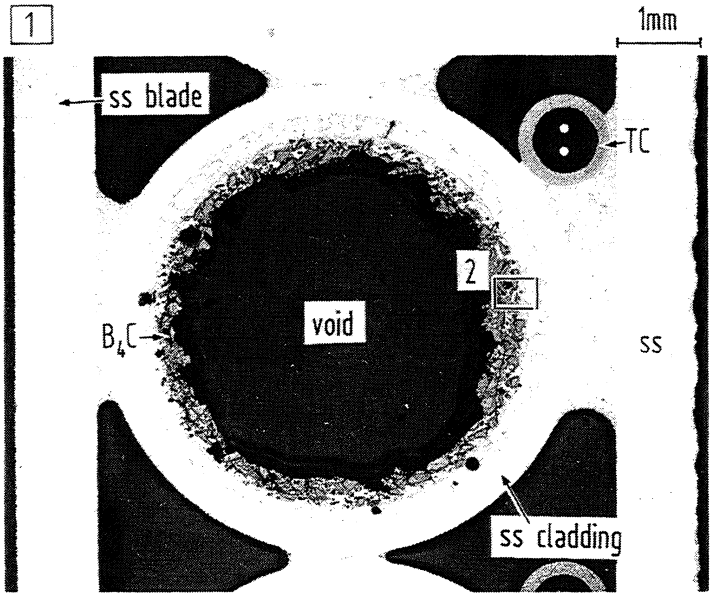

cross-section of B_4C absorber rod

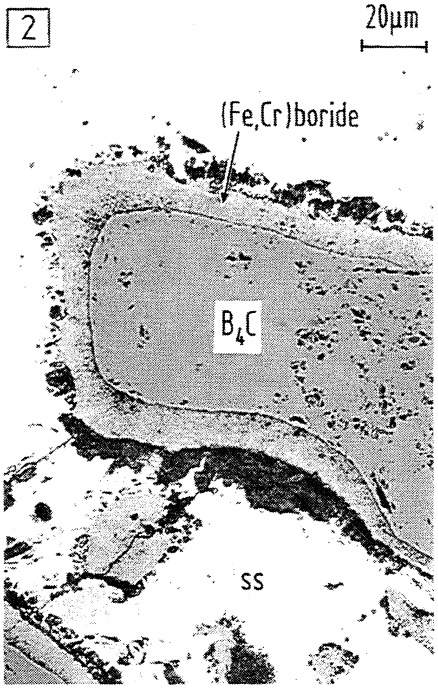

dissolution of B_4C particles

Fig. 65 Details of cross section CORA 16-08

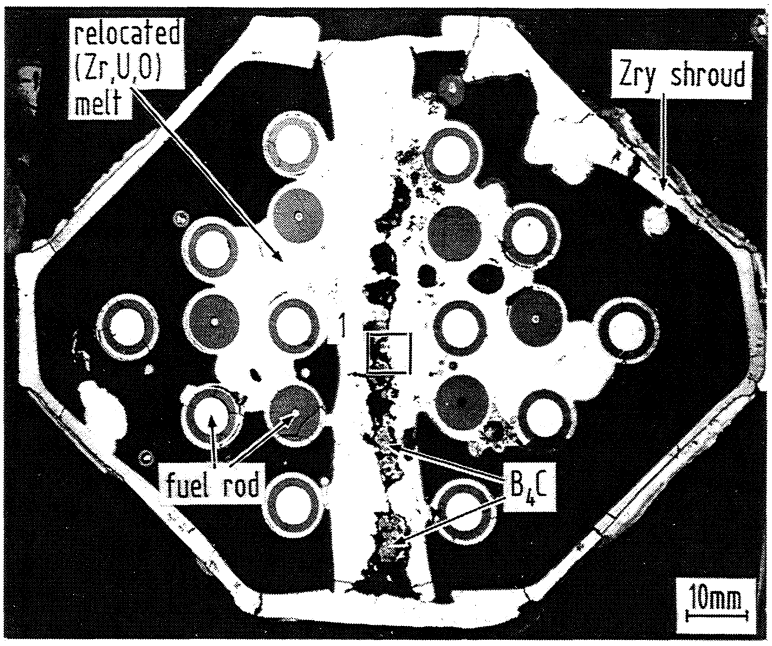

cross-section CORA 16-01 (110mm)

attack of the B_4C by ss

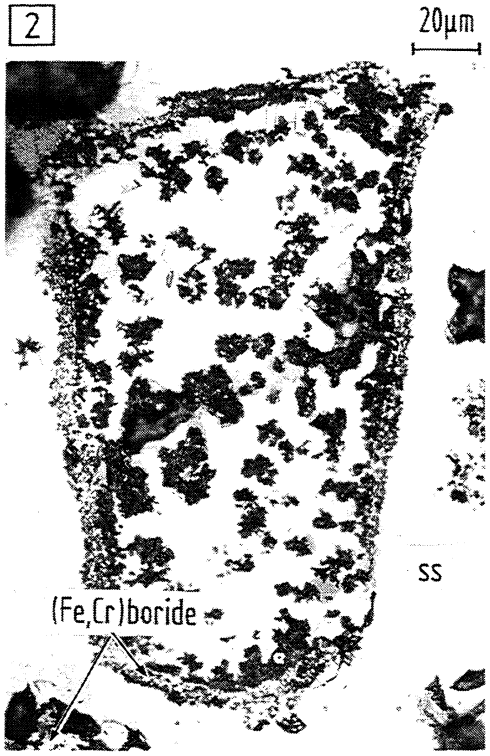

dissolution of B_4C particle

Fig. 66 Details of cross section CORA 16-01

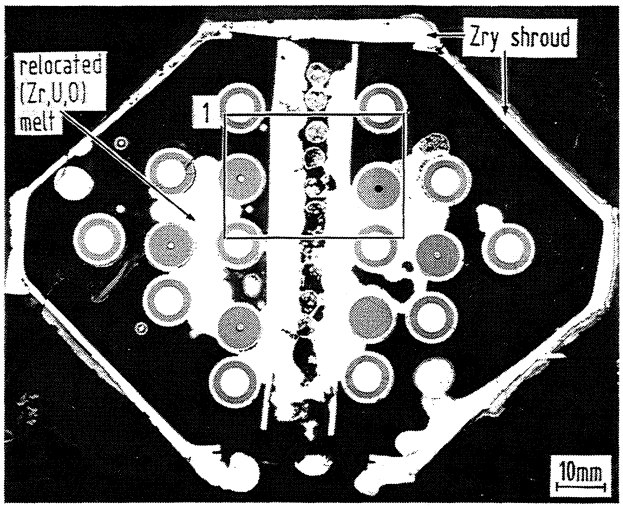

cross-section CORA 16-01 (97mm)

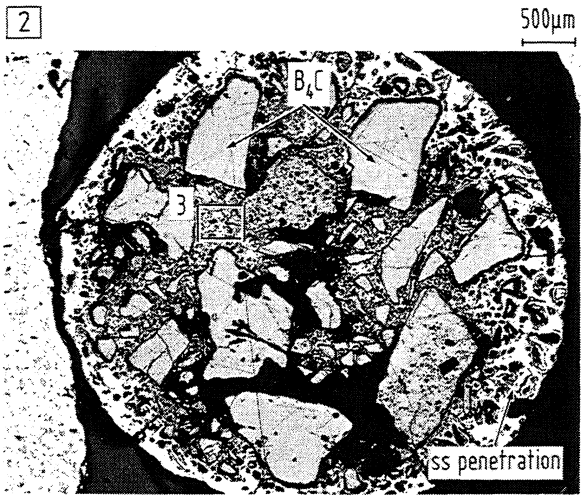

cross-section of attacked B_4C absorber rod

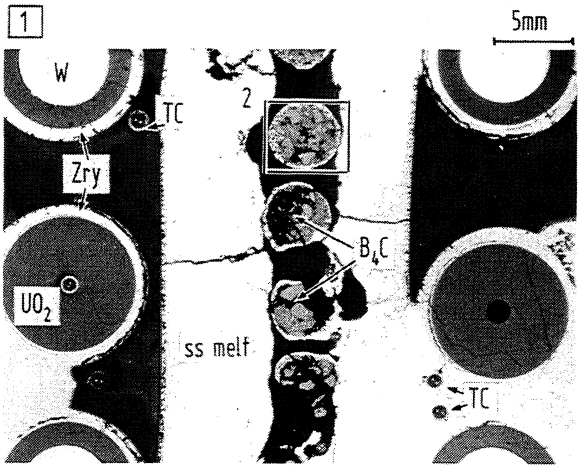

failure of B_4C absorber rods

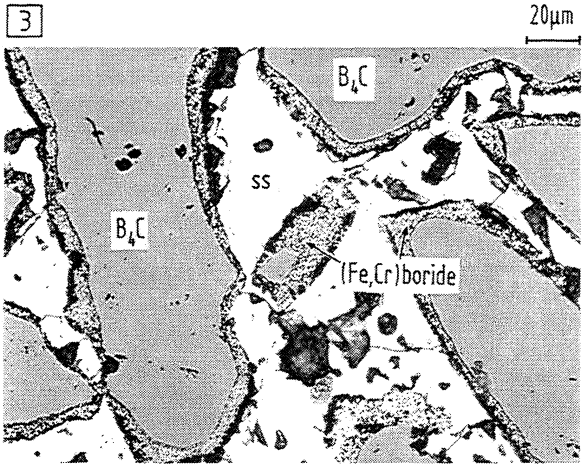

chemical interactions between B_4C and ss

Fig. 67: Details of cross section CORA 16-01, demonstrating the chemical behavior of B_4C absorber material

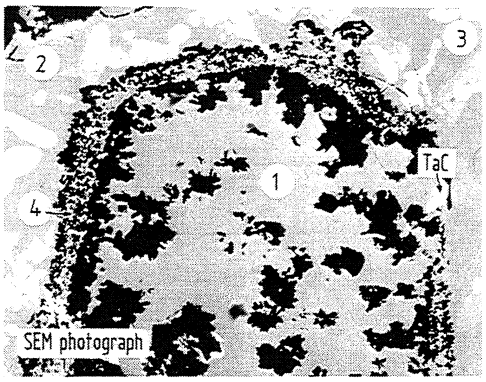

almost completely dissolved B_4C particle

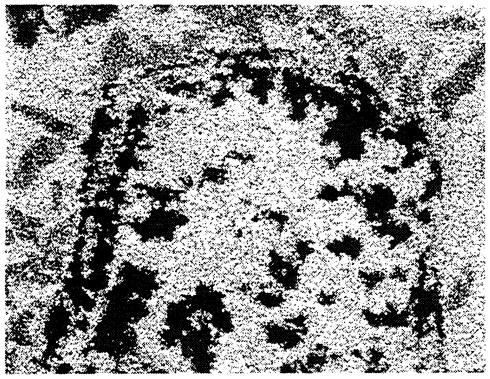

Fe map; EDX analysis

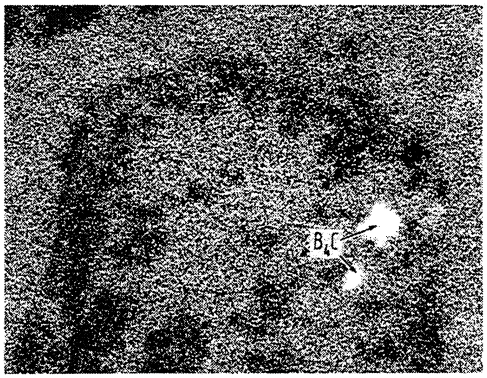

B map; WDX analysis

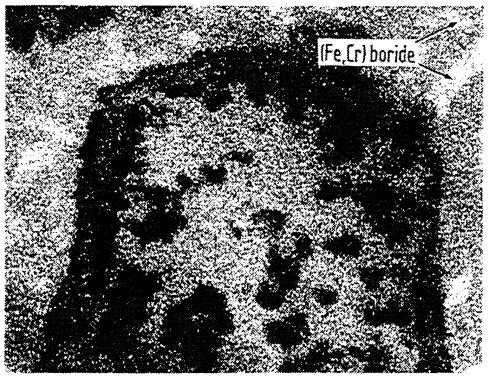

Cr map; EDX analysis

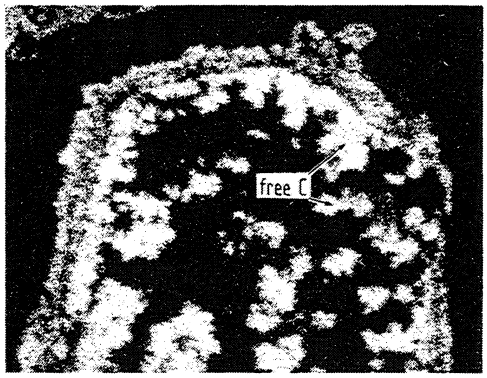

C map; WDX analysis

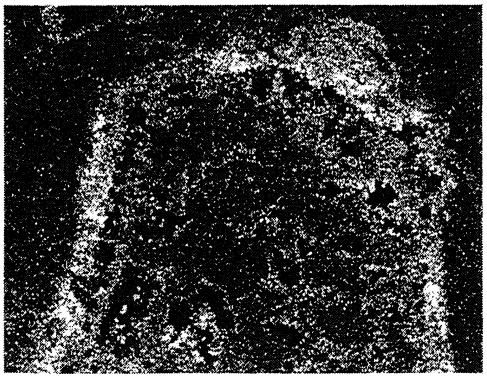

Ni map; EDX analysis — 20µm

wt. %	1	2	3	4
Fe	78	74	41	10
Cr	16	22	42	1
Ni	6	4	1	35
C	-----	-----	-----	54

CORA bundle 16
cross-section 16-01 (110mm)

Fig. 68 Distribution of elements of a B_4C particle attacked by metallic melt, cross section CORA 16-01

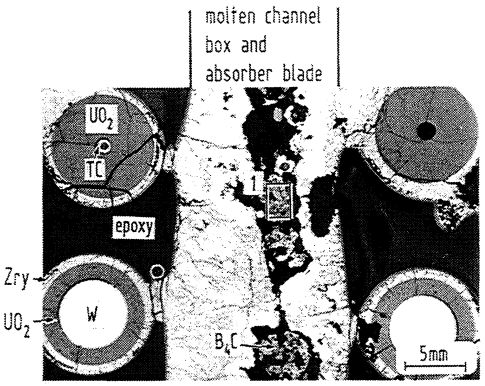

cross-section CORA 16-01 (110mm)

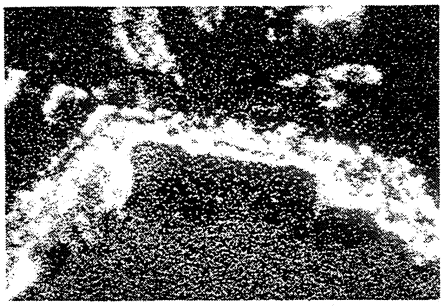

C map; WDX analysis

1

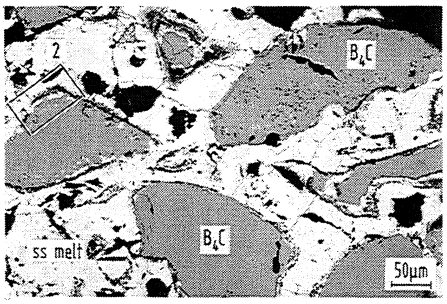

chemical interactions between B_4C and ss

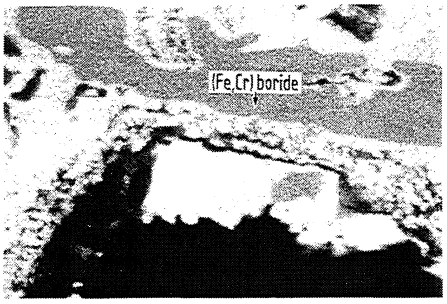

Fe map; EDX analysis

2

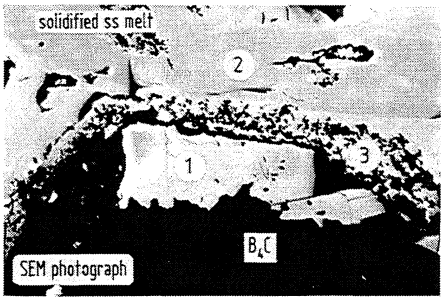

onset of B_4C dissolution by ss melt

Cr map; EDX analysis

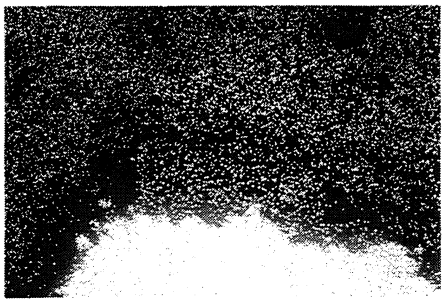

B map; WDX analysis

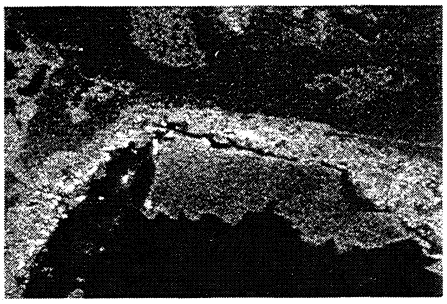

Ni map; EDX analysis — 20µm

wt. %	1	2	3
Fe	77	52	53
Cr	10	46	12
Ni	13	2	11

CORA bundle 16

Fig. 69 Distribution of elements within the metallic melt of cross section CORA 16-01

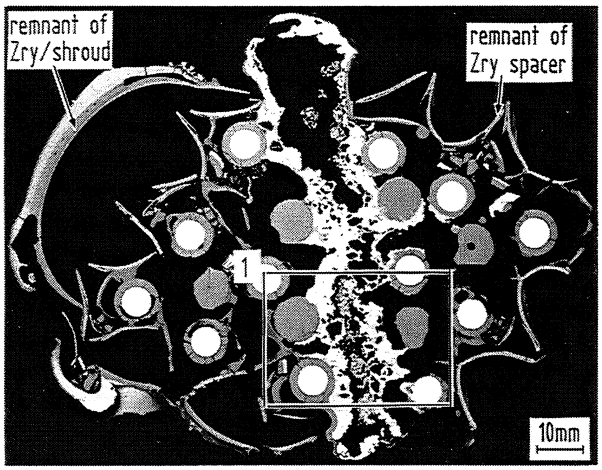

cross-section CORA 16-09 (525mm)

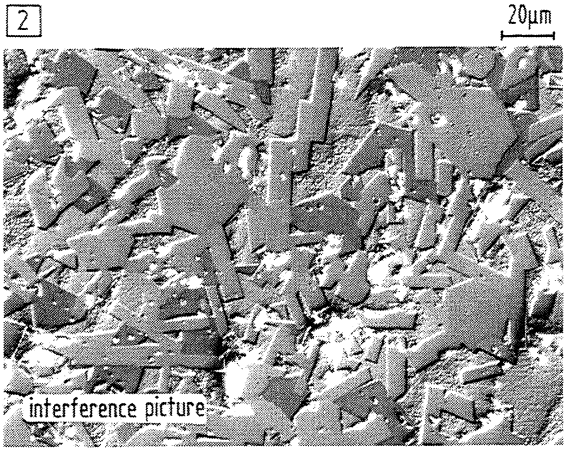

solidified B_4C-ss-Zircaloy melt

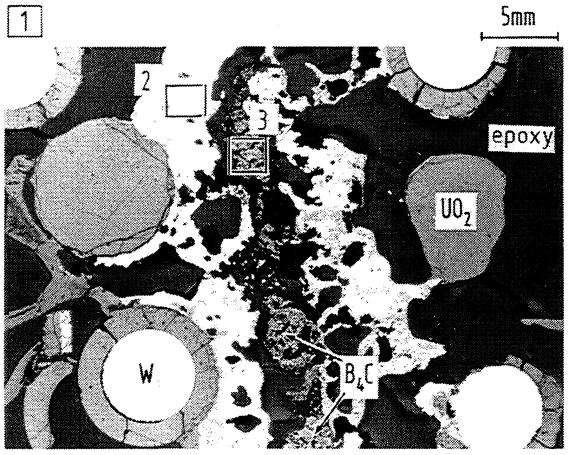

failure of the absorber blade and channel box

nearly completely dissolved B_4C by ss melt

Fig. 70 Severe dissolution of UO_2 and B_4C in metallic melt (cross section CORA 16-09)

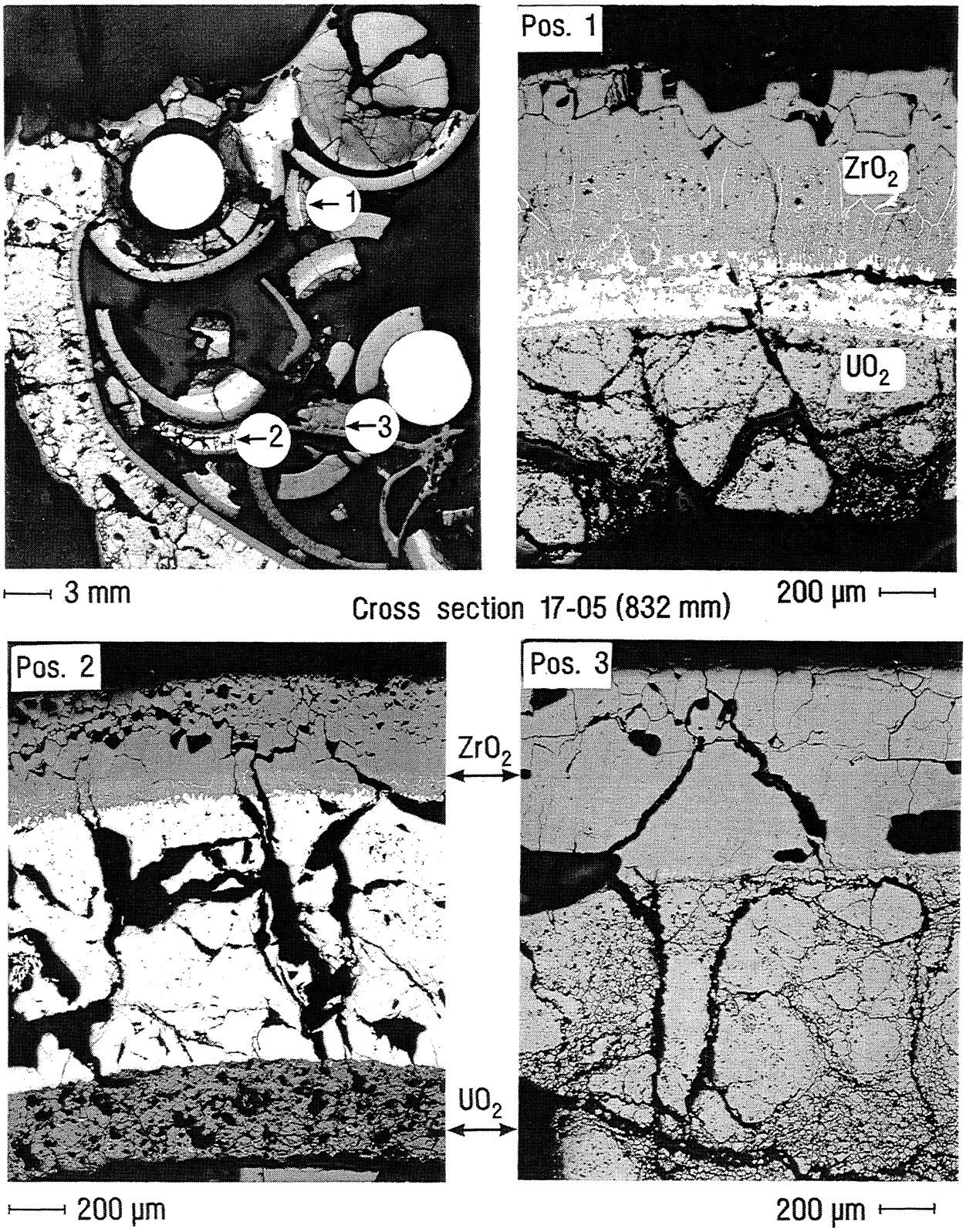

Fig. 71 Details of fuel rod fragments, accumulated at cross section CORA-17-05

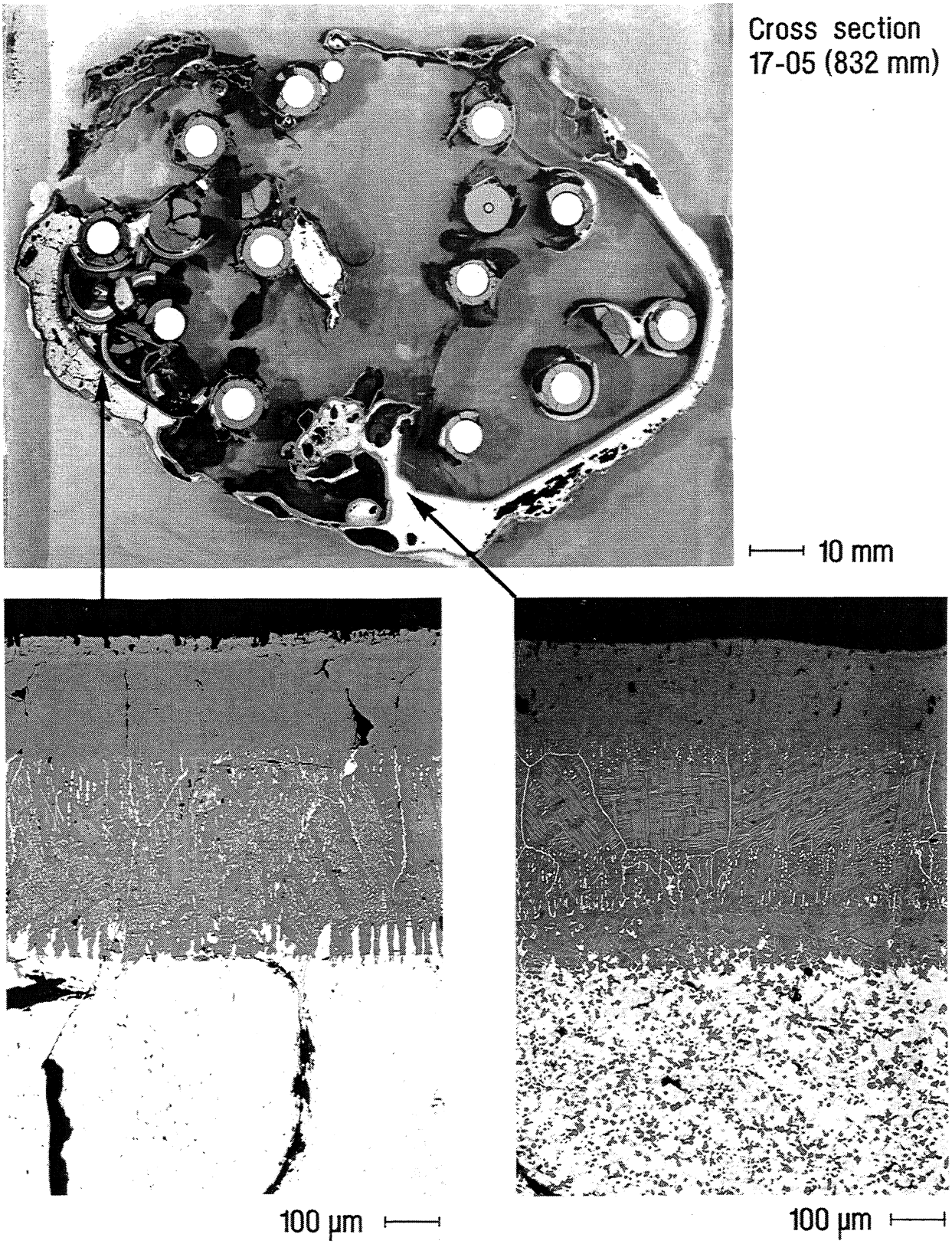

Fig. 72 Cross section CORA-17-05 with agglomerations of (Zr, O) melt at the external side of shroud

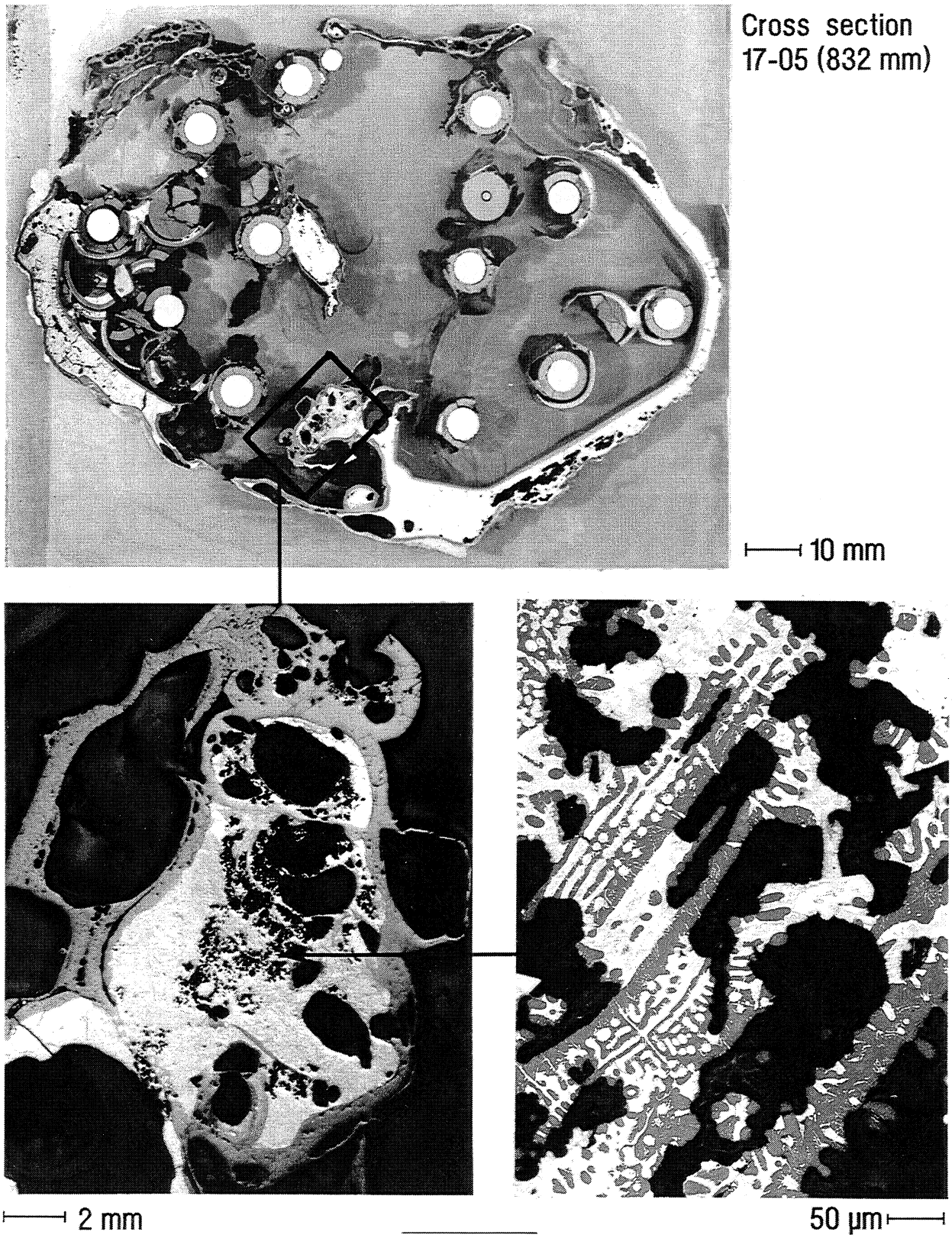

Fig. 73 Porous melt at cross section CORA-17-05

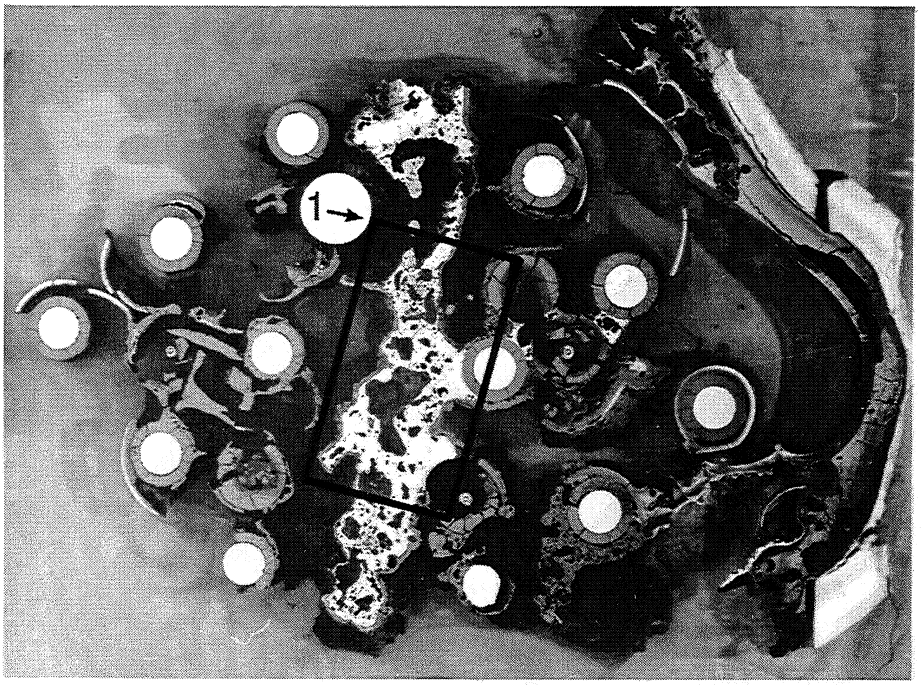

Cross section 17-02 (361 mm) 10 mm

Pos. 1

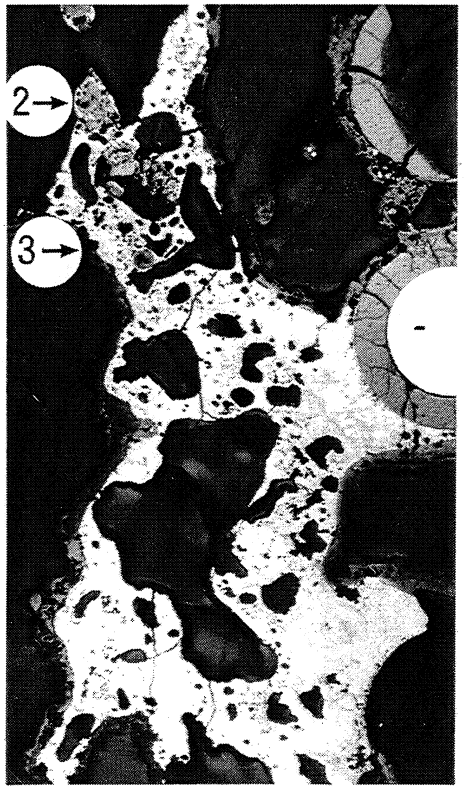

B_4C/ss melt 3 mm

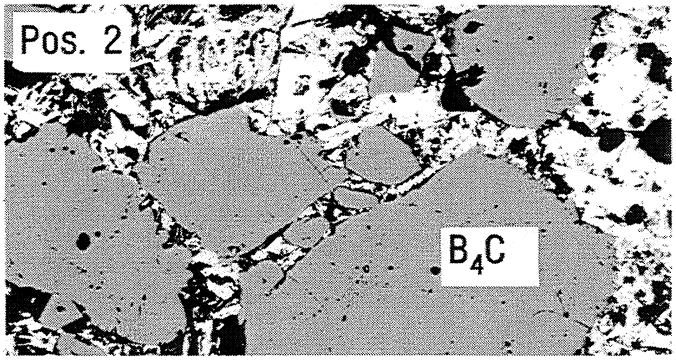

B_4C in melt 50 µm

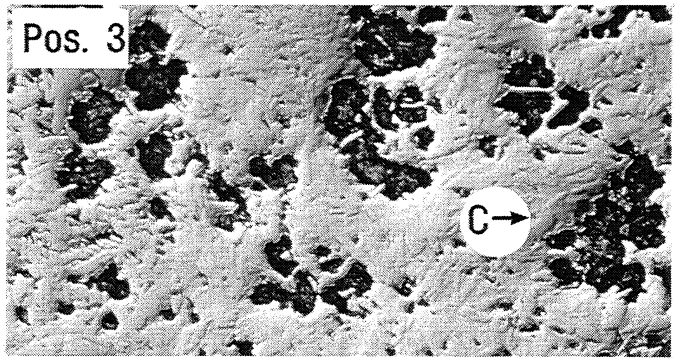

Free carbon in melt (Interf. contrast) 50 µm

Fig. 74 Cross section CORA-17-02, showing distrubution of melt from B_4C/ stainless steel interaction and free carbon as reaction product residues

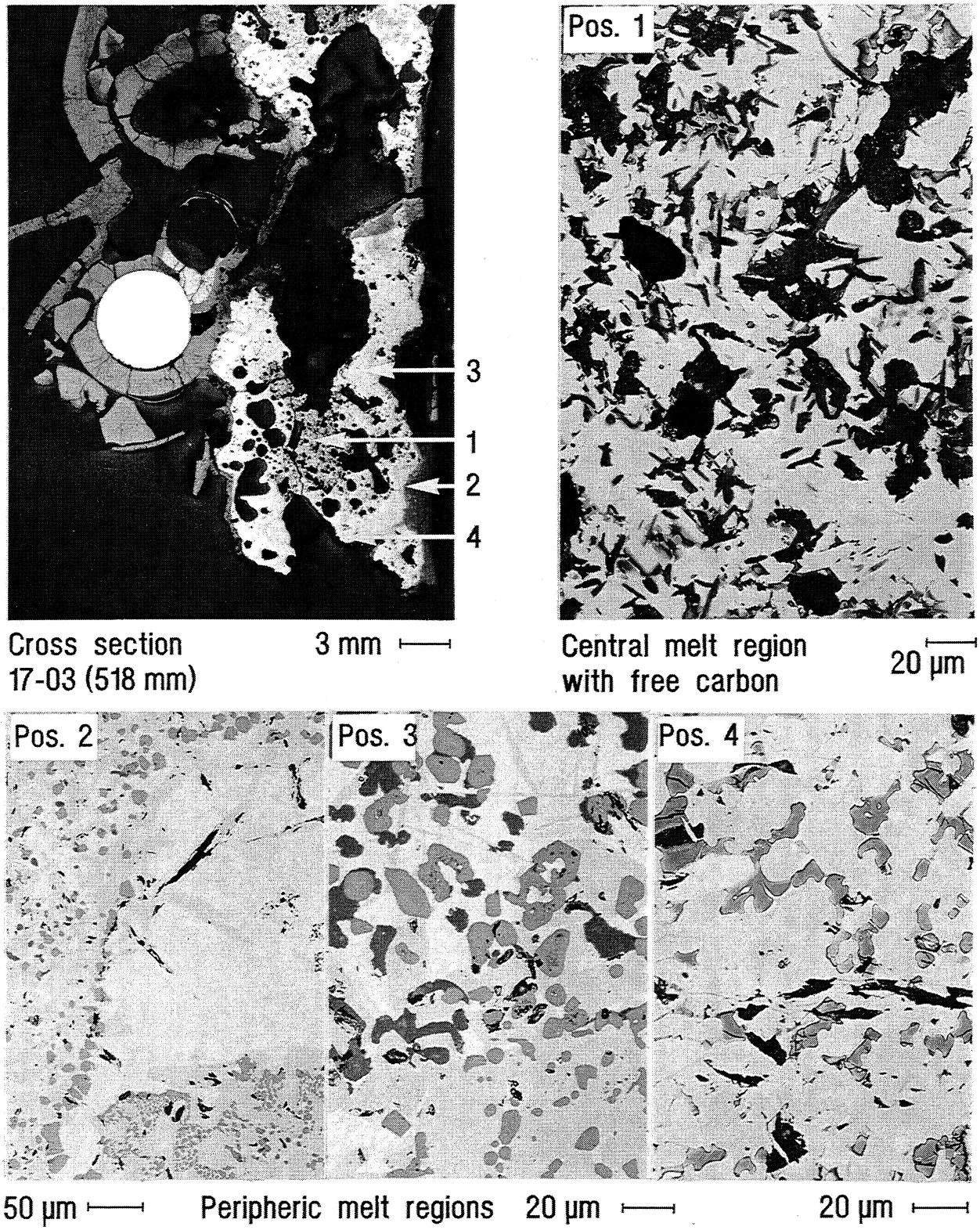

Fig. 75 Cross section CORA-17-03, showing melt from the disintegrated absorber unit, being rich in residual carbon at central positions

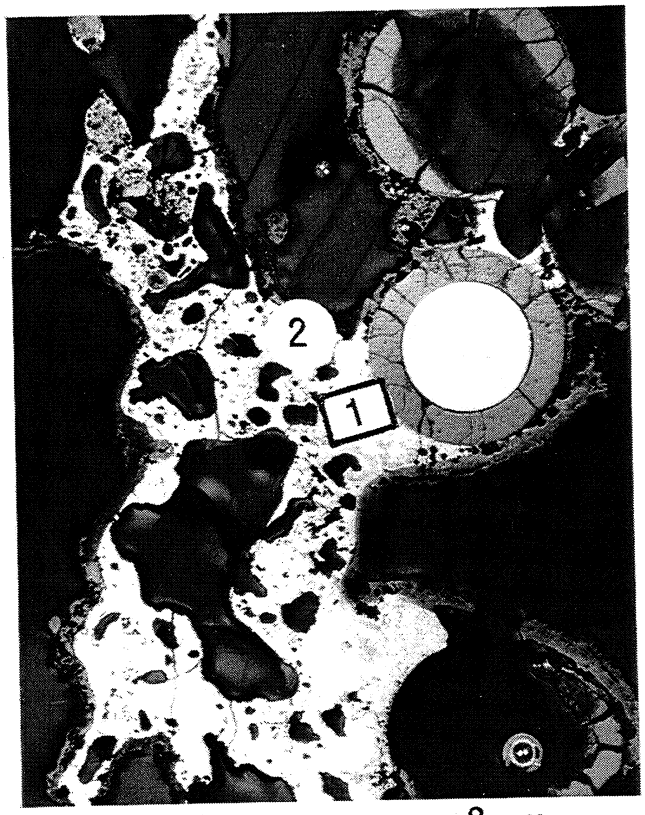

Cross section
17-02 (361 mm)

3 mm

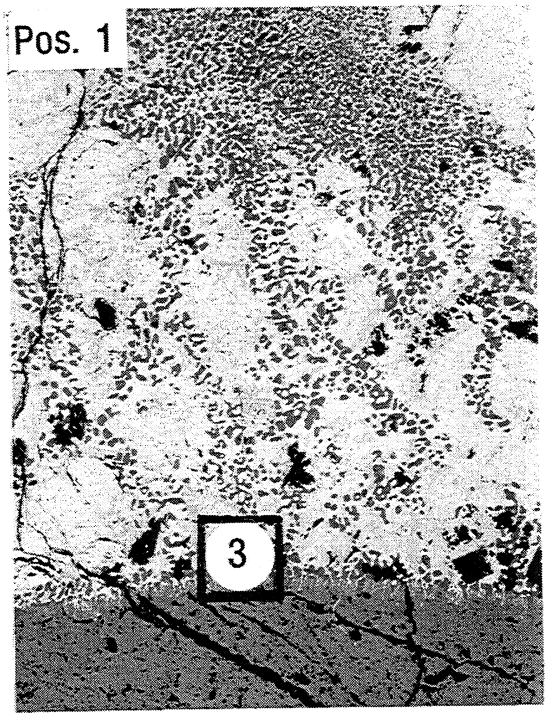

Contact zone
melt/UO_2 pellet

200 µm

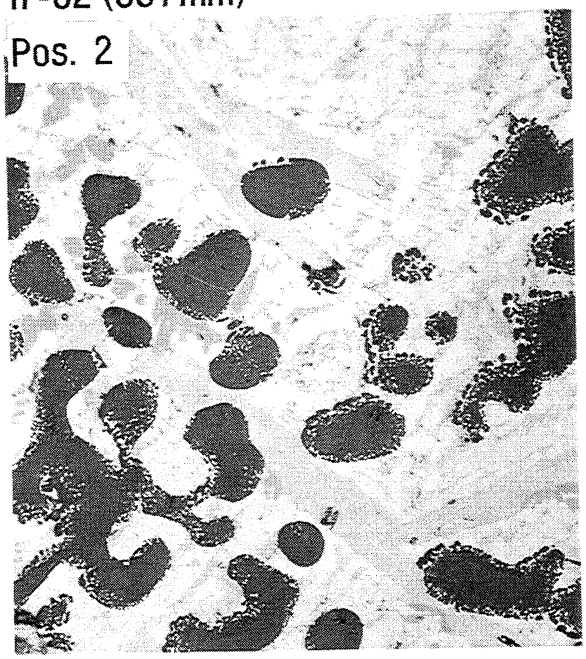

Melt

20 µm

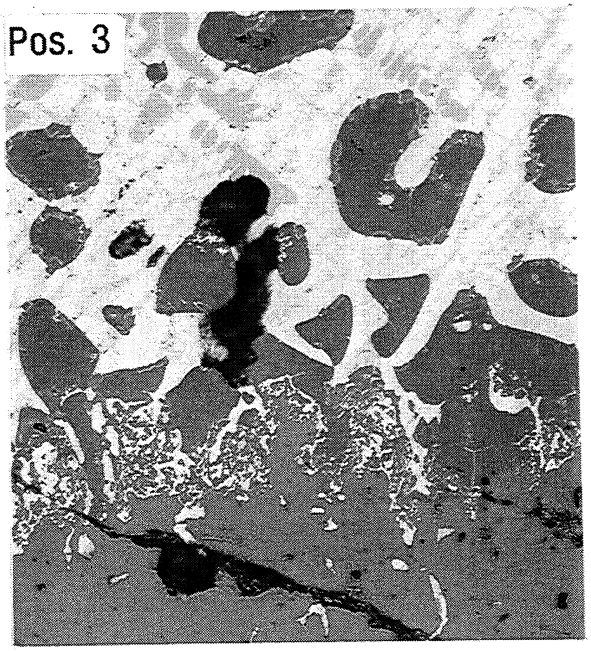

Contact zone

20 µm

Fig. 76 **Cross section CORA-17-02, showing contact between absorber melt and fuel rod; details of multicomponent product melt**

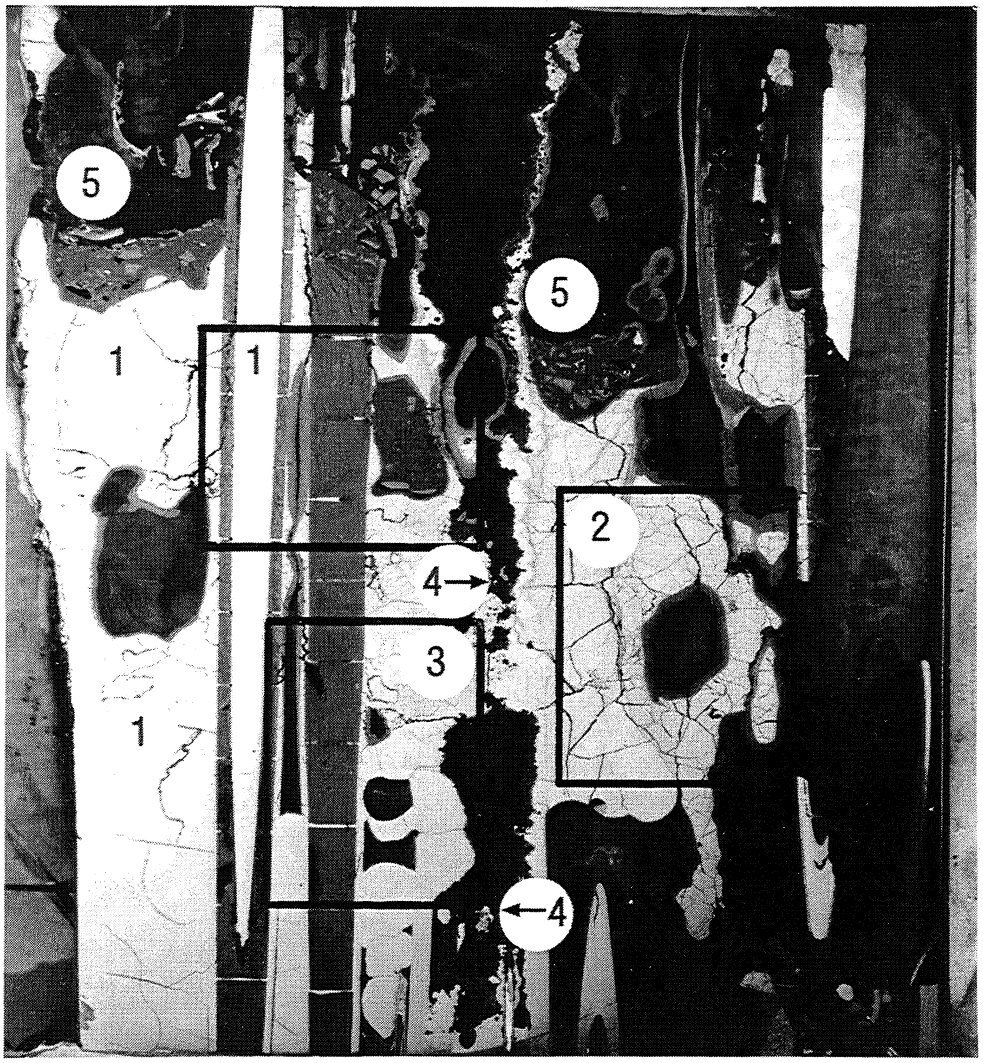

[1] Metallic (Zr, U, O) melt, with traces of steel components
[2] (Zr, U, O) melt, with higher oxygen content
[3] Metallic melt, rich in steel components
[4] Positions with isolated B_4C residues
[5] Rubble beds of cladding and fuel rod fragments

Fig. 77 Vertical section through blockage of CORA-17 bundle

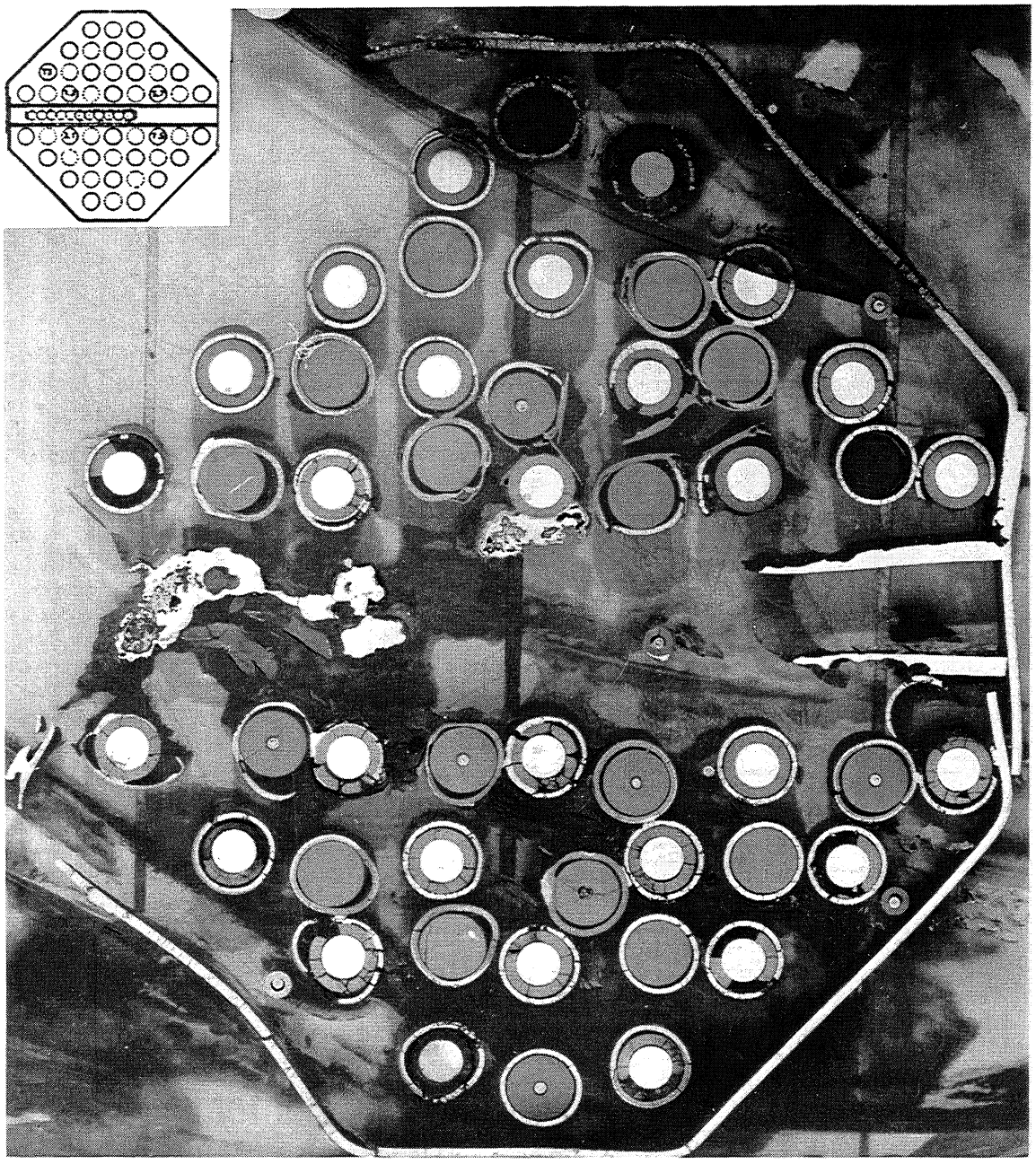

Cross Section 18-07, 874 mm, top view 10 mm

Fig. 78 Cross section through CORA-18 (BWR, large bundle)

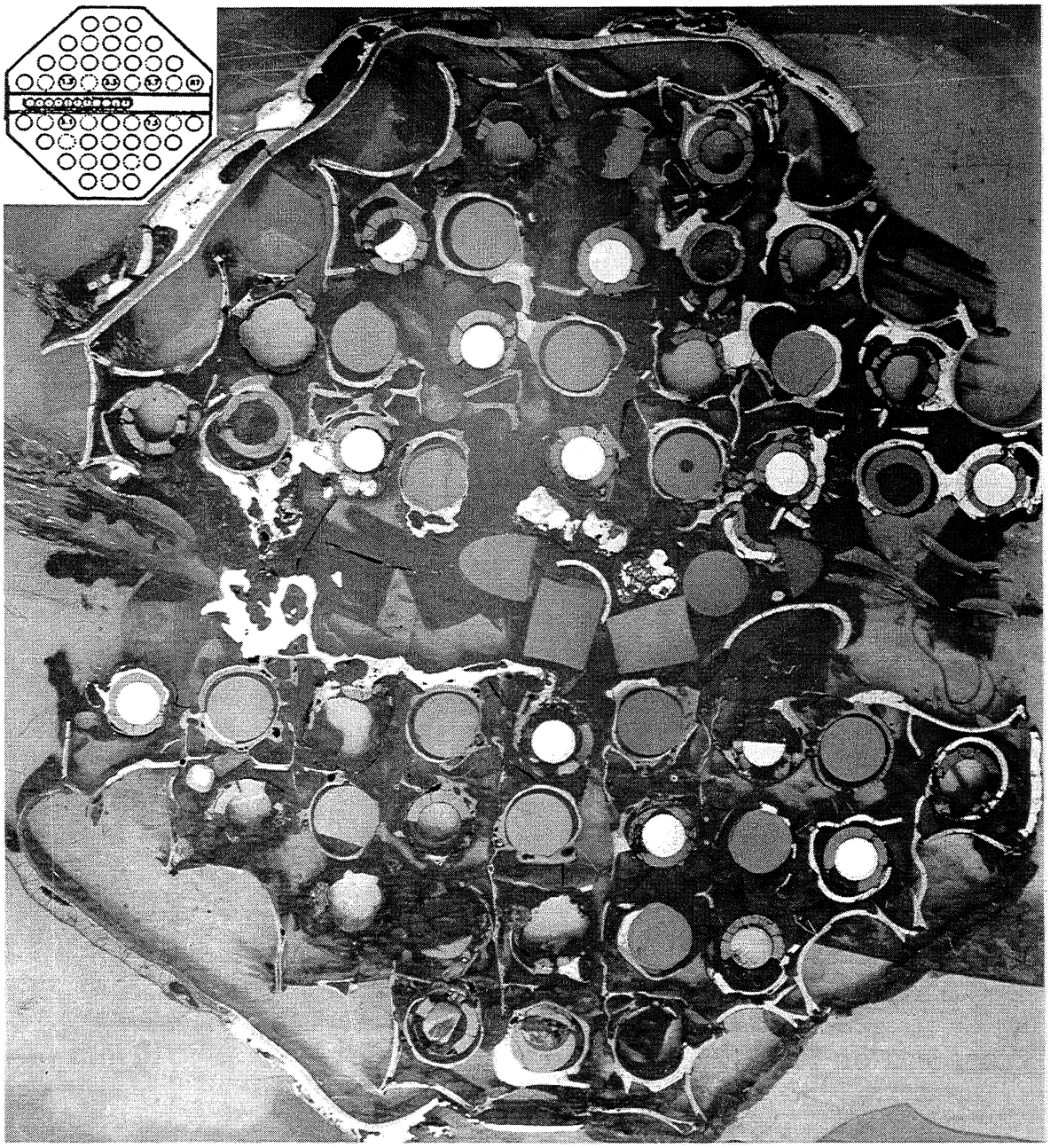

Cross Section 18-05, 560 mm, top view 10 mm

Fig. 79 Cross section through CORA-18 (BWR, large bundle)

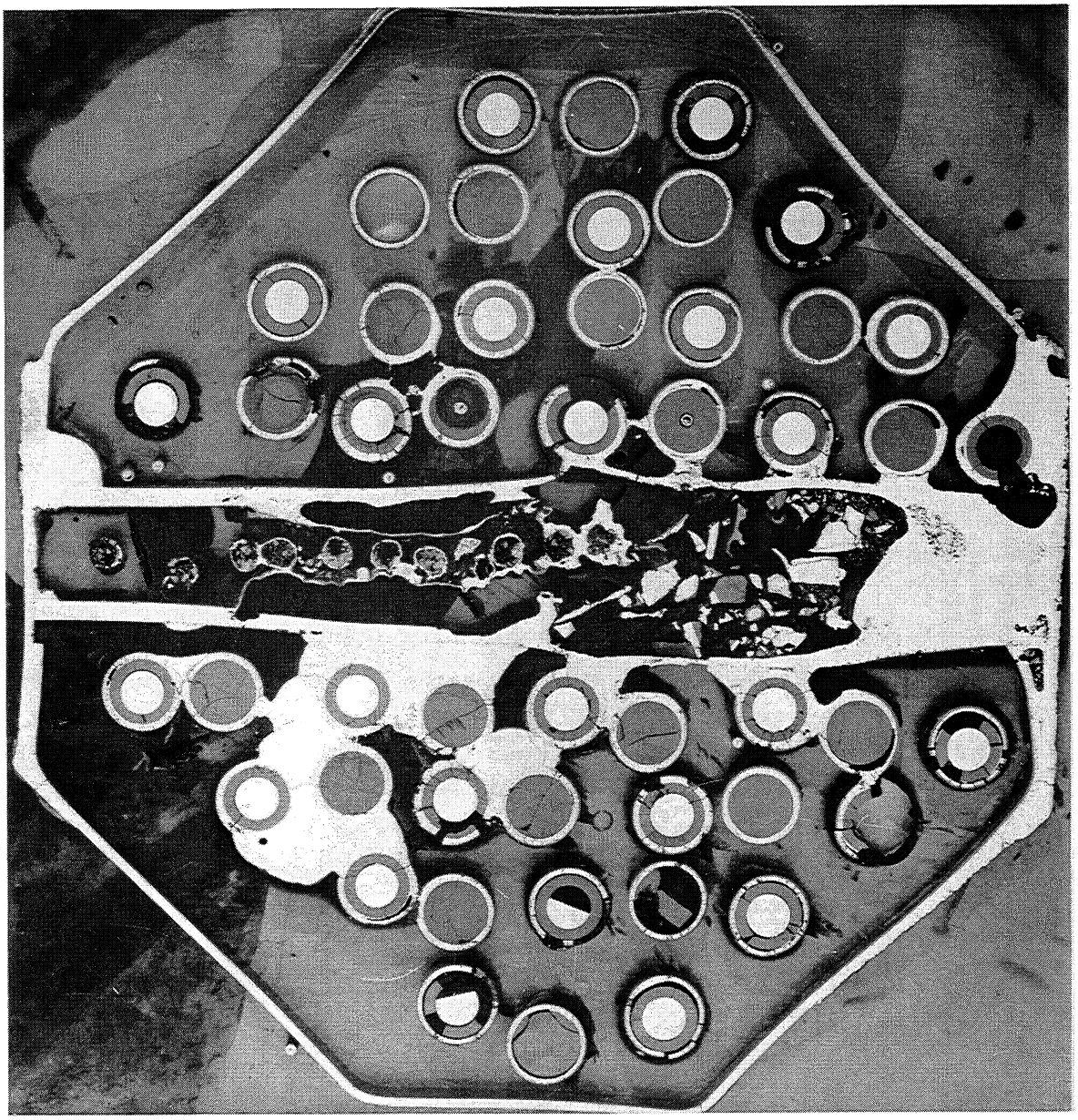

Cross Section 18-03, 269 mm, top view

10 mm

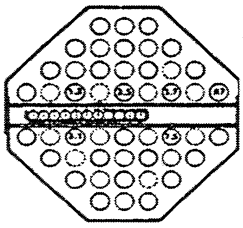

Fig. 80 Cross section through CORA-18 (BWR, large bundle)

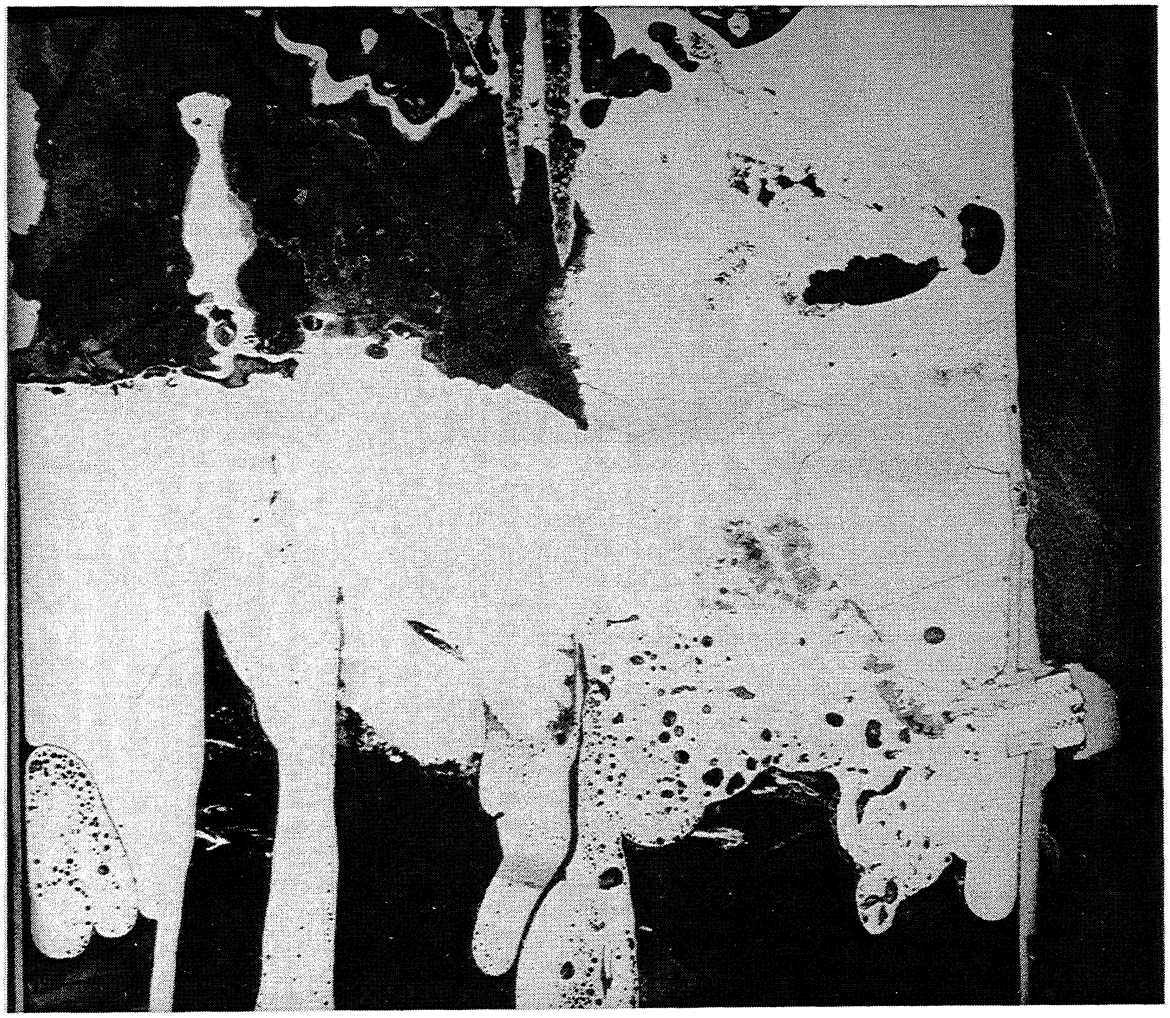

Vertical Section 18-c-L, 114 - 254 mm

10 mm

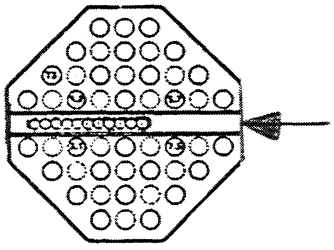

Fig. 81 Vertical section through CORA-18 (BWR, large bundle)

Appendix

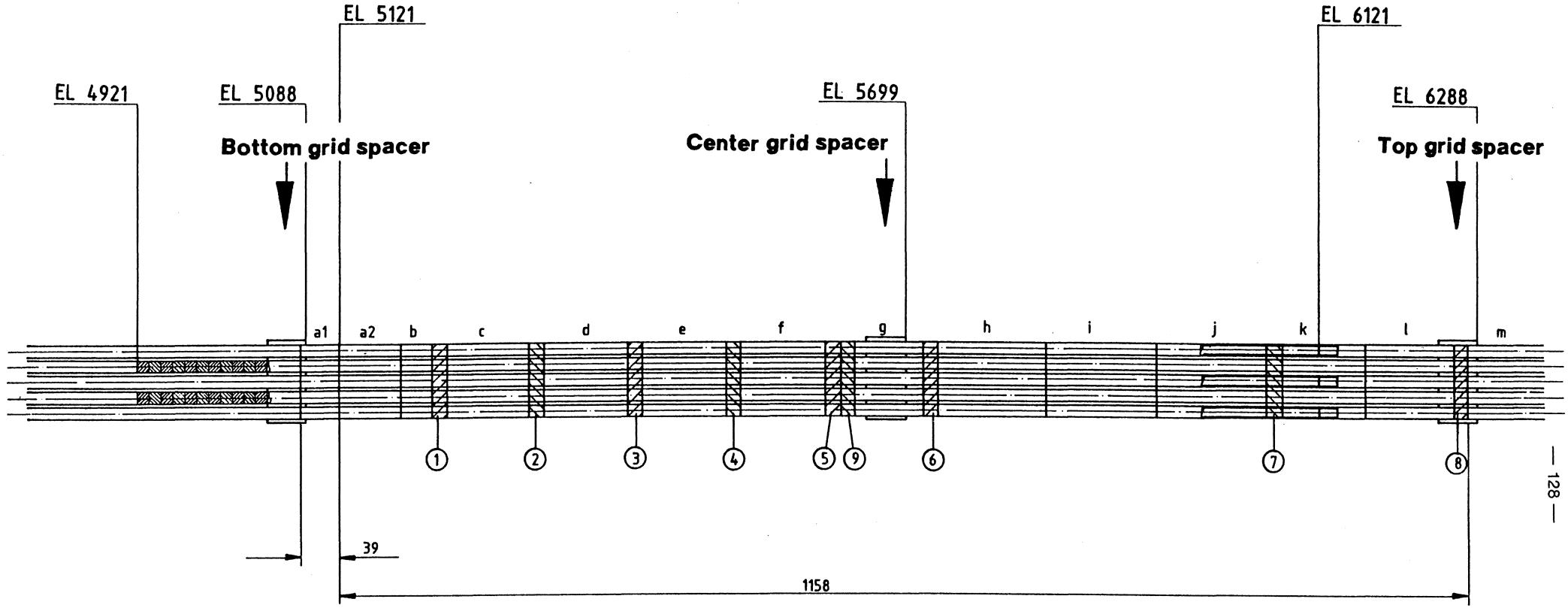

BWR-type bundle viewed from 30° and 210°, respectively

Vertical sections of remnants a2,b,c

Height of horizontal sample : 13mm (marking distance= 15mm)

Fig. A1: CORA-16
Bundle Sectioning

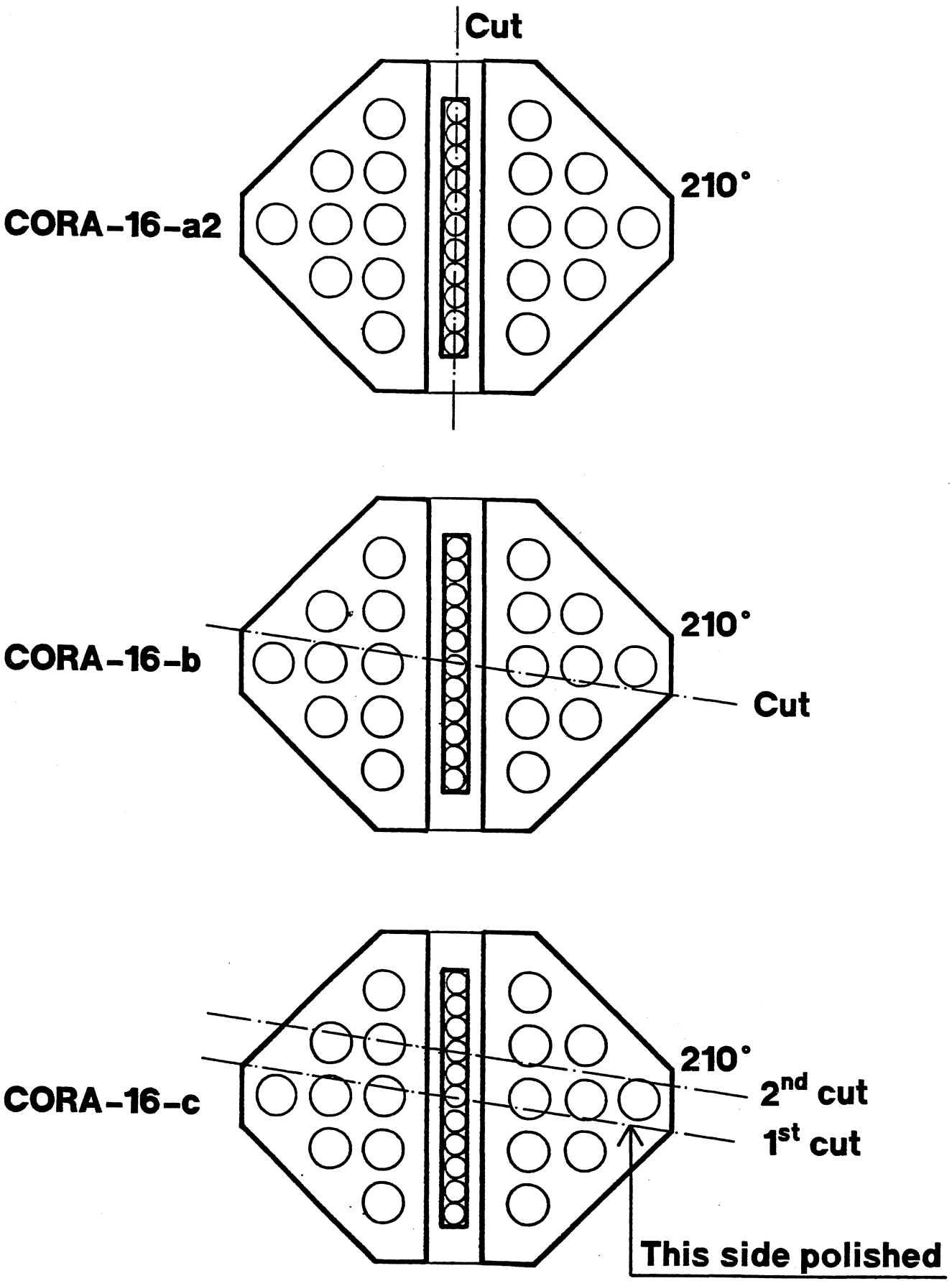

Fig. A2: CORA-16; Locations of vertical cuts through sections 16-a2, 16-b and 16-c (top-viewed)

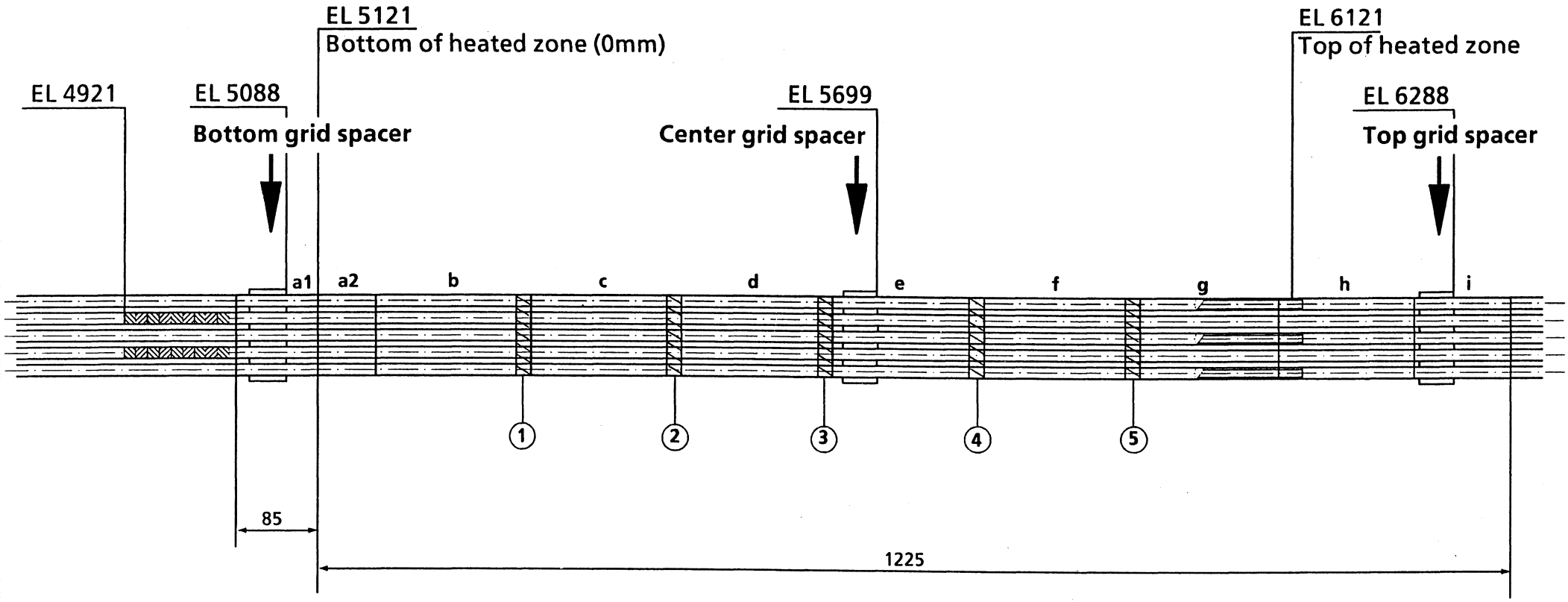

BWR-type bundle viewed from 30° and 210°, respectively

Vertical sections of remnants a2, b, c, d, e

Height of horizontal sample : 13mm (marking distance = 15mm)

Fig. A3: CORA-16
Bundle Sectioning

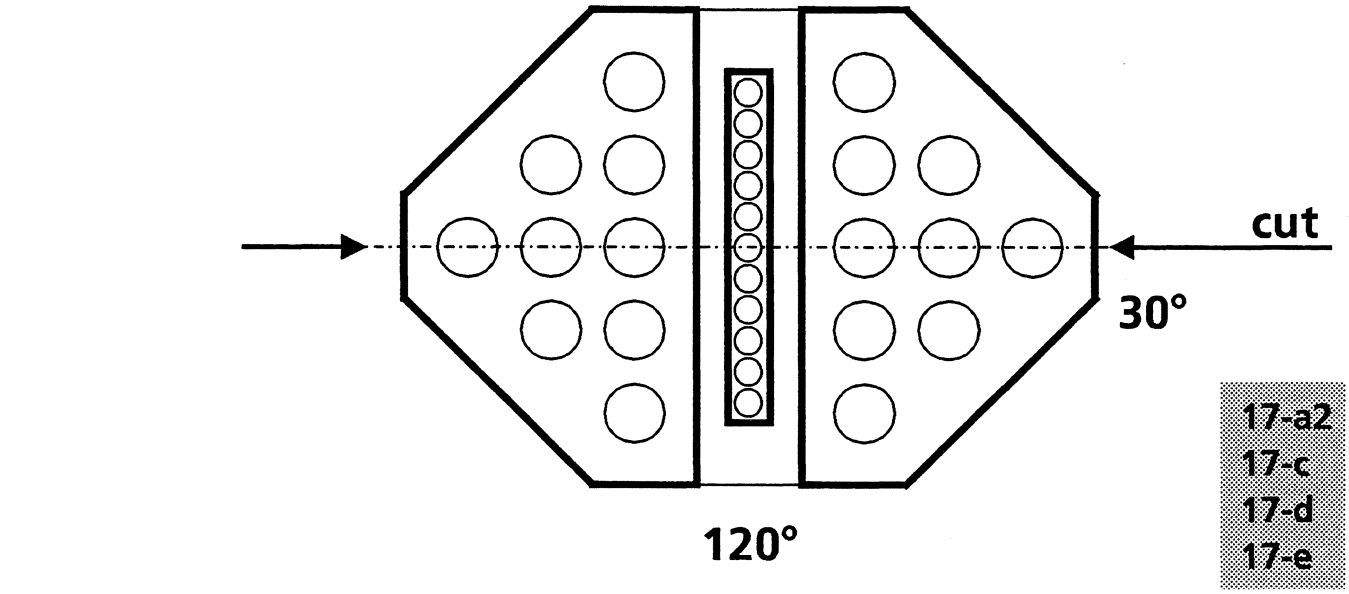

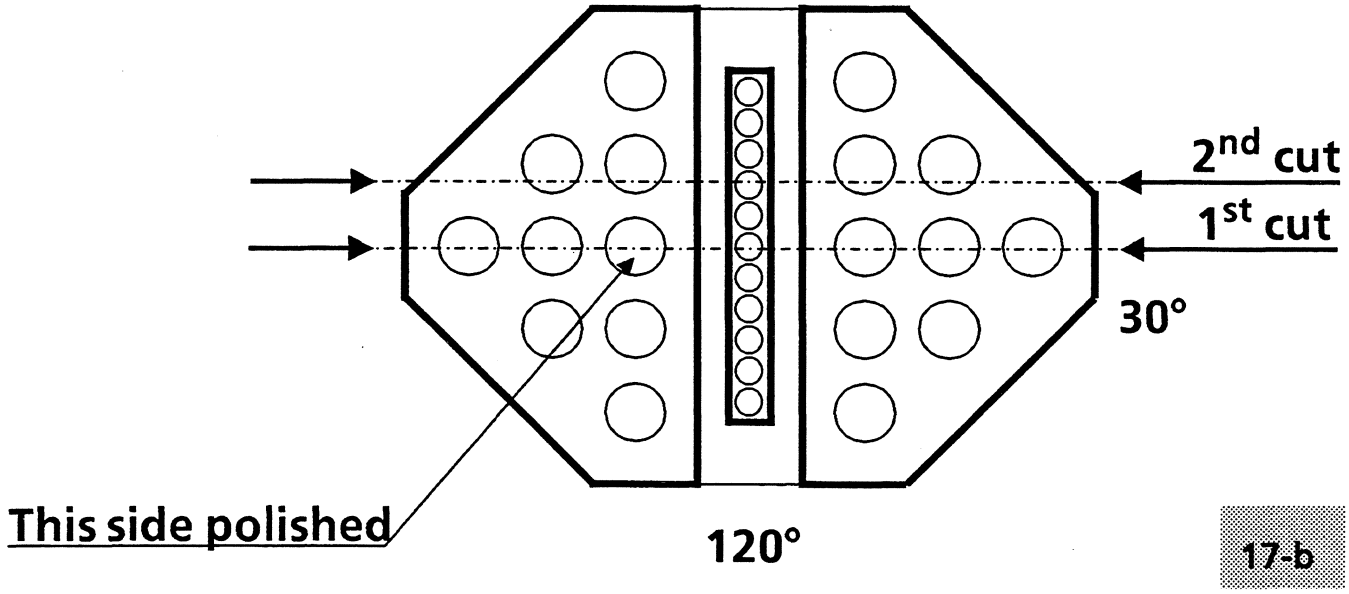

Fig. A4: CORA-17; Locations of vertical cuts through sections 17-a2, 17-b, 17-d and 17-e (top-viewed)

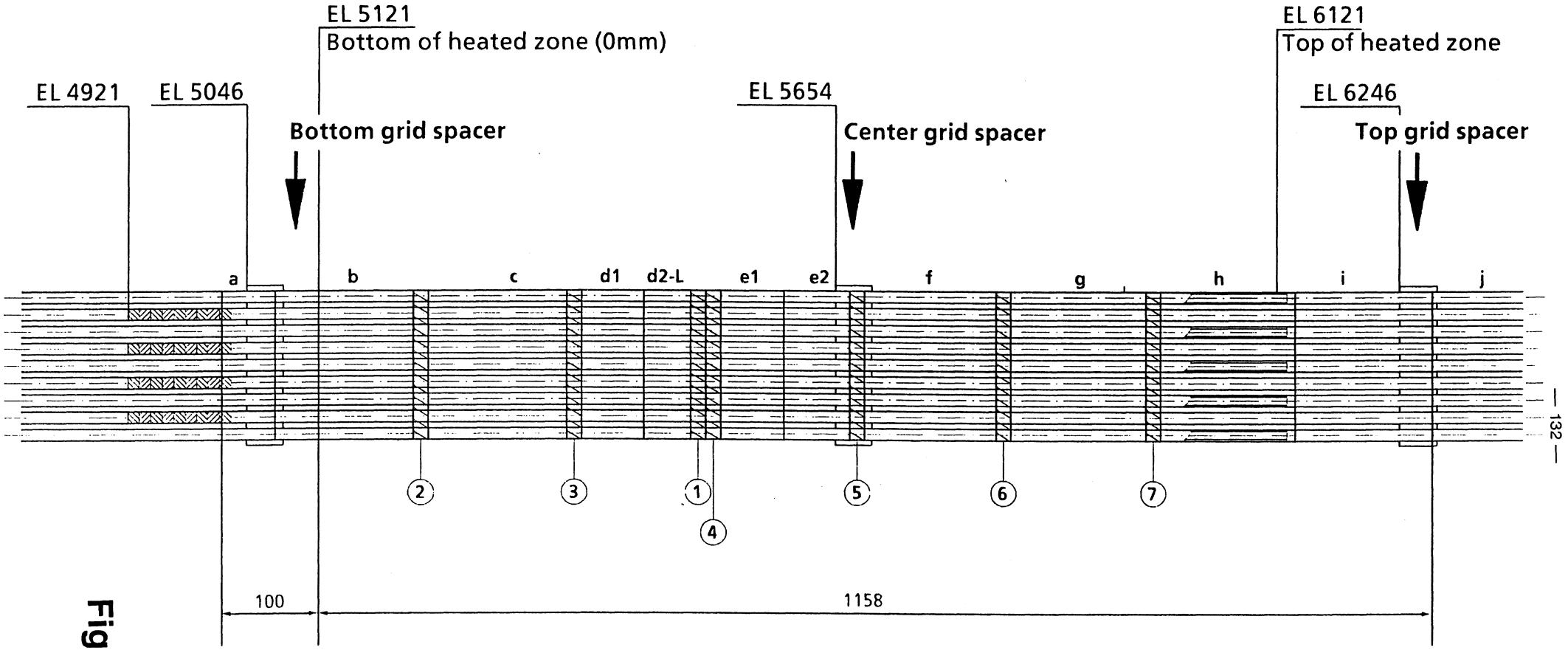

Fig. A5: CORA-18
Bundle Sectioning

Vertical sections of remnants c, d, e,

Height of horizontal sample : 13mm (marking distance = 15mm)

Bundle viewed from 30° and 210°, respectively

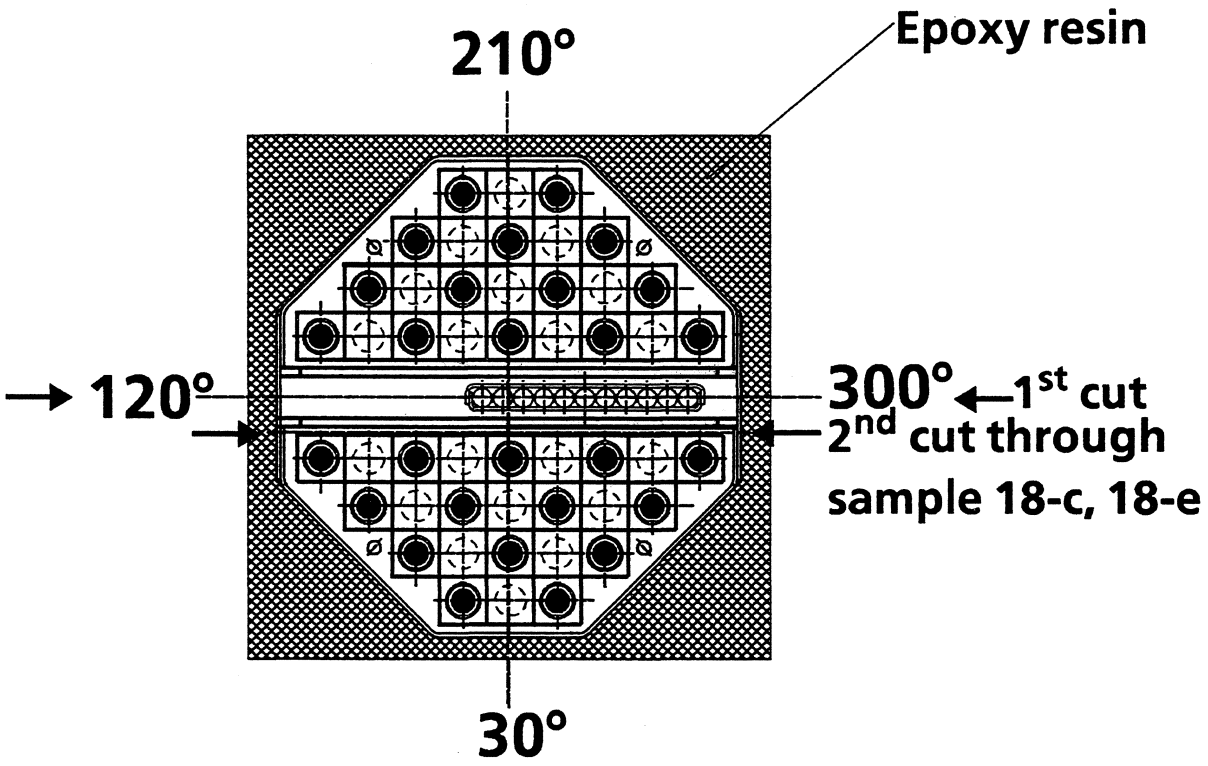

Fig. A6: CORA-18; Locations of vertical cuts through sections 18-c, 18-d and 18-e (1 st cut)